

**PNE-5009**

**DISTRIBUTION STATEMENT A**  
Approved for Public Release  
Distribution Unlimited

PNE-5009

**C.2**



**Plowshare**

civil, industrial and scientific uses for nuclear explosives

**UNITED STATES ARMY CORPS OF ENGINEERS**



## **THE FORMATION AND INITIAL STABILITY OF SLOPES ON COHESIONLESS MATERIALS**

**LOVELACE FOUNDATION**

**DOCUMENT LIBRARY**

B. N. MacIver

Engineer Waterways Experiment Station  
Vicksburg, Mississippi

26832

**U. S. Army Engineer Nuclear Cratering Group**  
Livermore, California

**ISSUED: August 1967**

PNE-5009

ENGINEERING PROPERTIES OF NUCLEAR CRATERS, REPORT 4  
THE FORMATION AND INITIAL STABILITY OF SLOPES ON  
COHESIONLESS MATERIALS

B. N. MacIver

U. S. Army Engineer Waterways  
Experiment Station  
Corps of Engineers  
Vicksburg, Mississippi

August 1967

20010711 072

## FOREWORD

The U. S. Army Engineer Waterways Experiment Station (WES) is conducting a program of studies at the request of the U. S. Army Engineer Nuclear Cratering Group (NCG) to develop analytical and empirical methods for evaluating the stability of nuclear craters. One phase of the program is concerned with the slopes on cohesionless fallback material, which comprise a major portion of the visible crater. This aspect of the overall slope stability problem was studied intermittently during the period March 1964 through December 1966 by Mr. B. N. MacIver, Embankment and Foundation Branch, Soils Division. Project Director was Mr. W. C. Sherman, Jr., Embankment and Foundation Branch, Soils Division.

This report was prepared by Mr. MacIver under the direction of Messrs. W. J. Turnbull, A. A. Maxwell, J. R. Compton, and W. C. Sherman, Jr., Soils Division, and was reviewed by Mr. S. J. Johnson.

Directors of the NCG during the study and the preparation of this report were LTC Ernest C. Graves, Jr., CE, and LTC Walter J. Slazak, CE. Directors of the WES were COL Alex G. Sutton, Jr., CE, and COL John R. Oswalt, Jr., CE. Technical Director of the WES was Mr. J. B. Tiffany.

## CONTENTS

	<u>Page</u>
FOREWORD. . . . .	iii
GLOSSARY. . . . .	ix
CONVERSION FACTORS, BRITISH TO METRIC UNITS OF MEASUREMENT. . . . .	xiii
SUMMARY . . . . .	xv
PART I: INTRODUCTION . . . . .	1
Purpose and Scope of Study. . . . .	1
Scope of Report . . . . .	1
PART II: CONCEPTS AND DEFINITIONS OF SLOPES AND SLOPE ANGLES . . . .	3
Failures of Slopes. . . . .	3
Angle of Repose . . . . .	5
Angle of Deposition . . . . .	6
PART III: FACTORS AFFECTING SLOPE ANGLES . . . . .	8
Characteristics of Individual Particles . . . . .	8
Characteristics of Aggregations of Particles. . . . .	17
Geometrical Characteristics of Slopes . . . . .	24
PART IV: CONSIDERATIONS AFFECTING FACTORS OF SAFETY. . . . .	30
Stability of Particles on Slopes. . . . .	30
Movement of Particles on Slopes . . . . .	35
Comparison of Slope Angles with Angles of Internal Friction . .	39
Comparison of Angle of Repose with Angle of Deposition. . . . .	45
PART V: EMPIRICAL DATA . . . . .	47
Angles of Deposition. . . . .	47
Angles of Repose. . . . .	49
PART VI: CONCLUSIONS . . . . .	51
LITERATURE CITED. . . . .	53
APPENDIX A: EMPIRICAL DATA ON COHESIONLESS SLOPES (EXCLUDING CRATERING STUDIES) . . . . .	A1
Laboratory Investigations . . . . .	A1
Stockpiles and Waste Dumps. . . . .	A10
Rock-fill Dams. . . . .	A12



	<u>Page</u>
Quarries and Open-Pit Mines . . . . .	A15
Natural Deposits. . . . .	A16
Handbooks and Codes . . . . .	A20
APPENDIX B: COHESIONLESS SLOPES IN EXPLOSION-PRODUCED CRATERS. . . .	B1
Explosion-Produced Craters. . . . .	B1
Crater Formation. . . . .	B3

## FIGURES

1. Failure of slope on cohesive material. . . . .	3
2. Failure of low slope on dry cohesionless material. . . . .	4
3. Hypothesized relation between angle of repose and relative density . . . . .	6
4. Effect of particle orientation on angle of repose. . . . .	6
5. Dimensions of particle . . . . .	11
6. Classes of particle shape. . . . .	11
7. Radii of curvature of particle corners . . . . .	12
8. Examples of classes of particle angularity . . . . .	13
9. Method of plotting particle-size (gradation) analysis. . .	14
10. Variation in gradations of materials having same average particle size. . . . .	15
11. Examples of gradation curves . . . . .	16
12. Elemental methods of deposition. . . . .	20
13. Hypothesized relations between angle of repose and angle of deposition for various rates of deposition. . .	23
14. Dimensions of slope linear in plan . . . . .	24
15. Dimensions of slope curved in plan . . . . .	25
16. Dimensions of hyperbolic representation of apparent, explosion-produced crater profile below preshot ground surface . . . . .	27
17. Variation in apparent crater profile with shape and roundness ratios . . . . .	29
18. Forces acting on particle. . . . .	30
19. Stability of particle on slope against overturning . . . .	32
20. Stable and hyperstable slopes formed by regular stacking of uniform spheres . . . . .	34
21. Kinetic energy of particle sliding on a slope of constant coefficient of sliding friction . . . . .	36
22. Variation in kinetic energy due to change in coefficient of sliding friction. . . . .	37
23. Relation between normal and shear stresses in direct shear test . . . . .	39
24. Relation between maximum and ultimate angles of internal friction. . . . .	40
25. Strength envelope of a cohesionless material reported by Seed and Goodman . . . . .	41
26. Comparisons of angles of repose with maximum angles of internal friction. . . . .	43

	<u>Page</u>
27. Comparisons of angles of deposition with ultimate angles of internal friction. . . . .	44
28. Comparisons of angles of deposition with maximum angles of internal friction found in tests by Metcalf . . . . .	44
29. Comparisons of angles of repose with angles of deposition . . . . .	45
A1. Relation between angle of deposition and initial slope angle found in model tests by Bustamante . . . . .	A6
A2. Summary of values of angle of repose given in handbooks and codes. . . . .	A22
B1. Section through Sedan crater showing crater nomenclature and dimensions and coordinate axes used for slope stability studies. . . . .	B2
B2. Variation in average fallback slope angle with depth of burst of single 1-lb TNT charges in sand found in experiments by Fulmer. . . . .	B5
B3. Variation in average fallback slope angle with depth of burst of single 1-lb C <sup>4</sup> charges in sand found in results of Project Zulu II . . . . .	B6
B4. Typical and average profiles of apparent crater of Project Sedan produced by single 100-kt nuclear explosion in desert alluvium . . . . .	B7
B5. Variation in average fallback slope angle with depth of burst of single explosions in desert alluvium. . . . .	B9
B6. Profile shape and roundness ratios for explosion-produced craters. . . . .	B10
B7. Typical and average profiles of apparent crater of Row H (at charge No. 5) of Project Pre-Buggy II produced by row of 1000-lb nitromethane explosions in desert alluvium . . . . .	B12
B8. Typical and average profiles of apparent crater of Project Danny Boy produced by single 0.42-kt nuclear explosion in basalt. . . . .	B13
B9. Comparison of particle size distribution of ejecta with natural joint spacing distribution at Danny Boy crater . . . . .	B14
B10. Variation in average fallback slope angle with depth of burst of single explosions in basalt of Buckboard Mesa . . . . .	B16
B11. Typical and average profiles of apparent crater of Project Dugout produced by row of 40,000-lb nitromethane explosions in basalt . . . . .	B17
B12. Profiles along bearing S40°W of apparent crater of Project Pre-Schooner II showing steepening of slope by undermining. . . . .	B19
B13. Comparison of selected average apparent crater profiles. . . . .	B20

#### TABLES

1. Relative Influence of Various Factors on Angles of Deposition and Repose. . . . .	9
--	---

	<u>Page</u>
2. Description of Elemental Methods of Deposition. . . . .	21
A1. Results of Tests by Morris <sup>27</sup> of Uniform Materials, and Inferred Characteristics of Individual Particles . . . . .	A8
A2. Results of Tests by Metcalf <sup>6</sup> of Crushed Materials. . . . .	A9
A3. Slope Angles Formed by Construction of Dumped Rock- Fill Dams . . . . .	A14
B1. Dimensions of Selected Explosion-Produced Craters . . . . .	B8

## GLOSSARY

- b width (or intermediate dimension) of particle, in.
- BF bulking factor, dimensionless
- c cohesion, psf or tons/sq ft
- $c_i$  cohesion intercept of strength envelope of cohesionless material, psf or tons/sq ft
- $C_c$  coefficient of curvature, dimensionless
- $C_u$  coefficient of uniformity, dimensionless
- D size (or diameter) of particle, in.
- $D_a$  apparent crater depth, ft or  $\text{ft}/\text{kt}^{1/3.4}$
- $D_{\text{avg}}$  average particle size, in.
- $D_d$  relative density, percent
- $D_{\text{max}}$  maximum particle size, in.
- $D_{\text{ob}}$  depth of burst, ft or  $\text{ft}/\text{kt}^{1/3.4}$
- $D_{10}$  effective particle size, in.
- $D_{30}$  size of particle larger in size than 30 percent (by weight) of material, in.
- $D_{50}$  average particle size, in. or ft
- $D_{60}$  size of particle larger in size than 60 percent (by weight) of material, in.
- $D_{100}$  maximum particle size, in.
- e void ratio, dimensionless
- $e_{\text{max}}$  maximum void ratio, dimensionless
- $e_{\text{min}}$  minimum void ratio, dimensionless
- $e_o$  original or preshot void ratio, dimensionless
- $E_f$  energy wasted in overcoming friction, ft-lb
- $E_k$  kinetic energy, ft-lb

$E_p$  potential energy, ft-lb  
 $F_k$  force due to kinetic friction, lb  
 $F_s$  force due to static friction, lb  
 $FS$  factor of safety, dimensionless  
 $g$  acceleration due to gravity, ft/sec<sup>2</sup>  
 $G$  specific gravity, dimensionless  
 $G_m$  bulk specific gravity, dimensionless  
 $G_s$  specific gravity of solids, dimensionless  
 $H$  height (or vertical height) of slope, ft  
 $H_{al}$  apparent crater lip crest height, ft or ft/kt<sup>1/3.4</sup>  
 $J$  curvature factor of slope in plan, dimensionless  
 $L$  length (or horizontal distance measured normal to cross section) of slope, ft  
 $l$  length (or longest dimension) of particle, in.  
 $n$  porosity, percent  
 $n_o$  original or preshot porosity, percent  
 $N$  normal force, lb  
 $r$  radius of particle or radius of largest circle inscribed in outline of particle, in.  
 $r_c$  radius of curvature of particle corner, in.  
 $R$  maximum radius of slope curved in plan (positive for concave slopes and negative for convex slopes), ft  
 $R_a$  apparent crater radius, ft or ft/kt<sup>1/3.4</sup>  
 $R_{al}$  apparent crater lip crest radius, ft or ft/kt<sup>1/3.4</sup>  
 $R_c$  cavity radius, ft or ft/kt<sup>1/3.4</sup>  
 $s$  spacing of charges, ft or ft/kt<sup>1/3.4</sup>  
 $S$  slant height of slope, ft  
 $t$  thickness (or smallest dimension) of particle, in.  
 $T$  tangential force, lb  
 $w$  water content, percent  
 $W$  weight of particle, lb (main text)  
 $W$  weight of explosive or energy yield of explosion, lb or kt (Appendix B)  
 $W_a$  apparent crater width, ft or ft/kt<sup>1/3.4</sup>  
 $W_{al}$  apparent crater lip crest width, ft or ft/kt<sup>1/3.4</sup>  
 $x$  longitudinal distance or horizontal distance parallel to toe of slope, ft or ft/kt<sup>1/3.4</sup>

$y$  lateral distance or horizontal distance perpendicular to toe of slope, ft or  $\text{ft}/\text{kt}^{1/3.4}$   
 $z$  vertical distance, ft or  $\text{ft}/\text{kt}^{1/3.4}$   
 $Z_a$  location of apparent crater bottom above origin of coordinate system base on average fallback slope angle, ft or  $\text{ft}/\text{kt}^{1/3.4}$   
 $Z_i$  location of apparent crater bottom above intersection of asymptotes to hyperbola representing apparent crater profile, ft or  $\text{ft}/\text{kt}^{1/3.4}$   
 $\beta$  angle of slope, deg  
 $\beta_a$  fallback slope angle, deg  
 $\beta_i$  inclination of asymptotes to hyperbola representing apparent crater profile, deg  
 $\gamma$  unit weight, pcf  
 $\gamma_{\text{max}}$  maximum unit weight, pcf  
 $\gamma_{\text{min}}$  minimum unit weight, pcf  
 $\gamma_o$  original or preshot unit weight, pcf  
 $\delta$  angle of deposition, deg  
 $\rho$  angle of repose, deg  
 $\rho_{\text{max}}$  maximum angle of repose, deg  
 $\rho_{\text{min}}$  minimum angle of repose, deg  
 $\sigma$  normal stress, psf or tons/sq ft  
 $\sigma_1$  major principal stress, psf or tons/sq ft  
 $\sigma_3$  minor principal stress, psf or tons/sq ft  
 $\tau$  shear stress, psf or tons/sq ft  
 $\tau_f$  maximum shear stress, psf or tons/sq ft  
 $\tau_u$  ultimate shear stress, psf or tons/sq ft  
 $\phi$  maximum angle of internal friction or inclination of strength envelope based on maximum shear stresses, deg  
 $\phi_i$  maximum angle of stress obliquity, deg  
 $\phi_u$  ultimate angle of internal friction or inclination of strength envelope based on ultimate shear stresses, deg  
 $\psi_k$  angle of kinetic sliding friction, deg  
 $\psi_s$  angle of static friction against sliding, deg

# CONVERSION FACTORS, BRITISH TO METRIC UNITS OF MEASUREMENT

British units of measurement used in this report can be converted to metric units as follows:

<u>Multiply</u>	<u>By</u>	<u>To Obtain</u>
inches	25.4	millimeters
feet	0.3048	meters
square feet	0.92903	square meters
cubic feet	0.0283168	cubic meters
pounds	0.45359237	kilograms
tons	907.185	kilograms
pounds per square foot	4.88243	kilograms per square meter
pounds per cubic foot	16.0185	kilograms per cubic meter
foot-pounds	0.138255	meter-kilograms
feet per second	0.3048	meters per second

## SUMMARY

The purpose of the study of engineering properties of nuclear craters is to identify and describe the physical properties that will control the use of a nuclear crater for engineering purposes. One of the prime considerations in the engineering use of a nuclear crater is the stability of the crater slopes. The late time mechanism of explosion crater formation is a deposition phenomenon.

The inclination of a slope formed by deposition of cohesionless material is termed the angle of deposition. The angle of repose is defined in this report as the maximum possible inclination of a slope of cohesionless material. This definition differs from some common definitions of angle of repose. The factor of safety of a slope formed by deposition is defined as the ratio of the tangent of the angle of repose to the tangent of the angle of deposition. Variations are recognized in the angle of deposition with the manner of deposition, and in the angle of repose with varying relative density and particle orientation.

Such factors as particle size, shape, and angularity, structure of particle aggregations, manner of deposition, and geometry of slopes are discussed with regard to their relative influence on each of the aforementioned angles. A few simple analytical relations are given to aid in understanding the behavior of particles during deposition and their stability on an inclined surface. Empirical data from laboratory tests, stockpiles, rock-fill dams, natural slopes, explosion-produced craters, etc., are presented and compared.

It is concluded that angles of deposition for cohesionless rock and soil materials vary between 22 and 42 deg, and generally lie between 34 and 37 deg for angular particles, whereas angles of repose range between 27 and 47 deg, and generally lie between 37 and 47 deg for angular particles. The initial factor of safety of a slope formed by deposition will probably exceed 1.1 but will be no more than 1.5 in most cases.



# ENGINEERING PROPERTIES OF NUCLEAR CRATERS

## THE FORMATION AND INITIAL STABILITY OF SLOPES ON COHESIONLESS MATERIALS

### PART I: INTRODUCTION

#### Purpose and Scope of Study

1. The broad objective of the study of engineering properties of nuclear craters is to identify, describe, and assign usable engineering parameters to the geologic and physical properties that will control the behavior of a nuclear crater from an engineering standpoint. One of the most important factors that will control a crater's use is the stability of its slopes. The fallback and ejecta portions of a crater are formed during the latter portion of the cratering process by a type of depositional phenomenon. This results in physical characteristics that are generally those of cohesionless materials. This study (a) investigates the process of the formation and stability of slopes on cohesionless materials in general, (b) compares the information developed on formation and stability of slopes on cohesionless materials in general, and (c) compares the information developed on formation and stability with cratering experience obtained to date in dry material.

#### Scope of Report

2. This report considers only the first purpose of the overall study; that is, the inclination and stability of slopes immediately upon formation. The behavior of only dry, perfectly cohesionless materials under gravity forces is considered. The effect of environmental factors (groundwater, surface waters, seismic accelerations, settlement, mechanical or chemical weathering, etc.) and the long-term stability of slopes on cohesionless materials are beyond the scope of this report.

3. Almost all of the information reviewed for this report is contained in published literature. The information reviewed includes

---

empirical data and hypotheses regarding the angle of repose, descriptions of the properties of cohesionless materials, and measured slope dimensions of rock-fill dams, taluses, craters, etc. The concepts and definitions being followed in the overall study were established in this report.

## PART II: CONCEPTS AND DEFINITIONS OF SLOPES AND SLOPE ANGLES

4. A slope is an unrestrained, inclined surface of a mass of material. The slope angle is that angle between a horizontal plane and the slope surface. A slope failure is a change in the overall inclination of a slope due to movement of the material beneath the slope. The tendency toward failure may be described in terms of geometric and material properties. For the infinite slope case (that is a slope of constant inclination and of infinite height) the only geometric parameter is the slope angle. The significance of using the slope angle as a measure of the tendency toward failure is discussed in the following paragraphs by comparing the concept of the mode of failure of an intact cohesive material and a cohesionless material.

### Failures of Slopes

#### Cohesive materials

5. The slope of a mass of cohesive material such as moist clay will fail when the shearing stress along any potential surface of sliding exceeds the resistance to shearing along that surface. The material will slide en masse upon the resulting discontinuity, as illustrated in fig. 1a.

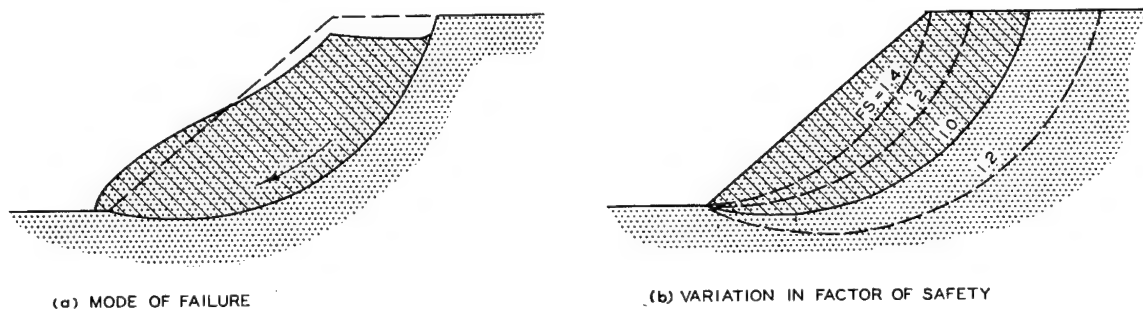


Fig. 1. Failure of slope on cohesive material

Both the shearing stress and the shearing resistance for any possible failure surface depend on the height as well as the inclination of the slope. The ratio of average shearing resistance to average shearing stress within a material is called the factor of safety. When the factor of safety

falls below unity, the slope fails by shearing.

6. When a slope of given height in a relatively homogeneous and isotropic cohesive material is formed too steeply, failure occurs along a surface that is curved (essentially circular) in section and passes deeply within the material. This is shown in fig. 1b by the decrease in factor of safety with increasing depth of the potential failure surface beneath the slope. Thus, even a slightly excessive slope angle will cause the movement of a substantial block of material along a relatively deep, interior sliding surface.

#### Cohesionless materials

7. A mass of cohesionless material such as dry sand or rock fragments will not fail by en masse sliding of material along a deep-seated curved surface as in the case of cohesive material. Rather, when a slope is formed at too large an angle in cohesionless material, the slope will recede to a stable inclination by a series of progressive slides along plane surfaces slightly beneath the slope, as shown in fig. 2a. The increase in factor of safety with decreasing slope angle is illustrated in fig. 2b; the potential surface of sliding having the lowest factor of safety is coincident with the slope. Therefore, the controlling shearing and resisting stresses are independent of the height of the slope, being functions solely of the inclination.

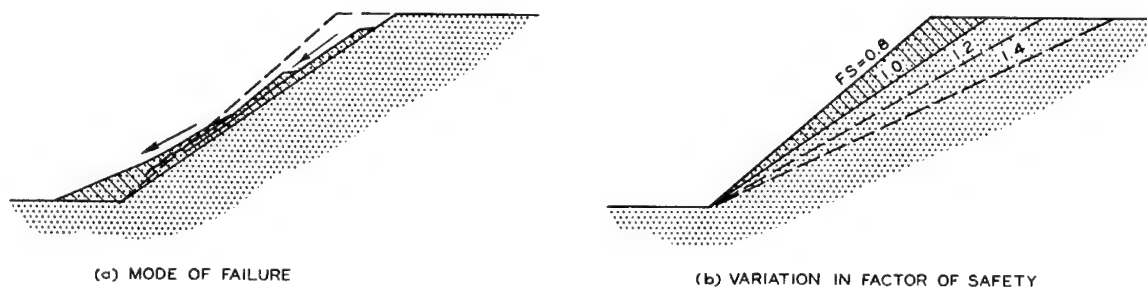


Fig. 2. Failure of low slope on dry cohesionless material

8. Because of the surficial character of a slope failure in cohesionless material and because of the uncomplicated and time-independent shearing resistance of such a material, a slope of cohesionless material is generally considered safe for many engineering purposes even if the factor of safety is small.

### Angle of Repose

9. The angle of repose most commonly is defined as the angle (measured from the horizontal) of the steepest slope at which a loose, cohesionless material can be piled.<sup>1,2,3,4</sup> Such a definition qualifies the relative density of the material (loose) and the manner of forming the slope (piled), and implies that the angle of repose represents the angle at which a mass of material in motion will come to rest.

10. In this study a new definition of the angle of repose is used which recognizes a static condition at which surficial movement begins that is separate and distinct from a kinetic condition at which surficial movement ceases. This distinction has been recognized by such authors as Bustamante<sup>1</sup> and Field.<sup>5</sup> On the other hand, Metcalf<sup>6</sup> concluded that a static angle of repose is a transient phenomenon that can generally be destroyed by a small addition of energy. For purposes of this study the angle of repose  $\rho$  is the maximum possible inclination of a slope of a given mass of cohesionless material. This slope might be formed by excavating into the material or through the steepening of an existing slope by settlement or erosion. In the laboratory this could be accomplished by placing the material in a shallow box or pan and then tilting the box until surface movement begins. The range over which this angle can vary for any material is considered in the following paragraphs.

11. The limiting values are the minimum angle of repose  $\rho_{\min}$  and the maximum angle of repose  $\rho_{\max}$  corresponding respectively to the least stable and the most stable possible arrangements of particles. In a mass of relatively equidimensional and rounded particles, the variation in particle arrangement would correspond to the variation in relative density  $D_d$ ; that is, the minimum angle of repose would be found for the material at zero relative density, and the maximum angle of repose would be attained by the material at 100 percent relative density. A hypothesized variation of angle of repose with relative density is shown in fig. 3 to illustrate the relation.

12. When the particles of a material are block-like or plate-like in shape, the correlation between the angle of repose and the relative density is affected by the particle orientation with regard to the slope

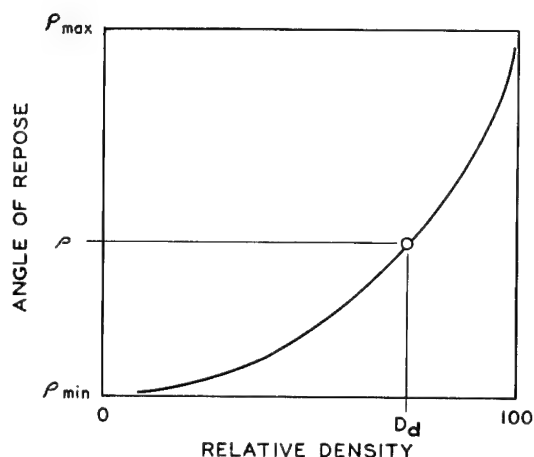


Fig. 3. Hypothesized relation between angle of repose and relative density

and the interlocking characteristics of the particles. As illustrated in fig. 4, a particle orientation parallel to the slope would give a minimum angle of repose and an orientation perpendicular to the slope would give a maximum angle.

13. Angles of repose approaching the minimum and maximum values can be measured by laboratory tests in which the material is placed in extreme conditions of relative density and particle orientation before the mass is tilted. Both limiting values would represent meaningful

parameters of the material consistent with the methods used to obtain the minimum and maximum densities of a cohesionless material.<sup>7,8</sup> The difference between the two values might also serve as an index of the properties of the material, the difference being small for uniform, rounded particles and large for nonuniform or flat particles.

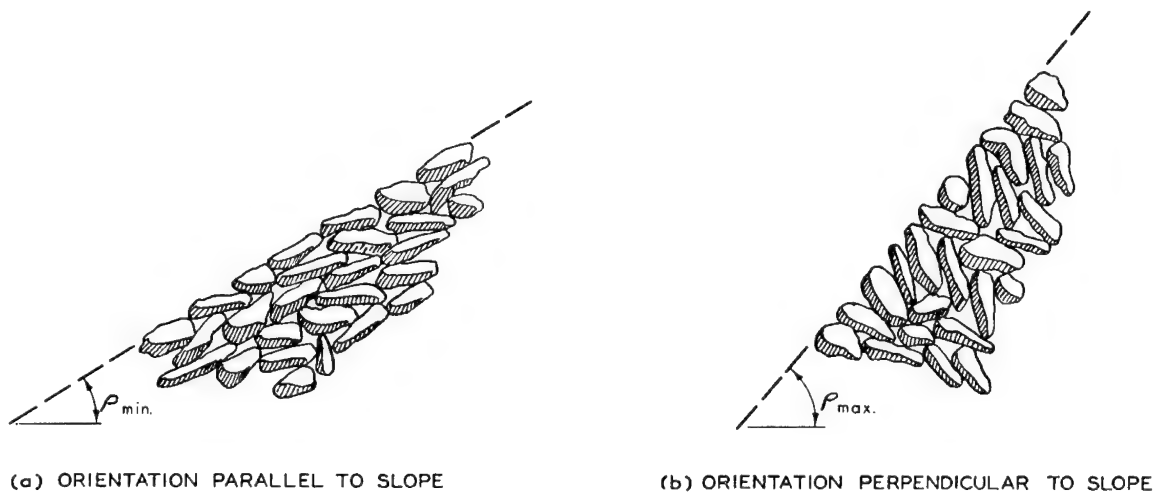


Fig. 4. Effect of particle orientation on angle of repose

#### Angle of Deposition

14. When a slope is formed by, not after, the deposition of material,

the slope angle corresponds to the kinetic condition at which surficial movement ceases and is defined as follows: angle of deposition  $\delta$  is the inclination of a slope formed by the deposition of cohesionless material. This is the angle of the slope when the particles stop moving, and it applies to the initial slopes of deposits such as taluses, stockpiles, dumped rock-fill dams, or the fallback in an explosion-produced crater.

15. A slope formed by dumping or dropping dry cohesionless material will have an inclination less than the angle of repose of the resulting deposit and will, therefore, have against the resumption of movement a factor of safety greater than unity.

---

### PART III: FACTORS AFFECTING SLOPE ANGLES

16. The initial inclination of a slope formed by deposition of a cohesionless material depends on the physical characteristics (size, shape, etc.) of the individual particles and on the manner of placing the material on the slope. The subsequent stability of the slope depends on the aggregate characteristics (relative density, orientation, etc.) of the material as well as the characteristics of the individual particles. These different types of factors and their relative influences on the slope angle are discussed in the following paragraphs. This part also discusses slope nomenclature as a basis for usage in the present and in future reports.

17. Table 1 gives the several factors discussed in this section and the estimated relative influence of these factors on the angles of deposition and repose. The influence of each factor is indicated by the extent to which the slope angle would be increased or decreased by a change in the factor.

#### Characteristics of Individual Particles

##### Size

18. The size of the particles is often considered to be the predominant factor affecting the angle of repose. Perhaps this emphasis reflects the ease with which size can be measured and expressed, whereas such factors as shape and angularity cannot be as readily given in numerical terms. Authors of most published works<sup>1,4,9,10</sup> imply, or explicitly state, that the angle of repose or the angle of deposition increases with increasing size of the particles. Other investigators<sup>4</sup> take the contrary view that the angle of repose is inversely related to particle size, and a few<sup>4,6,11</sup> claim that any relation between particle size and angle of repose is insignificant. Laboratory shear tests of cohesionless materials have led to similar disagreements; some investigators<sup>12,13,14</sup> have suggested that the angle of internal friction is essentially independent of particle size, whereas others<sup>15,16,17</sup> have indicated an increase with size,



Table 1  
Relative Influence of Various Factors on Angles of Deposition and Repose

Factor	Change in Factor	Effect of Change in Factor*			
		Angle of Deposition		Angle of Repose	
		Low Rate of Deposition	High Rate of Deposition	Minimum	Maximum
Characteristics of Individual Particles					
Average size	Increase	Decrease (S-M)	Decrease (S)	No effect	No effect
Shape	More bulky	Decrease (M)	Decrease (S-M)	Increase (M)	Decrease (M-L)
Angularity	Increase (sharper)	Increase (L)	Increase (L)	Increase (L)	Increase (L)
Surface texture	Rougher	Increase (M-L)	Increase (L)	Increase (L)	Increase (L)
Specific gravity	Increase	Decrease (S)	Decrease (S)	Decrease (S)	Decrease (O-S)
Characteristics of Aggregations of Particles					
Relative density	Increase	Angle of Deposition		Angle of Repose	
		Bulky Particles	Nonbulky Particles	Bulky Particles	Nonbulky Particles
Gradation	Increase (wider graded)	Not applicable	Not applicable	Increase (M-L)	Increase (S-M)
		Decrease (S-M)	Decrease (S)	Increase (M)	Increase (S-M)
Particle orientation	Increase in alignment { Perpendicular to slope Parallel to slope	Not applicable	Not applicable	Increase (O-S)	Increase (L)
		Not applicable	Not applicable	Decrease (O-S)	Decrease (L)
Manner of deposition**	Rate of deposition { Initial velocity { Vertical component Horizontal component	Increase (M-L)	Increase (M-L)	Decrease (S-M)	Increase (M)
		Decrease (S)	No effect	Increase (M)	Increase (M)
		Decrease (L)	Decrease (L)	Increase (S)	Increase (S)
Geometrical Characteristics of Slope					
Slant height	Increase	Decrease (S-M)		No effect	
Ratio of slant height to average particle size	Increase (up to 100†)	Decrease (S-M)		Decrease (S-M)	
Curvature factor	Slope concave in plan { Slope convex in plan	Increase (S-M)		Increase (S)	
		Decrease (S-M)		Decrease (S)	

\* Assuming that all other factors remain constant, O = negligible, S = slight, M = moderate, and L = large change in angle.  
 \*\* Affects the angle of repose as it affects the relative density and particle orientation of the resulting deposit.  
 † At ratios of slant height to average particle size greater than about 100, this ratio has negligible effect.

and still others<sup>18</sup> have shown a decrease.

19. Laboratory tests by van Burkalow,<sup>4</sup> using small uniform particles of similar character, showed a slight to moderate decrease in the angle of deposition with a severalfold increase in particle size. This relation suggests that the greater kinetic energy of larger particles is not completely offset by the increased energy losses resulting from the greater surface irregularities associated with larger particle size.

20. The confusion regarding the effect of particle size may stem from (a) failure to distinguish between an angle of repose and an angle of deposition, (b) inability to isolate the effect of size from other influences, and (c) trying to express with a single number the multitude of different particle sizes present in a graded material. If it were possible to obtain and test several samples of uniformly sized particles, each sample being of a different particle size but identical in all other characteristics (material, particle shape, and angularity, etc.), it is believed that the angle of repose would be found to be independent of particle size. Such an investigation would require that each sample contain the same number of particles or, in more meaningful terms, that enough particles be involved in each test to ensure that the mass would behave as a continuous body rather than as a mechanism of interacting bodies. Therefore, in view of the contradictory evidence available it is suggested as a working hypothesis that particle size will have negligible influence on the angle of repose.

#### Shape

21. Probably the most influential characteristics of particles are shape and angularity. Shape refers to the relative difference in dimensions of a particle measured in different directions, and angularity refers to the relative sharpness of the corners and edges of a particle. Numerous methods for measuring and numerically expressing these properties have been advocated.<sup>19,20,21,22,23</sup> For the present purposes, only the common qualitative classifications will be considered.

22. The shape of a particle might be classified<sup>24</sup> as follows:

Class	Description	$t/b$	$b/l$
Bulky	Equidimensional, chunky	$>2/3$	$>2/3$
Elongated	Rod-like, prolate	$>2/3$	$<2/3$
Flat	Plate-like, disk-shaped	$<2/3$	$>2/3$
Bladed	Triaxial	$<2/3$	$<2/3$

where  $l$  is the length,  $b$  is the width (or breadth), and  $t$  is the thickness of the particle measured along mutually perpendicular axes, such that  $l > b > t$ , as shown in fig. 5. The width  $b$  is essentially equal to the particle size  $D$ , whereas  $l$  and  $t$  are the maximum and minimum dimensions, respectively, of the particle. Fig. 6 illustrates the

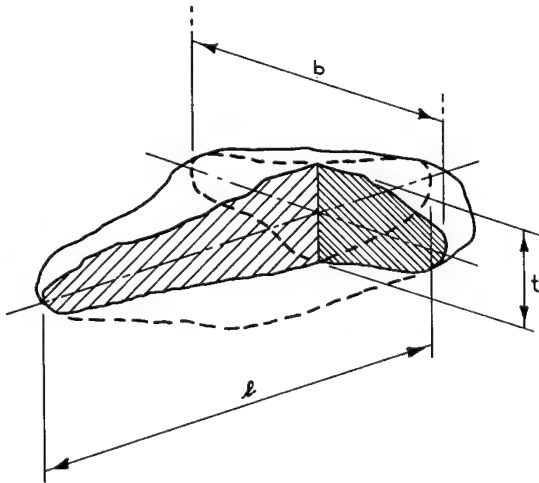


Fig. 5. Dimensions of particle

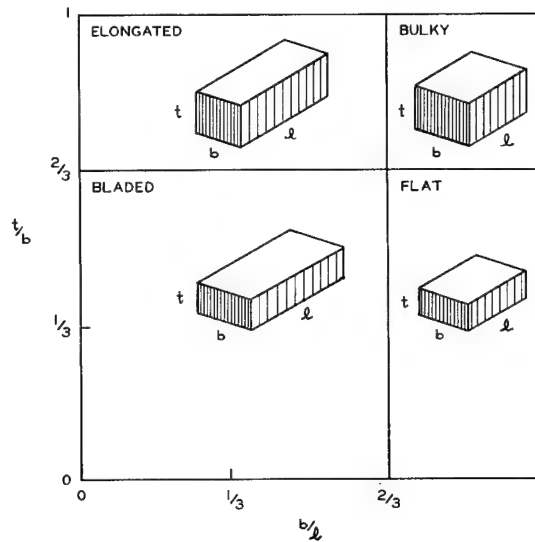


Fig. 6. Classes of particle shape

four classes of particle shape. It should be noted that for many civil engineering purposes (concrete aggregate,<sup>25</sup> slope protection against wave action,<sup>26</sup> etc.) particles are classified according to a ratio of  $1/3$ . To classify a mass of material, the percentage of the particles (preferably by weight rather than number of particles) in each shape class is often used.

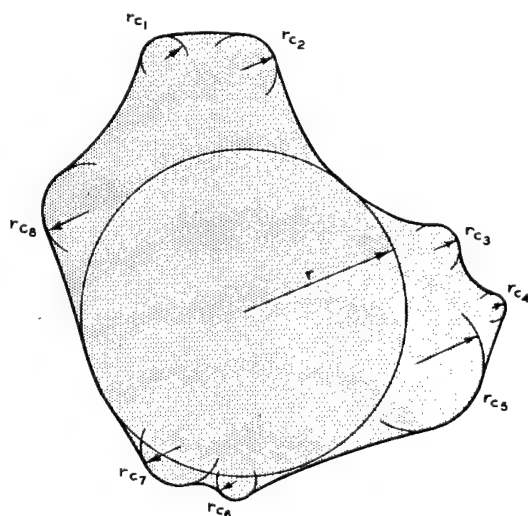
23. As particles become less bulky, their orientation with respect to each other and to the slope becomes more significant. In general, the less bulky the particles, the smaller the minimum angle of repose and the larger the maximum angle of repose, assuming a parallel particle

orientation in each case. The angle of deposition will be increased in most cases by a decrease in bulkiness, since such particles will tend to slide rather than roll when in motion. This behavior is dependent on the manner of deposition and, in some instances, on the mineral composition of the material.

### Angularity

24. The angularity of a particle can be expressed in terms of the degree to which the curvature of the corners and edges approaches the maximum curvature possible. Considering the projection of the particle outline in each of the three principal, mutually perpendicular planes, the ratio of the radius  $r_c$  of any curved surface to the radius  $r$  of the largest circle that could be inscribed in the same plane can be estimated, as shown in fig. 7. It should be noted that  $r$  would be essentially

equal to either  $b/2$  or  $t/2$ . A particle then might be classified as follows:<sup>24</sup>



AVERAGE  $\frac{r_c}{r} = 0.21$   
CLASS: SUBANGULAR

Fig. 7. Radii of curvature of particle corners

mass of material, the percentage of the particles (preferably by weight) in each class of angularity might be used.

25. The effect of a decrease in angularity is a marked decrease in both the angle of repose and the angle of deposition due to the decrease

Class	$r_c/r$
Angular	0 to 0.15
Subangular	0.15 to 0.25
Subrounded	0.25 to 0.40
Rounded	0.40 to 0.60
Well-rounded	0.60 to 1.00

where the value of  $r_c/r$  is the average of all curved surfaces (excluding reentrant corners and values of  $r_c/r$  greater than 1.00) in the three principal planes. Fig. 8 illustrates the five classes of particle angularity. To describe a

of particle interlocking and increased freedom to roll. Particles of blasted rock will generally be angular, or at least subangular, even when thrown for long distances through the air. The impact of a freshly broken particle may split the particle but probably would not decrease its angularity. However, further movement (bouncing or rolling) or interaction among particles after impact could reduce its angularity.

#### Surface texture

26. The surface texture of a particle might be classified as rough or smooth solely on visual evaluation, but few bases are available for a more detailed classification.<sup>21</sup> The fine surface irregularities of small particles have been indexed<sup>13</sup> by the absorption of kerosene on these surfaces. Despite the difficulties of expressing surface texture, this property strongly affects the coefficient of friction between particles, and both the angles of repose and of deposition will decrease as the particles become smoother. This effect is shown clearly by the results of laboratory tests by Morris.<sup>27</sup>

#### Specific gravity

27. The specific gravity  $G$  of a particle is the ratio of the weight of the particle to the weight of an equal volume of water; it represents the unit weight of the material constituting the particle. The specific gravity of solids  $G_s$  considers only the solid mineral constituents of each particle. For material that may contain internal voids, the bulk specific gravity  $G_m$  may be preferred.<sup>7</sup> This is determined by considering each particle to be internally homogeneous, thus averaging the weight of the solid constituents with that of the internal voids.

28. Model tests by van Burkalow<sup>4</sup> showed a slight decrease (1 to






PARTICLE	AVERAGE $\frac{r_c}{r}$	CLASS
	0.12	ANGULAR
	0.20	SUBANGULAR
	0.32	SUBROUNDED
	0.50	ROUNDED
	0.80	WELL ROUNDED

Fig. 8. Examples of classes of particle angularity

2 deg) in angle of deposition with an increase in specific gravity of 250 percent. This effect is relatively minor compared to other factors, especially since the variation in specific gravity among most common rocks is not large (e.g. 2.3 to 2.9, or about 25 percent variation). Simons and Lane<sup>28</sup> found that small-scale tests indicated no change in angle of deposition when the slope was completely submerged in water (equivalent to a decrease in specific gravity of about 40 percent). It is suggested, therefore, that the angles of repose and deposition will decrease but slightly, if at all, with increasing specific gravity of the particles.

#### Other characteristics

29. Mineral composition, hardness, soundness, and absorption of particles are indexes of the durability and weatherability of slopes. As these properties affect primarily the long-term stability of slopes, they will not be considered in this report.

#### Gradation

30. A uniform material contains particles of various sizes. The results of gradation analyses are presented by plotting the percentage of material finer than each sieve against the logarithm of the sieve opening, as shown in fig. 9. The particle size corresponding to a given percentage

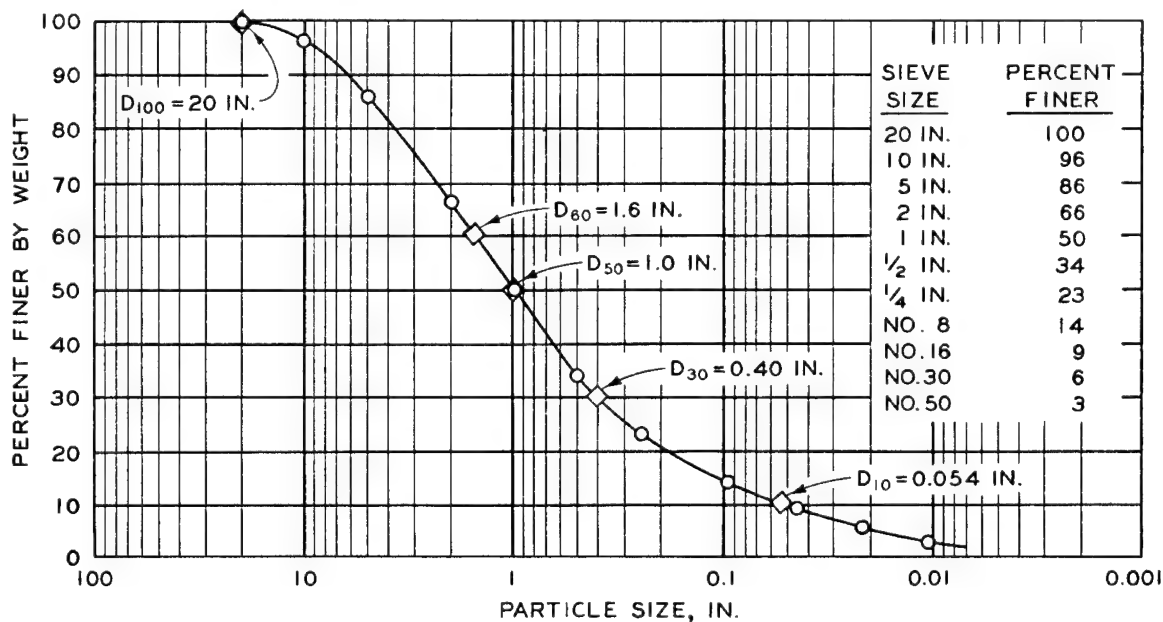


Fig. 9. Method of plotting particle-size (gradation) analysis

of the material can be found from the gradation curve, and several size percentages are considered meaningful. The average particle size  $D_{avg}$  (or  $D_{50}$ ) is the only value reported in some studies of cohesionless materials, though the gradation of the material cannot be defined by a single number, as illustrated in fig. 10. The effective particle size  $D_{10}$  was

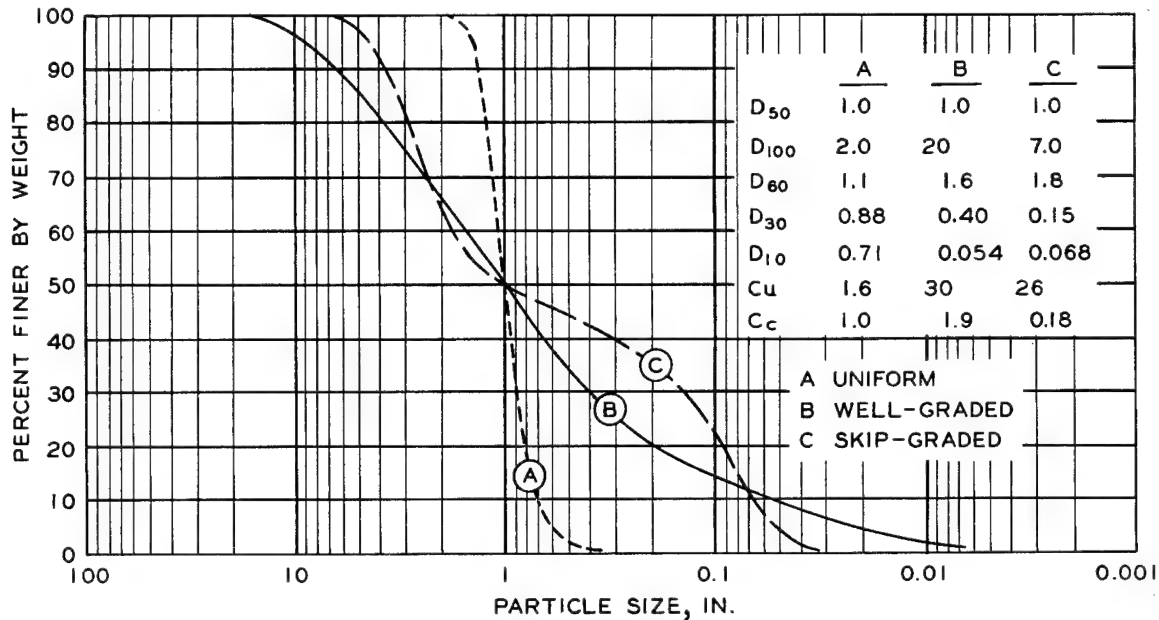


Fig. 10. Variation in gradations of materials having same average particle size

initially selected as an index of the permeability of filter sands,<sup>29</sup> as was the coefficient of uniformity  $C_u$  defined as

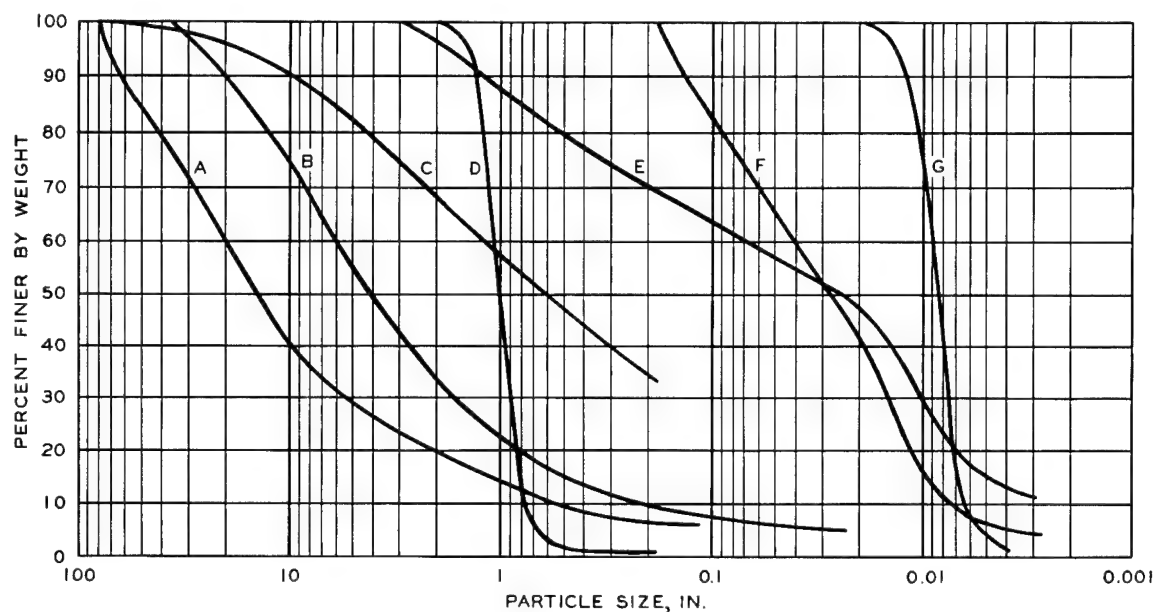
$$C_u = \frac{D_{60}}{D_{10}}$$

A complementary ratio is the coefficient of curvature  $C_c$  defined as

$$C_c = \frac{(D_{30})^2}{(D_{60})(D_{10})}$$

31. A material can be classed roughly as either uniform (poorly graded) when relatively few different particle sizes are present, or

graded when the material contains a wide range of different particle sizes. Graded materials, in turn, can be subdivided into well-graded when the material contains a wide variety of intermediate particle sizes, and skip-graded or gap-graded (also poorly graded) when there is a deficiency of intermediate particle sizes. More specific criteria for well-graded materials require that (a) the coefficient of curvature lie between 1 and 3, and (b) the coefficient of uniformity be greater than 6 for sands (0.003 to 0.2 in.\*) and greater than 4 for gravels (0.2 to 3 in.).<sup>8</sup> Gradation curves for several materials are shown in fig. 11.



CURVE	MATERIAL	D <sub>50</sub>	D <sub>100</sub>	D <sub>60</sub>	D <sub>30</sub>	D <sub>10</sub>	C <sub>u</sub>	C <sub>c</sub>
A	EJECTA OF DANNY BOY CRATER <sup>30</sup>	15	72	20	5.5	0.58	35	2.6
B	ROCKFILL OF DERBENDI KHAN DAM <sup>31</sup>	4.3	36	6.2	1.7	0.24	26	1.9
C	FALLBACK OF PRE-SCHOONER II CRATER <sup>32</sup>	0.63	75	1.2	0.15	0.020	60	0.90
D	CRUSHED LIMESTONE AGGREGATE <sup>28</sup>	1.0	2.0	1.1	0.90	0.78	1.4	0.94
E	FALLBACK OF SEDAN CRATER <sup>33</sup>	0.025	3.0	0.070	0.010	0.002	35	0.71
F	SAND OF PROJECT ZULU II <sup>34</sup>	0.028	0.19	0.042	0.015	0.0077	5.5	0.70
G	DUNE SAND OF LIBYAN DESERT <sup>35</sup>	0.0085	0.023	0.0090	0.0076	0.0064	1.4	1.0

Fig. 11. Examples of gradation curves

32. Widening the range of particle sizes in a material results in an increase in unit weight and number of particle-to-particle contacts in the material and, therefore, a larger angle of repose. As the average

\* A table of factors for converting British units of measurement to metric units is presented on page xiii.



particle size of a material increases, the range of particle sizes will widen as a rule, encouraging the presumption of a direct relation between average particle size and angle of repose. However, the most stable and dense arrangement results when the larger particles are in contact with one another and the smaller particles occupy the voids among the larger particles. If the smaller particles separated the larger ones at the points of contact, a less stable arrangement would exist, and the angle of repose would be smaller. This latter condition may develop in certain skip-graded materials or when the materials contain large proportions of fine particle sizes.

33. The effect of gradation on the angle of deposition may depend on the manner of deposition and the degree of segregation of particle sizes that may occur over the length of the slope. As each increment of the material being deposited moves down the slope, the larger particles can ride over the smaller particles and not be arrested until they reach even larger particles near the bottom of the slope. The smaller-than-average particles will be caught in interstices at the upper portion of the slope. This natural sorting of particle sizes, which is a function of the height of the slope and the manner of deposition, will tend to produce a concave slope. With widening gradation, the difference in inclination between the upper and lower portions of the slope should increase, and the average surface of the slope should become smoother as the smaller particles chink the spaces among the larger ones. Since these effects would tend to increase the velocity of particles moving on the upper portion of the slope, it is believed that the angle of deposition will decrease as gradation widens, whereas it was previously stated that the angle of repose will increase with widening gradation. This inference is offered only as a working hypothesis.

#### Characteristics of Aggregations of Particles

##### Relative density

34. The most important aggregate characteristic of a material is its structure, or interparticle geometry. Under static conditions (as would apply to the angle of repose), structure may be represented in part

by the closeness with which the particles fit against one another and the space between them. This fitting or denseness can be described<sup>29</sup> by:

(a) void ratio  $e$  , which is the ratio of the volume of void space among the particles to the volume of the particles or solids; (b) porosity  $n$  , which is the ratio (usually expressed as a percentage) of the volume of voids to the total volume (voids plus solids) of the material; and (c) unit weight  $\gamma$  , which is the weight of the material per unit of total volume. One other parameter closely related to the denseness of a material is the bulking factor  $BF$  , which is used to describe the increase in volume due to disturbance of the material, and particularly the increase in volume of the fallback and ejecta material of an explosion-formed crater over the volume of this material before the explosion.<sup>36</sup> The bulking factor is defined as the ratio of the original or preshot unit weight  $\gamma_o$  to the resulting postshot unit weight  $\gamma$  , or

$$BF = \frac{\gamma_o}{\gamma} = \frac{1 + e}{1 + e_o} = \frac{100 - n_o}{100 - n}$$

where the subscript  $o$  indicates, in each case, the original condition. Postshot void ratio can be computed as

$$e = (1 + e_o) BF - 1$$

and porosity as

$$n = 100 - \frac{100 - n_o}{BF}$$

or, if the material disturbed was originally a tightly jointed rock, so that

$$e_o \sim n_o \sim 0$$

then

$$e \sim BF - 1$$

and

$$n \sim \frac{BF - 1}{BF} \times 100$$

35. However, none of the above parameters can, by itself, indicate whether an aggregation of particles is in a loose or a dense condition. Rather, this determination must be expressed in terms of the range of possible density, that is, as a relative density. The relative density  $D_d$  is defined<sup>29</sup> as

$$D_d = \frac{e_{\max} - e}{e_{\max} - e_{\min}} \times 100$$

where  $e_{\max}$  is the void ratio of the material in the loosest state and  $e_{\min}$  the void ratio of the material in the densest state that can be attained by specified laboratory procedures.<sup>7</sup> However, it is usually more convenient to compute the relative density as

$$D_d = \frac{\gamma_{\max} (\gamma - \gamma_{\min})}{\gamma (\gamma_{\max} - \gamma_{\min})} \times 100$$

where  $\gamma_{\min}$  and  $\gamma_{\max}$  are, as above, the unit weights corresponding to the loosest and densest states, respectively. Thus, the relative density is zero percent when the material is as loose as possible and 100 percent when it is as dense as possible. The angle of repose will generally increase with increasing relative density.

#### Particle orientation

36. The orientation of one particle to another (extent of preferred orientation) and the orientation with respect to the slope (direction of preferred orientation) affect the angle of repose. A numerical description of particle orientation requires a statistical survey not unlike the survey of joints in nondisarranged rock masses.<sup>21</sup> Such a survey would be practicable for a mass of cohesionless material since a knowledge of the orientation of only those particles at or near the surface is required. The effect on the angle of repose of an increasing extent of preferred orientation depends on the direction of preferred orientation. An alignment

of flat or elongated particles parallel to the slope generally decreases the angle of repose whereas an alignment perpendicular to the slope increases this angle, as illustrated in fig. 4. The extent of preferred

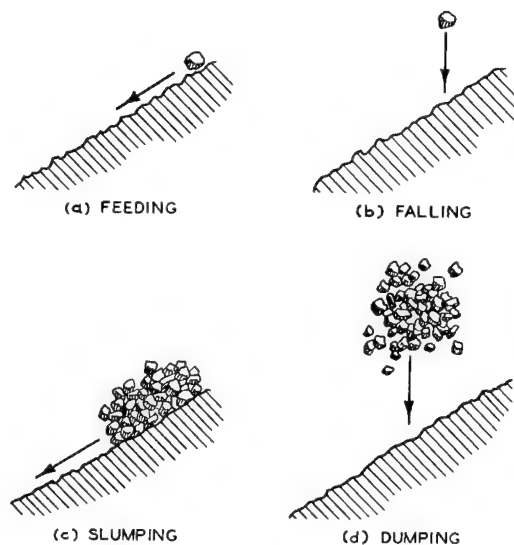


Fig. 12. Elemental methods of deposition

during a given time. Four methods of deposition, shown in fig. 12, illustrate the effects of these interrelated factors.

- a. Feeding. The material is either placed at the top of a slope or is dislodged from the surface so the particles trickle or spill down the slope at a low rate (for example, the construction of dumped rock-fill dams by truck haul).
- b. Falling. The material is allowed to fall freely onto a slope at a low rate (for example, stockpiling by means of conveyor belts, talus slope development).
- c. Slumping. A mass of material on a slope is set in motion either by removing lateral support from the mass or by tilting the slope so the material slides or spills down the slope at a high rate (for example, undercutting a stockpile or a riverbank, emptying a dump truck of small particles, many laboratory model tests of slopes of cohesionless materials).
- d. Dumping. A mass of material is dropped onto a slope at a high rate (for example, filling a truck from a hopper).

38. These methods and inferred characteristics of the material after deposition are described in table 2 in order of decreasing density of the deposited material. The methods are basic manners of deposition,

orientation increases with increasing relative density. Thus, if the direction of preferred orientation is unfavorable, an increase in relative density results in a decrease in the angle of repose.

#### Manner of deposition

37. In order to describe a manner of deposition, the initial velocity of the material, the direction of movement relative to the slope, and the rate of deposition must be considered. The rate of deposition is defined as the quantity of material reaching the slope

Table 2

Description of Elemental Methods of Deposition

<u>Method of Deposition</u>	<u>Manner of Deposition</u>		<u>Initial Direction</u>	<u>Mode of Particle Movement</u>	<u>Inferred Characteristics After Deposition</u>	
	<u>Rate of Deposition</u>	<u>Initial Velocity</u>			<u>Grading of Particles</u>	<u>Orientation of Particles*</u>
Falling	Low	High	Vertical	Rolling	Sorted	Parallel
Feeding	Low	Low	Inclined	Rolling	Sorted	Parallel
Dumping	High	High	Vertical	Sliding	Random	Random
Slumping	High	Low	Inclined	Sliding	Random	Random
						Densest
						Dense
						Loose
						Loosest

\* Relative to slope.

and actual cases may be more complex and involve features of more than one method. The main basis for inferring the characteristics of the material after deposition is that particles moving separately are free to roll or even bounce whereas those moving as masses are constrained to a predominantly sliding mode of movement. Thus, at a low rate of deposition, particles will tend to segregate down the slope according to size and will be free to assume a preferred orientation parallel to the slope.<sup>37</sup> Particles moving individually will seek positions of rest giving greater density and stability to the deposited material than would be in the case when inter-particle interference restricted their movement.<sup>6</sup> Finally, the higher the initial vertical velocity, the larger will be the dynamic compaction effort and, therefore, the greater will be the density, though this effect is not as strong as that of the rate of deposition.<sup>37,38</sup>

39. The shape of the particles influences these effects and plays a major role in the mechanics of deposition. The effect of particle shape can be illustrated by considering only two shapes, bulky and nonbulky, as representing particles that would tend to roll and those that would tend to slide, respectively, during deposition. When particles have the shape and freedom to permit rolling, the angle of deposition will be decreased. The tendency to roll will be increased by an increased initial velocity of each particle. However, a high rate of deposition will cause the particles to come to rest more quickly, thus increasing the angle of deposition. Therefore, the angle of deposition of bulky particles will be increased by higher rates or lower initial velocities. Since particle orientation is of minor importance for bulky particles, the angle of repose is directly related to the density of the deposited material. High rates of deposition or lower initial velocities would result in lower densities and, hence, in smaller angles of repose. These inverse relations are summarized as follows:

Bulky Particles		
<u>Method of</u> <u>Deposition</u>	<u>Angle of</u> <u>Deposition</u>	<u>Angle of</u> <u>Repose</u>
Falling	Smallest	Largest
Feeding	Small	Large
(Continued)		

Bulky Particles		
Method of Deposition	Angle of Deposition	Angle of Repose
Dumping	Large	Small
Slumping	Largest	Smallest

40. In the case of nonbulky particles, the extent of particle orientation parallel with the slope would be greater with lower initial velocities or lower rates of deposition, resulting in a smaller angle of deposition. The angle of repose in this case would be affected by particle orientation in the same manner as the angle of deposition, and the two angles would be directly related, as shown in the following tabulation:

Nonbulky Particles		
Method of Deposition	Angle of Deposition	Angle of Repose
Feeding	Smallest	Smallest
Falling	Small	Small
Slumping	Large	Large
Dumping	Largest	Largest

41. From the relation between the manner of deposition and the structure of the resulting deposit (fig. 13), the following tentative conclusions can be drawn. First, it appears that the rate of deposition should have a greater effect on both the angle of deposition and the angle of repose than the initial velocity of the material. However, this conclusion assumes that the material does not have a high initial horizontal velocity component. Second, it is believed that increasing the rate of deposition will increase both the angle of deposition and the angle of repose

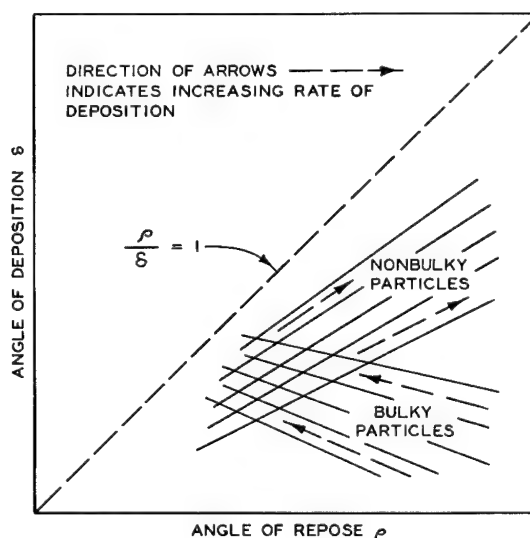


Fig. 13. Hypothesized relations between angle of repose and angle of deposition for various rates of deposition

for nonbulky (e.g. flat) particles. On the other hand, for bulky particles, the angle of deposition may approach the angle of repose as the rate increases, as illustrated schematically in fig. 13.

#### Water content

42. The final characteristic of aggregations of particles to be mentioned here is water content  $w$ , which is defined as the ratio (usually expressed as a percentage) of the weight of water in a mass of material to the weight of the dry particles. Even a trace of moisture (such as would be expected in an outdoor stockpile in a nonarid climate) can strongly increase the slope angle of a low mass of fine particles (for example, vertical slopes of limited height can be cut into a damp sand). The effect of a small amount of water in an otherwise cohesionless material is to give the material an apparent cohesion by forming menisci at interparticle contacts and increasing the pressure of these contacts by surface tension. Since the inclination of a slope on a material having some cohesion is not independent of its height, the term angle of repose has no meaning for a damp or moist mass of fine particles. Complete submergence of a slope will eliminate the apparent cohesion as will the complete drying of the material.

### Geometrical Characteristics of Slopes

#### Dimensions

43. Slopes are generally described in a two-dimensional cross section by a slope height  $H$  measured vertically from the crest to the toe and a slope angle  $\beta$  measured from the horizontal to the line connecting the crest and the toe, as shown in fig. 14. The slant height  $S$  of the slope is the length of the line connecting the crest and the toe, and is computed as

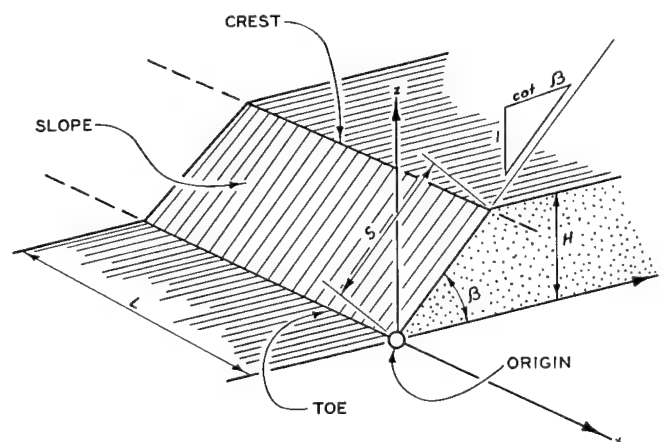


Fig. 14. Dimensions of slope linear in plan



$$S = \frac{H}{\sin \beta}$$

The slope length  $L$  is the horizontal extent of the slope measured perpendicularly to the cross section. To consider a slope stability problem in a two-dimensional analysis,  $L$  should be at least equal to  $2S$ . The inclination of a slope, expressed as the angle  $\beta$  in degrees, is termed the slope angle for the purposes of this study.

44. To obtain a valid measure of either the angle of repose or the angle of deposition, the slant height must be sufficiently great to permit a large number of particles to lie along the slope at any cross section; too small a slope height should increase the slope angle. A ratio of slant height to average particle size of at least 100 is recommended.

#### Curvature in plan

45. When a slope is curved in plan, as shown in fig. 15, the slope

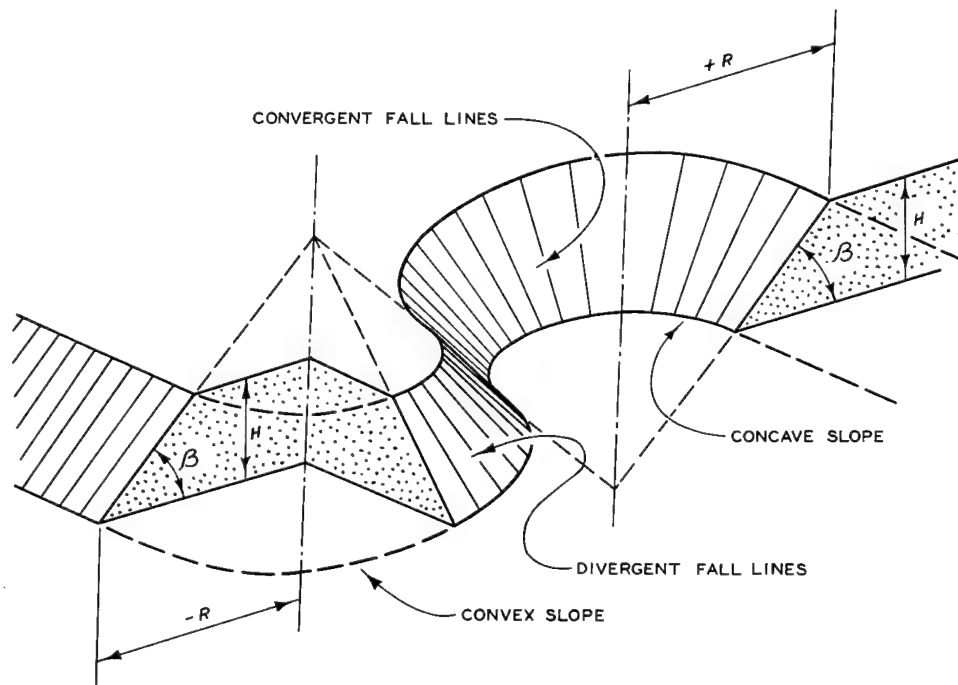


Fig. 15. Dimensions of slope curved in plan

radius  $R$  is measured in a horizontal plane at the level of maximum radius, that is, at the toe of a slope convex in plan and at the crest of a slope concave in plan. An index relating the radius to the height of the slope is the curvature factor  $J$ , defined as

$$J = \frac{H \sin \beta}{R}$$

which has an upper limit of

$$J < \frac{H}{R}$$

for the case of a vertical slope, that is, for a right circular cylinder, and a lower limit of

$$J > \frac{H}{R} \sin \arctan \frac{H}{R}$$

for a right circular cone. For a typical slope on a cohesionless material (e.g.  $\beta$  about 37 deg), the maximum height-to-radius ratio possible would be about 0.8 for a completely conical slope, so the curvature factor would never exceed 1/2. By giving an algebraic sign to the slope radius, as shown in fig. 15, the curvature factor becomes positive for a slope concave in plan and negative for a slope convex in plan. When the radius of a slope is more than about three times the height (or when  $J$  is less than 1/6 for a slope on cohesionless material), the slope can be considered linear for most practical purposes.

46. It would appear logical for the angle of repose to be larger for a concave slope in plan and to be smaller for a convex slope, as shown in fig. 15, due to the horizontal arching effect that would give more lateral support to each particle in a concave curvature and less to each particle in a convex one. Similarly, the angle of deposition might be larger for a concave slope, since the downwardly convergent fall lines (or lines of maximum inclination on the slope) would indicate an interparticle wedging that would aid in arresting the movement. A few tests by van Burkalow<sup>4</sup> showed that the angle of depositon is slightly larger for a concave slope and smaller for a convex slope than that measured from a linear slope identical in all other respects. However, a contrary relation might be observed in slopes having large curvature factors and relatively large central angles, where the deposited material converging down a concave slope would overfeed the lower portion of the slope and produce a small angle of deposition. In the case of a convex slope the material would

diverge and approach the angle of deposition for a linear slope.

47. The effect of curvature in plan may be especially pertinent to the difference between the shape of cross sections through craters produced by single explosions and those produced by linear rows of several explosions. The slopes of single craters are less plane in section than those of row craters of the same depth, and are much more rounded at the bottom. The steeper upper portion of a single crater may be due, in part, to the horizontal arching or wedging effect resulting from the concave areal curvature, and the convergence of fallback material during deposition in a single crater causes the flattening (rounding) of the lower portion.

#### Curvature in section

48. It is generally assumed in this report that slopes are planar in section and can, thus, be considered to have a single slope angle. This assumption is satisfactory in most cases since slopes tend to form on cohesionless materials with little curvature except at the crest and toe. In the case of the fallback slope in an explosion-produced crater, however, the curvature of the bottom represents a significant portion of the apparent crater surface and is important in the evaluation of the crater for engineering purposes. Therefore, a description of this curvature is

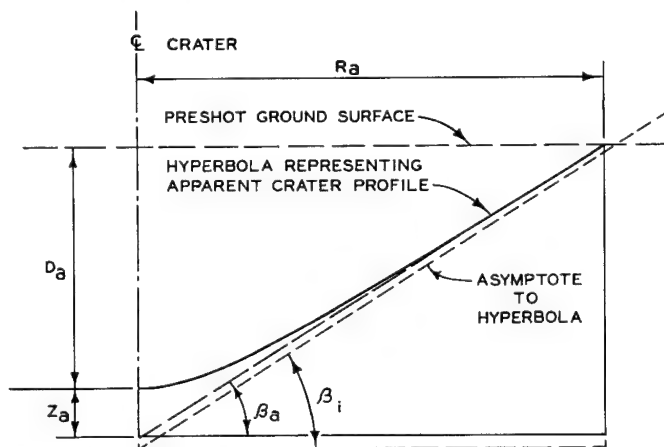


Fig. 16. Dimensions of hyperbolic representation of apparent, explosion-produced crater profile below preshot ground surface

needed, even though the curvature is not a factor affecting the slope angle.

49. As described in fig. 16, a fallback slope is considered to have an inclination  $\beta_a$  and to intersect the preshot ground surface at a distance  $R_a$  from the center line of the crater. The depth of the apparent crater surface below the preshot ground surface at the center line is  $D_a$ . One additional dimension is

required to describe the curvature:  $Z_a$ , which is the vertical distance between the bottom of the apparent crater and the intersection of the center line with an extension of the fallback slope at a constant angle  $\beta_a$ . That is,

$$Z_a = R_a \tan \beta_a - D_a$$

50. The overall shape of the apparent crater surface in section is often assumed (for prediction purposes) to be parabolic.<sup>39</sup> However, detailed analyses by Hughes, Benfer, and Foster<sup>40</sup> of the average cross sections of 20 medium to large craters have shown that a hyperbolic shape is a generally more satisfactory assumption. This approximation considers a hyperbola passing through two well-defined points: (a) the center line of the crater at the apparent crater depth and (b) the preshot ground surface at the apparent crater radius; the hyperbola is horizontal at the first point and inclined to the fallback slope angle at the second point. Thus, the profile of a crater can be computed, with the expressions given in fig. 16, from the values for three dimensions:  $R_a$ ,  $D_a$ , and  $\beta_a$ .

51. Helpful indexes of the apparent crater profile may be the ratios  $D_a/R_a$ , which is termed herein the profile shape ratio, and  $Z_a/D_a$ , which is termed the profile roundness ratio. The values for  $D_a$  and  $R_a$  are measurable.  $Z_a$ , which is the vertical distance between the bottom of the apparent crater and the intersection of the center line with an extension of the fallback slope at a constant angle,  $\beta_a$ , as shown in fig. 16, is computed as:

$$Z_a = R_a \tan \beta_a - D_a$$

Fig. 17 illustrates the variation in apparent crater profile with varying shape and roundness ratios.

#### Inclination of base

52. In the foregoing discussion of factors affecting slope angles, it is assumed that the material at the toe of a slope is fully supported against horizontal movement and that the material moves over similar

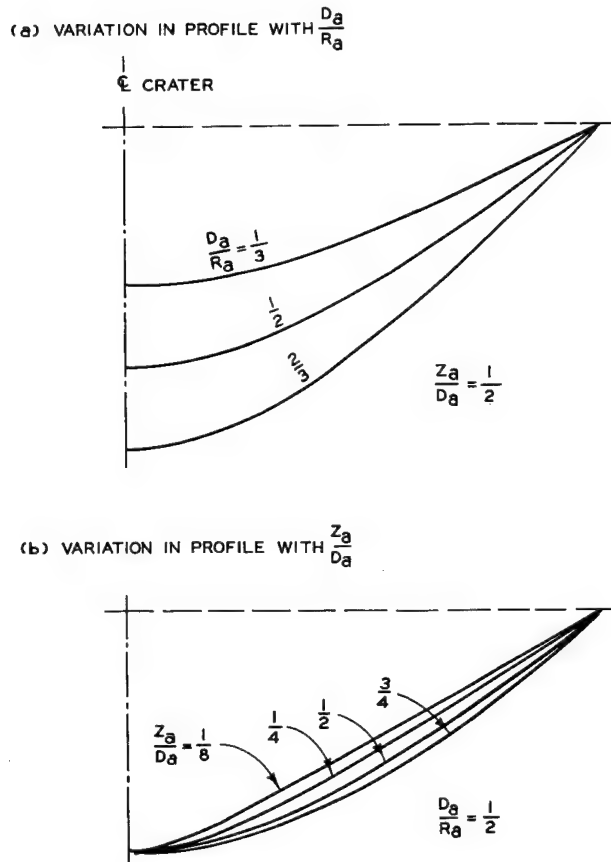


Fig. 17. Variation in apparent crater profile with shape and roundness ratios

material both during deposition and in the case of a failure. Although this assumption may not always be valid, model tests<sup>4,6</sup> have indicated that the inclination of the surface supporting a deposit of cohesionless material has no influence on the angle of deposition. Therefore, it is assumed in this report that angles of deposition and repose are affected only by characteristics of the deposited material and are independent of the base on which it is deposited.

#### PART IV: CONSIDERATIONS AFFECTING FACTORS OF SAFETY

53. Surface stability of cohesionless media<sup>12,41</sup> have been largely avoided in recent theoretical studies because: (a) difficulties have arisen in combining the concept of individual particle behavior, which involves sliding, rolling, etc., with that of mass particle behavior, which involves particle interaction; and (b) few of the factors affecting a slope angle can be expressed numerically. The stability of cohesionless media can be described in terms of the angle of static friction, the angle of sliding friction, the angle of internal friction, the angle of repose, and the angle of deposition. The following discussion considers the relation between a factor of safety and these various parameters.

##### Stability of Particles on Slopes

54. When a particle is at rest on a plane slope, as shown in fig. 18a, all forces acting on the particle are in balance and known.

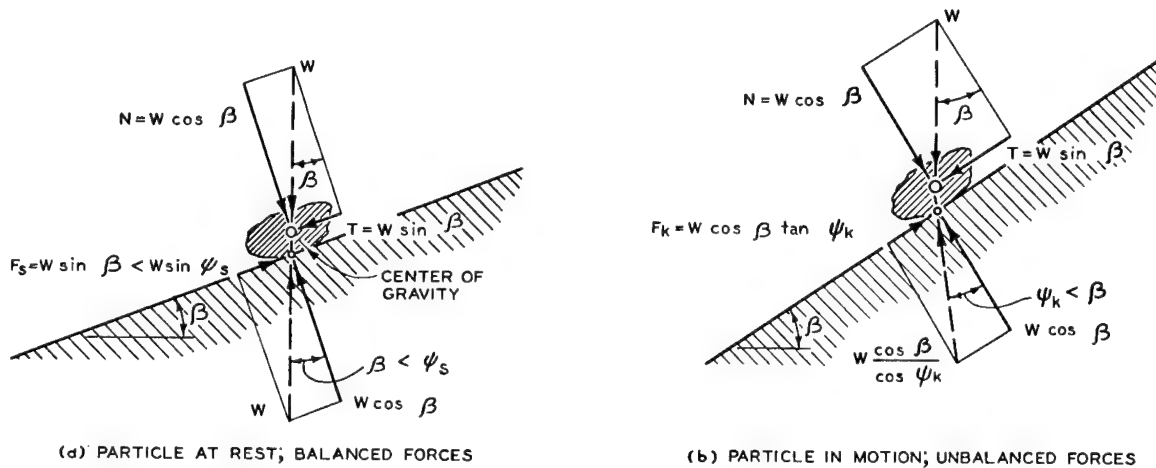


Fig. 18. Forces acting on particle

This state of equilibrium can be upset by increasing the inclination  $\beta$  of the slope until the particle either slides or overturns.

55. In the first condition (sliding), the tangential forces (forces parallel to the slope) become unbalanced and the particle slides. The particle weight  $W$  can be resolved into two components. The component

tangential to the slope is

$$T = W \sin \beta$$

and the component normal to the slope is

$$N = W \cos \beta$$

The maximum value that can be attained by the force due to static friction  $F_s$  is

$$F_s = N \tan \psi_s = W \cos \beta \tan \psi_s$$

where  $\psi_s$  is the angle of static friction and  $\tan \psi_s$  is the coefficient of static friction. Therefore, the particle will not slide so long as

$$T < F_s$$

or, expressing these forces in terms of particle weight and rearranging terms, as long as

$$\tan \beta < \tan \psi_s$$

the factor of safety FS against sliding is

$$FS = \frac{\tan \psi_s}{\tan \beta}$$

56. The second condition (overturning) occurs when the summation of moments about the center of gravity of the particle becomes unbalanced. As shown in fig. 19a, a particle will overturn if the line of action through the center of gravity is to the left of the pivot point. Assuming that the particle is a rectangular prism with rounded corners, the particle will not overturn so long as

A diagram showing a rectangular block of width  $b$  and thickness  $t$  resting on an inclined plane. The plane is at an angle  $\beta$  to the horizontal. The block's center is at a distance  $r_c$  from the bottom-left corner. The distance from the bottom-left corner to the point where the block's bottom edge meets the plane is  $\frac{t}{2} = r$ . The distance from the bottom-left corner to the point where the block's top edge meets the plane is  $\frac{b}{2} - r_c$ . The distance from the bottom-left corner to the point where the block's right edge meets the plane is  $\frac{t}{2} \tan \beta$ . The weight  $W$  acts vertically downwards from the center of the block.

The graph plots Slope Angle  $\beta$ , DEG (Y-axis, 0 to 90) against the ratio  $t/b$  (X-axis, 0 to 1.0). It shows curves for nonbulky particles and bulky particles with varying  $r_c/r$  ratios (0, 0.15, 0.25, 0.4, 0.6, 1.0). A vertical line at  $t/b = 0.33$  is labeled with the formula  $\tan \beta = \frac{b}{t} - \frac{r_c}{r}$ . The right side of the graph is divided into five regions: Angular, Subangular, Subrounded, Rounded, and Well-Rounded.

Fig. 19. Stability of particle on slope against overturning



$$\frac{t}{2} \tan \beta < \frac{b}{2} - r_c$$

or, rearranging terms, so long as

$$\tan \beta < \frac{b}{t} - \frac{r_c}{r}$$

where  $b/t$  and  $r_c/r$  are ratios classifying the shape and angularity of particles, respectively. Therefore, it is possible to relate the maximum possible slope inclination to the shape and angularity of this idealized particle, as shown in fig. 19b, with regard to overturning, not sliding. Under this assumption, the factor of safety against overturning is

$$FS = \frac{1 - \frac{t}{b} \left( \frac{r_c}{r} \right)}{\frac{t}{b} \tan \beta}$$

57. In the actual case of a cohesionless material, surface particles are supported by other particles; only particles much larger than average could be considered to be resting on a plane. One approach to analyzing the stability of interacting particles is to view the mass as a systematic stacking of spheres. Fig. 20 shows two slopes for each of a few possible stackings of uniformly sized spheres: a stable (steeper) slope and a hyperstable (flatter) one. The hyperstable slope in each case has one less sphere in each higher adjacent layer than the stable slope. The stable slope will not fail until it is tilted up to an angle of 90 deg (even for frictionless spheres, assuming the basal layer to be fixed in position), and no particle will move on the hyperstable slope until the slope angle is increased to 90 deg minus the difference between the stable and hyperstable slope angles. Such regular stackings were considered by Bustamante<sup>1</sup> to be too simplified for predicting slope angle, but helpful in understanding the extensive, progressive surface movements he observed on the slopes of his models. He noted that if any single particle were disturbed on a hyperstable slope, the remainder of the surface particles would not be affected, but the disturbance of any particle on the steeper stable slope would cause movement of the entire surface layer.

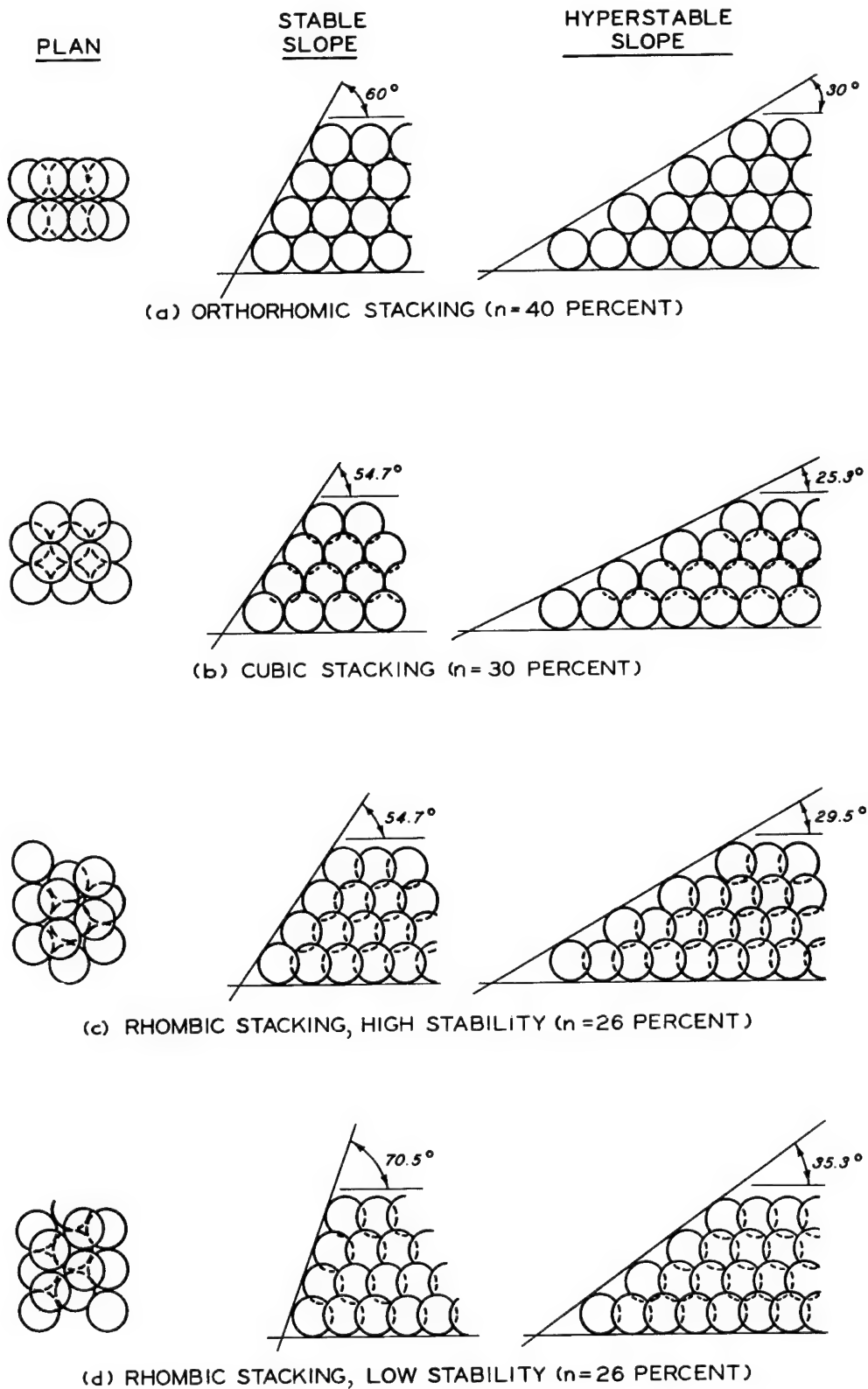


Fig. 20. Stable and hyperstable slopes formed by regular stacking of uniform spheres

58. The study of systematic stackings (or packings) of spheres, especially as randomness in sizes and stackings is introduced,<sup>12</sup> may contribute to the understanding of surficial stability. However, much progress is needed in this area before granular systems amenable to theoretical analysis that would meaningfully model the shape, angularity, and orientation of real particles of fragmented rock can be conceived.

### Movement of Particles on Slopes

#### Sliding

59. When a particle is sliding with nonuniform velocity on a plane slope, as shown in fig. 18b, the tangential forces acting on the particle are not balanced. The tangential component of the particle weight is, as in the case of a particle at rest,

$$T = W \sin \beta$$

but the force due to kinetic friction  $F_k$  is limited to a maximum of

$$F_k = N \tan \psi_k = W \cos \beta \tan \psi_k$$

where  $\psi_k$  is the angle of kinetic sliding friction and  $\tan \psi_k$  is the coefficient of kinetic sliding friction. Thus, the unbalanced force acting on the particle is

$$T - F_k = W \sin \beta \left( 1 - \frac{\tan \psi_k}{\tan \beta} \right)$$

and the particle will slide as long as

$$\tan \beta > \tan \psi_k$$

60. If the particle started from a position of rest, the kinetic energy  $E_k$  after the particle had descended the slope for a vertical distance  $z$  would be

$$E_k = Wz \left( 1 - \frac{\tan \psi_k}{\tan \beta} \right)$$

which is the product of the unbalanced force acting on the particle and the distance over which this force acts.<sup>42</sup> Since the total energy must remain constant, the loss of potential energy

$$E_p = Wz$$

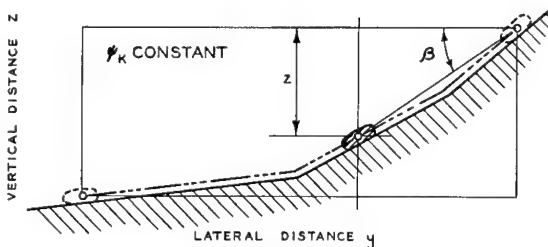
due to the decrease in elevation of the particle, must equal the sum of the gain in kinetic energy plus the energy wasted in overcoming friction, which is

$$E_f = Wz \frac{\tan \psi_k}{\tan \beta}$$

that is,

$$E_k = E_p - E_f$$

(a) PATH OF PARTICLE



The particle will slide as long as

$$E_k > 0$$

or as long as

$$E_p > E_f$$

(b) KINETIC ENERGY OF PARTICLE,  $E_k = Wz \left( 1 - \frac{\tan \psi_k}{\tan \beta} \right)$

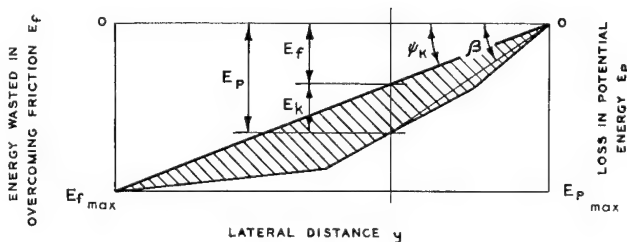


Fig. 21. Kinetic energy of particle sliding on a slope of constant coefficient of sliding friction

61. In fig. 21 are shown: (a) the path and (b) the kinetic energy of a particle sliding from an initial position of rest on a slope to a final position of rest. Several features illustrated in this figure are helpful in understanding the deposition of particles. If the angle

of kinetic sliding friction is constant over the length of the slope, the particle will move as long as

$$\tan \beta > \tan \psi_k$$

where  $\tan \beta$  is the inclination of a straight line from the position of the particle at any time to its initial position of rest. If the angle of kinetic sliding friction increases with distance down the slope (as might be the case where coarser particles had been previously deposited near the toe), the line of energy lost to friction would curve concave downward, intersecting the potential energy line earlier, as shown in fig. 22a. Such an increase in friction with distance could also arrest particles in motion on a slope that is not curved in section.

62. The coefficient of static friction of individual particles is always greater than the coefficient of kinetic sliding friction, or

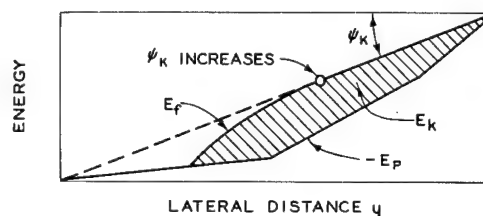
$$\tan \psi_s > \tan \psi_k$$

which suggests that the factor of safety against the resumption of sliding by a particle that has come to rest might be

$$FS = \frac{\tan \psi_s}{\tan \psi_k}$$

63. Several investigators have considered the relation between the angle of static friction developed by individual particles tending to slide against each other and the angles of repose and deposition. Laboratory tests by van Burkalow<sup>4</sup> were performed by placing 1- to 3-in. particles of traprock on an inclined planar slab of the same material. The results showed angles of static friction over 10 deg smaller than the angle of

(a) INCREASING COEFFICIENT OF SLIDING FRICTION



(b) CHANGING FROM SLIDING TO ROLLING

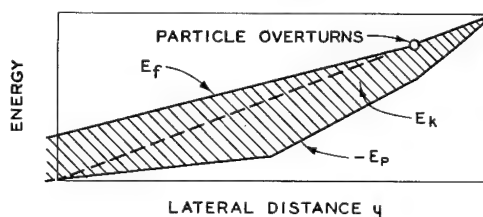


Fig. 22. Variation in kinetic energy due to change in coefficient of sliding friction

deposition of particles of the same material. Similar tests by Bustamante<sup>1</sup> showed that the angle of static friction between individual particles is smaller than either the angle of repose or the angle of deposition. On the other hand, Koons<sup>43</sup> concluded from field observations that the angle of static friction of particles on bare rock surfaces (averaging 35 deg) is always greater than the slope angle of the talus resting on such surfaces (averaging 32 deg); he verified the angle of static friction by means of laboratory tests.

64. A direct correlation of slope angles with angles of sliding friction was proposed by Melton.<sup>11</sup> From repeated laboratory tests of individual particles on an inclined slab of siliceous mica schist he found the angles of static and kinetic sliding friction to average about 34 and 28 deg, respectively. From numerous measurements of debris-covered non-colluvial slopes (the source of the particles tested) he found that the maximum inclination of such slopes is about 36 deg, whereas 28 deg is about the minimum inclination of a slope on which a dropped particle will roll. Based on these data, he hypothesized that the angle of repose (the maximum slope angle) is equal to the angle of static friction, and the angle of deposition (the maximum slope angle that precludes continued particle movement) is equal to the angle of kinetic sliding friction.

65. The most positive correlation of slope angles to angles of sliding friction was made by Metcalf<sup>6</sup> on the basis of laboratory tests. For several different crushed materials, and for angles ranging from 30 to 39 deg, he measured angles of deposition, which he found to be in close agreement with measured angles of kinetic sliding friction. His explanation for this correlation is that the movement of cohesionless materials on slopes occurs by aggregation rather than by individual particles. The movement of a mass of material will induce along the surface of movement a characteristic packing of the particles that allows sliding of one particle over another but not rolling. Thus, the mass of material moves as if it were a single particle on a plane surface.

#### Rolling

66. If a particle sliding on a slope overturns and moves by rolling, the gain in kinetic energy with vertical distance, as shown in fig. 22b,

will increase at a more rapid rate since the energy lost to rolling friction (which is zero for an incompressible sphere or cylinder on a plane surface) would be much less than that lost to sliding friction. A single particle dropped on a slope will roll unless the particle is exceptionally flat or bladed. Ritchie,<sup>44</sup> in his study of individually falling rock particles, found that particle movement changes easily from rolling to bouncing. Although particle movements of this type are of concern where loosening of individual particles from a slope may occur, the movement of an aggregation of particles, in which movement is constrained and confined close to the slope, is of more general interest. Particle interaction, in this case, will resist a rolling-bouncing mode of movement and result in a sliding-rolling mode of movement. Therefore, the rolling of individual particles is not considered pertinent to the purpose of this report.

#### Comparison of Slope Angles with Angles of Internal Friction

67. When a mass of cohesionless material is confined under pressure for a direct laboratory test, as illustrated in fig. 23a, deformation of the mass will induce shearing stresses. Continued deformation will cause a surface of sliding to form through the mass when the induced shear stress along that surface reaches a critical value, as shown in fig. 23b. The maximum shear (or tangential) stress  $\tau_f$  acting on the sliding surface is

$$\tau_f = \sigma \tan \phi$$

where  $\sigma$  is the normal stress acting on the surface,  $\phi$  is the angle of

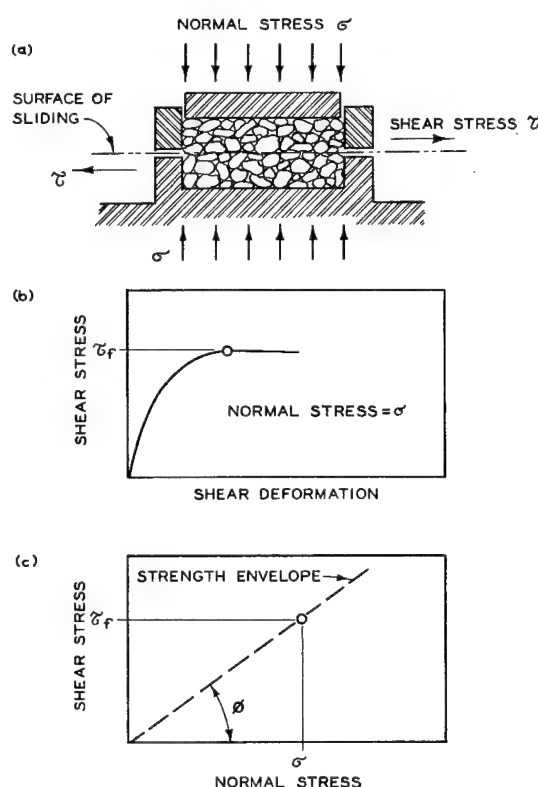


Fig. 23. Relation between normal and shear stresses in direct shear test

internal friction, and  $\tan \phi$  is the coefficient of internal friction. The relation between plotted values of maximum shear stress and normal stress, as shown in fig. 23c, is termed the strength envelope. By definition, a cohesionless material has a straight-line strength envelope that passes through the origin; that is, maximum shear stress is zero when normal stress is zero. Unlike the angle of sliding friction, the angle of internal friction expresses the behavior of an interacting aggregation of particles. The angle of internal friction, which increases with increased relative density of the aggregation<sup>12,13,16,27</sup> and with increased angularity and surface roughness of the particles,<sup>13,16,27,45</sup> is apparently independent of particle size.<sup>12,13,16</sup>

68. After the surface of sliding has developed and a maximum shear stress has been realized on this surface, the shear stress may decrease with continued deformation until it attains a constant or ultimate shear stress  $\tau_u$ , as shown in fig. 24a. The ratio of shear stress to normal

stress at this point is the ultimate coefficient of internal friction  $\tan \phi_u$ , where  $\phi_u$  is the ultimate angle of internal friction, as shown in fig. 24b. Whereas the angle of internal friction based on maximum shear stress can be considered to represent a static condition, the angle based on ultimate shear stress is somewhat kinematic since it reflects particle displacements and reorientations with movement. For a loose material the two angles are essentially the same, as shown in fig. 24; that is,

$$\tan \phi = \tan \phi_u$$

whereas for a dense material the maximum coefficient of internal friction is greater than the ultimate coefficient of internal friction, or

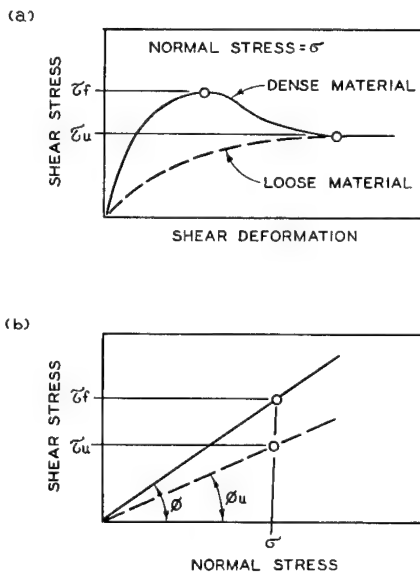


Fig. 24. Relation between maximum and ultimate angles of internal friction



$$\tan \phi > \tan \phi_u$$

which is similar to the relation between the coefficients of static and kinetic sliding friction.

69. When the factor of safety in slope stability analyses<sup>2,46,47</sup> is computed as

$$FS = \frac{\tan \phi}{\tan \beta}$$

the tacit assumption is made that the angle of repose equals the angle of internal friction. Some investigators<sup>15,17,48</sup> have emphasized the differences between these two angles, and this opinion stems mainly from the consideration of the constraint of internal particles compared with those at the surface. The strength envelope of a dense cohesionless material is typically curved concave downward;<sup>1,12,49</sup> consequently, the inclination of a straight line from the origin through the plotted maximum shear stress from each direct shear test (or tangent to the largest stress circle from each triaxial compression test) will decrease with increasing confining pressure, as shown in fig. 25 for the test results reported by Seed and Goodman.<sup>49</sup> This variable inclination is the maximum angle of stress obliquity<sup>47</sup>  $\phi_i$ , and is computed as

$$\phi_i = \arctan \frac{\tau_f}{\sigma}$$

for a direct shear test, and as

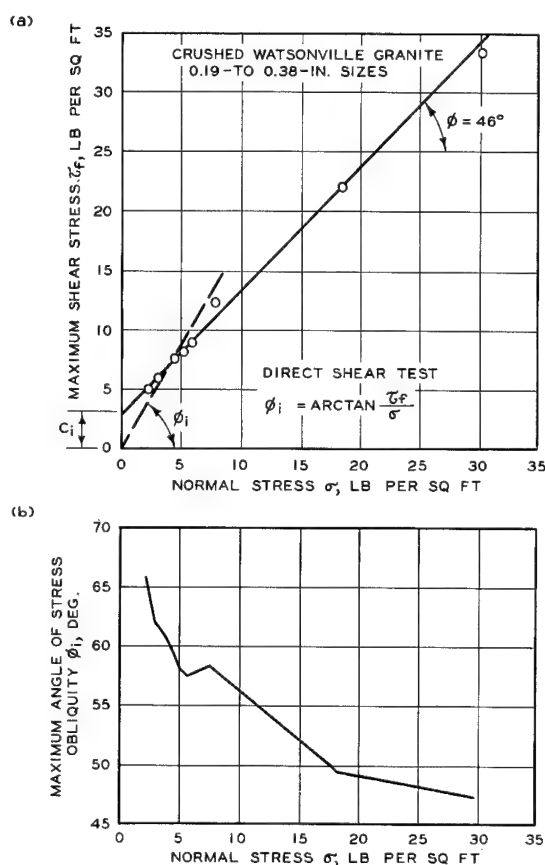
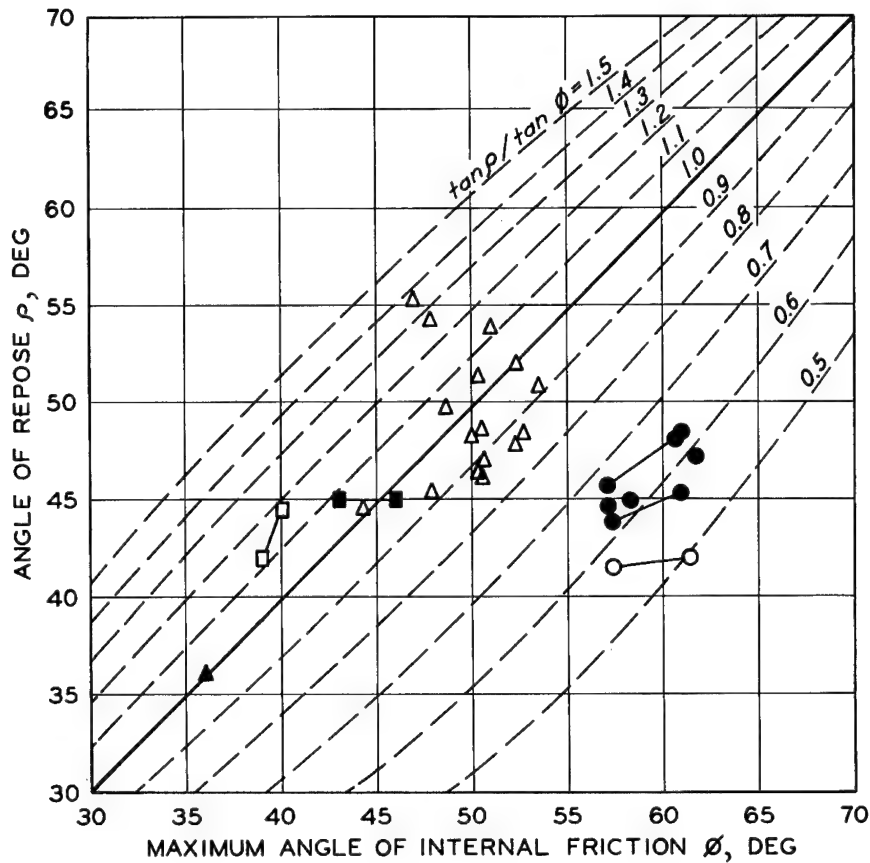


Fig. 25. Strength envelope of a cohesionless material reported by Seed and Goodman<sup>49</sup>

$$\phi_i = \arcsin \frac{\left(\frac{\sigma_1}{\sigma_3}\right)_f - 1}{\left(\frac{\sigma_1}{\sigma_3}\right)_f + 1}$$

for a triaxial compression test where  $(\sigma_1/\sigma_3)_f$  is the maximum ratio of the major principal stress  $\sigma_1$  and the minor principal stress  $\sigma_3$ . At extremely low confining pressures (near zero), the effect of particle interlocking can be quite significant. For example, if the test results reported by Seed and Goodman were interpreted on the basis of the best-fitted straight-line envelope, as shown in fig. 25a, the strength envelope would have a cohesion intercept  $c_i$  equivalent to the maximum shear stress mobilized by a normal stress essentially equal to the weight of a one-particle-thick layer of the material. On the other hand, if the maximum angle of internal friction were assumed to be equal to the maximum angle of stress obliquity, the angle of internal friction would exceed 60 deg under an equally low normal stress. Seed and Goodman have shown that the cohesion intercept due to interlocking is significant where surficial movement involves a layer several particle diameters thick.

70. Angles of repose for several materials are plotted in fig. 26 against the comparable angles of internal friction based on maximum shear stresses. The data from Bustamante<sup>1</sup> indicate angles of repose for sand as much as 15 deg smaller than the maximum angles of internal friction. On the other hand, some data from Morris<sup>27</sup> show angles of repose as much as 8 deg larger than the angles of internal friction. These data were determined by Morris using tilting-box tests and triaxial compression tests of 16 materials artificially fragmented and abraded to give a large variation in particle shape, angularity, and surface texture. However, every test specimen was prepared by the same vibratory compaction procedure. Thus, whereas the angle of repose increased continuously with increasing overall roughness and angularity of the particles, the angle of internal friction reached a maximum value and then decreased with further particle roughness. The decrease in angle of internal friction with increasing roughness is caused by an increase in porosity for a constant compaction



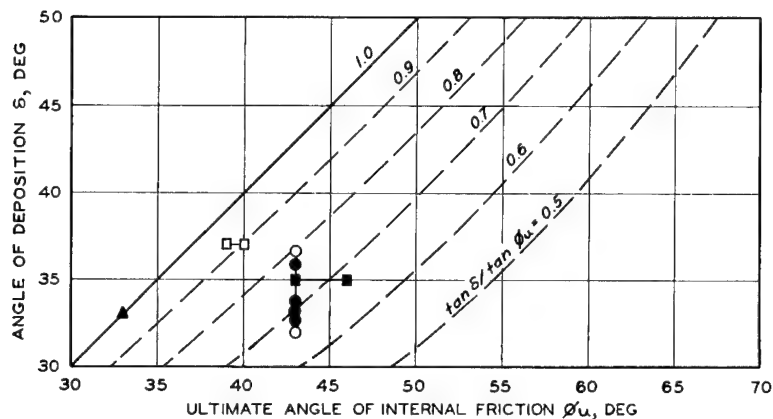
#### LEGEND

- SAND, TILTING MODEL EMBANKMENTS<sup>1</sup>
- SAND, TILTING-BOX TESTS<sup>1</sup>
- ▲ SAND, TILTING MODEL EMBANKMENTS<sup>50</sup>
- △ GRAVEL AND CRUSHED ROCK, TILTING-BOX TESTS<sup>27</sup>
- ROCKFILL, UNDERMINING EMBANKMENTS<sup>51</sup>
- RIVER GRAVEL, UNDERMINING STOCKPILES<sup>51</sup>

Fig. 26. Comparisons of angles of repose with maximum angles of internal friction

effort; this increase in porosity is due to the increased frictional resistance against the movement of particles relative to each other during compaction, a phenomenon reported by Vallergera, and others.<sup>13</sup>

71. In fig. 27 are plotted angles of deposition against the comparable angles of internal friction based on ultimate shear stresses. The angles of deposition are in no case larger than the ultimate angles of internal friction and are as much as 10 deg smaller. There are not enough



#### LEGEND

- SAND, FAILURE OF MODEL EMBANKMENT¹
- SAND, POURING ONTO PILE¹
- ▲ SAND, FAILURE OF MODEL EMBANKMENT⁵⁰
- ROCKFILL, END-DUMPING ONTO EMBANKMENT⁵¹
- RIVER GRAVEL, END DUMPING ONTO STOCKPILE⁵¹

Fig. 27. Comparisons of angles of deposition with ultimate angles of internal friction

data available to permit a comparison of the difference between the angles of repose and deposition with the difference between the maximum and ultimate angles of internal friction.

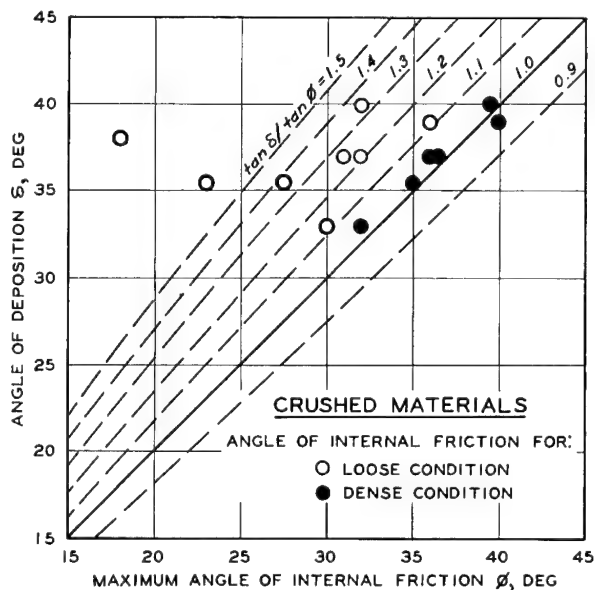


Fig. 28. Comparisons of angles of deposition with maximum angles of internal friction found in tests by Metcalf<sup>6</sup>

72. The single published investigation specifically intended to relate slope angle to angle of internal friction was conducted by Metcalf.<sup>6</sup> Metcalf found angles of deposition to be markedly and erratically larger than maximum angles of internal friction for material tested in an initially loose condition, but closely matching the angles of internal friction for material tested in an initially dense condition, as shown in fig. 28. These results are in direct contradiction and the view that the angle of repose (always larger than the

angle of deposition) is approximately equal to the angle of internal friction of the material in its loosest condition.

#### Comparison of Angle of Repose with Angle of Deposition

73. A useful relation between the angle of repose and the angle of deposition is the factor of safety against resumption of material movement. This can be expressed as the ratio of the tangent of the angle of repose to the tangent of the angle of deposition, that is,

$$FS = \frac{\tan \rho}{\tan \delta}$$

74. Plotted in fig. 29 are data comparing the angle of deposition to

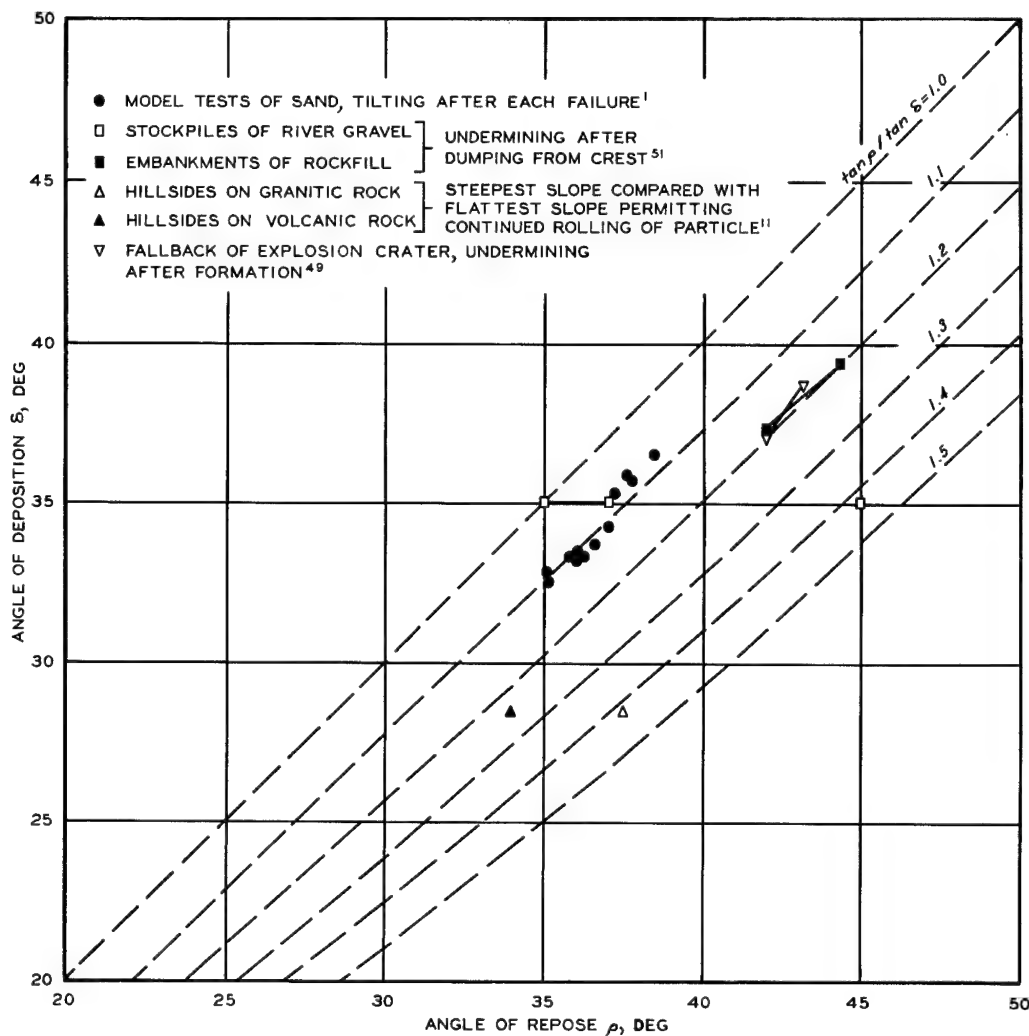


Fig. 29. Comparisons of angles of repose with angles of deposition

---

the angle of repose. The ratios of the tangents of the two angles approach 1.0 as a limit and do not exceed 1.5 in any case. The model tests of sand by Bustamante<sup>1</sup> gave ratios of about 1.1, and undermining the fallback slopes of the Pre-Schooner II crater<sup>32</sup> gave ratios of less than 1.2.

75. From the preceding considerations, it appears that the relation between the angle of repose and the angle of deposition is a better measure of the factor of safety of a cohesionless slope than the relation of either the angle of repose or angle of deposition to the angle of initial friction.

## PART V: EMPIRICAL DATA

76. Slopes formed on cohesionless materials in stockpiles, dumped rock-fill dams, and open-pit mines provide numerous opportunities for obtaining empirical data, and such observations are frequently reported in technical periodicals. Laboratory investigations and measurements of natural slopes also provide a valuable source of data concerning cohesionless slopes. Available data are reviewed in Appendix A. A considerable amount of information concerning cohesionless slopes has been developed in recent years in connection with cratering phenomenology in cohesionless media. This information is reviewed in Appendix B. The results of the surveys presented in Appendixes A and B are summarized below.

77. Summarizing the data contained in Appendixes A and B is handicapped by the variety of sources and the particular circumstances of slope formation or failure in each case. These varying circumstances require judgment in deciding whether the data refer to angles of repose or angles of deposition. Such judgment is especially needed in the case of excavating or undermining an existing slope since the resulting slope may be formed either mainly by the removal of material (tending to steepen the slope toward an angle of repose) or mainly by the redeposition of disturbed material. Most of the available data, however, refer to angles of deposition; measurements of slope angles that are clearly angles of repose are not available except for materials comprising relatively small-sized particles.

### Angles of Deposition

78. Laboratory measurements of angles of deposition by van Burkalow gave values ranging from 34 to 42 deg for slopes in material composed of angular, sand-sized (less than 0.2-in.) particles when existing piles were undermined. Angles as large as 50 deg were observed for material composed of larger (up to 0.75-in.) particles. Simons and Lane undermined stockpiles of sand, gravel, and crushed rock and found the resulting slope

angles varied from 29 to 39 deg for rounded particles and 32 to 42 deg for angular particles. Both rounded and angular gravel-sized (less than 2.5-in.) particles attained an angle of 40 deg when shoveled into piles by Rinkert,<sup>52</sup> whereas Bustamante poured sand onto a pile and found that the slope angle decreased from 37 to 32 deg as the pile grew. Metcalf measured angles of deposition between 30 and 40 deg for crushed, sand-sized particles in laboratory tests, with the average angle being 37 deg. Sand-sized particles deposited underwater were reported by Twenhofel<sup>53</sup> to form slopes ranging from 33 to 43 deg. Allen's<sup>54</sup> experiments showed that well-rounded sand deposited by flowing water could form a slope as steep as 38 deg. Wind-deposited sand dunes have lee slopes inclined at 30 to 34 deg.

79. Davis<sup>55</sup> found slopes on iron ore stockpiles varied in inclination from 34 to 45 deg, whereas other observations of piles of ore and mining wastes indicated slope angles ranging from 33 to 37 deg. Although slopes on dumped rock-fill dams vary between 36 and 40 deg for angular particles, they may be as flat as 30 deg for rounded particles. Blasted copper ore in open-pit mines formed slopes varying between 32 and 45 deg in inclination, with an average slope angle of 37 deg. Slope angles from handbooks and construction codes vary between 20 and 48 deg, averaging 38 deg. Both Behre<sup>56</sup> and Sharpe<sup>57</sup> gave a range in slope angle for taluses from 26 to 35 deg as a rule, with some as large as 36 deg and a very small number as large as 42 deg. Taluses formed beneath cliffs were found by Koons to have slopes with angles between 24 and 34 deg, whereas those around Buckboard Mesa in Nevada averaged 32 deg, with none steeper than 40 deg. Miner<sup>58</sup> measured slope angles of 38 to 40 deg on taluses composed of unusually angular and elongated particles. Melton suggested that bulky particles in motion on a slope would not be arrested unless the slope angle was smaller than 28 deg.

80. Angles of deposition for materials launched into motion by slope failures have been measured in laboratory studies. Tan found such angles ranged from 27 to 33 deg for both sand and gravel (up to 0.75 in. in size) and were inversely related to the inclination of the slope prior to failure. This relation was also observed by Bustamante for sand, with angles of 33 to 35 deg being reported. Slope failures of sand underwater



resulted in slope angles averaging 32 deg in the tests by Allen.

81. Fallback slope angles of explosion-produced craters may be affected by the depth of burst in some materials and are maximal at the optimum depth of burst. Fallback slope angles are also affected by the bulking factor of the fallback materials and by slope failures that may occur during crater formation. For near-optimum depths of burst, fallback slope angles were found to vary from 34 to 42 deg for desert alluvium and 31 to 37 deg for basalt, with the average of all angles being about 36 deg. A single cratering experiment in rhyolite produced a fallback slope angle of 38 deg. Row craters tend to have slightly flatter fallback slopes than single craters, and the slopes tend to be more planar in section.

82. The overall range of angles of deposition given above is not large, despite the wide variety of materials and manners of deposition. Excluding the extreme values found in handbooks, the angles vary between 24 and 50 deg, though a range of 27 to 42 deg is suggested as being more representative. Also, a very strong mode of 37 deg for angular particles can be seen. Fallback slope angles averaging about 36 deg appear to correlate well with the other values reported, considering the difference in manner of deposition.

#### Angles of Repose

83. Model embankments of sand and of gravel were tilted by Tan to slope angles ranging from 36 to 42 deg before failure, with the larger angles for the larger-sized particles. Bustamante tilted similar models of sand to angles of 45 to 47 deg when the material was dense, but the maximum slope angle did not exceed 36 deg once the material became loosened by slope failures. This sand was also tested by Bustamante in a tilting box, and the angle of repose was found to average 42 deg. Morris measured angles of repose between 44 and 55 deg for dense materials in tilting-box tests involving very angular and rough-textured particles.

84. Stockpiles of river gravel and angular rock fill were excavated to form slopes between 42 and 45 deg, according to Jones. Slopes on compacted rock-fill dams can be as steep as 45 deg. Nitchiporovitch<sup>59</sup> reported

slope angles ranging from 36 to 47 deg resulting from the undermining of piles of gravel and crushed rock. Debris-covered hillsides in an arid region were found by Melton never to be steeper than 34 deg for volcanic rock and 38 deg for granitic rock.

85. The fallback slope of one explosion-produced crater (Pre-Schooner II) was steepened by undermining to an inclination of about 43 deg from an initial slope angle of 38 deg.

86. These values of angles of repose vary between 34 and 47 deg if the data reported by Morris are excluded as being inapplicable to materials deposited by common methods. Where comparative angles of repose and deposition were given, the ratio of the tangents of the two angles was found not to exceed 1:5; the smallest ratio was about 1:1. For the Pre-Schooner II crater, the ratio of the tangents of the two angles was about 1:2.

## PART VI: CONCLUSIONS

87. There appear to be no theoretical bases yet available for predicting the initial inclination of the slope formed by the deposition of a given cohesionless material. Similarly, there are insufficient empirical data available to establish general relations between angles of deposition and the characteristics of materials. Nevertheless, some consistencies and trends among the data examined for this study suggest that reasonable estimates are possible of both the initial slope inclination and the factor of safety against the resumption of surficial movement by the deposited material.

88. An essential consideration with regard to slopes formed by the deposition of cohesionless material is the distinction between an angle of deposition, representing the cessation of particle movement, and an angle of repose, representing the resumption of particle movement; these conditions of slope formation and slope failure are often confused as being a single angle of repose. The ratio of the tangents of these two angles is a representation of the factor of safety of a slope formed by deposition. Based on the available data and hypotheses, the following conclusions are believed to be tenable:

- a. The angle of deposition is mainly a function of the gradation, shape, and angularity of the particles and the manner of deposition; it may be related to the angle of kinetic sliding friction between particles. Angles can range between 22 and 42 deg except in cases of unusual methods of deposition, and are generally 32 to 42 deg for angular particles, with angles of 34 to 37 deg to be expected in most cases.
- b. The angle of repose is mainly a function of the gradation, shape, and angularity of the particles and the structure (relative density and particle orientation) of the material. It is always larger than the angle of deposition of the same material. Angles can range between 27 and 47 deg except where a material has an unusual structure, and are generally 37 to 47 deg for angular particles.
- c. The factor of safety of a slope formed by deposition is mainly a function of the manner of deposition. Values probably range from about 1.1 to no more than 1.5 for the common methods of deposition.

---

89. The conclusions mentioned on the previous page are believed applicable to fallback slopes in explosion-produced craters. However, the volume and areal distribution of the redeposited material appear to be major factors, perhaps even more important than the characteristics of the individual particles. Thus, the fallback slope angles should be affected by both the type of material cratered (as this affects the release of explosive energy) and the geometry of the explosion (number and spacing of charges and depth of burst). Craters produced in rock by explosions near optimum depth of burst may have slope angles no larger than 38 deg and no smaller than 30 deg, and possibly no smaller than 34 deg for row craters. In such a material, the initial factor of safety against further movement of particles may lie between 1.1 and 1.5.

# LITERATURE CITED

1. Bustamante, J. I., Dynamic Behavior of Non-Cohesive Embankment Models. Ph. D. Thesis, University of Illinois, Urbana, Ill., 1964.
2. Jumikis, A. R., Mechanics of Soils: Fundamentals for Advanced Study. D. Van Nostrand, Princeton, N. J., 1964.
3. Terzaghi, Karl, "General wedge theory of earth pressure." Transactions, American Society of Civil Engineers, vol 106 (1941), pp 68-97.
4. van Burkalow, Anastasia, "Angle of repose and angle of sliding friction: an experimental study." Geological Society of America Bulletin, vol 56, No. 6 (June 1945), pp 669-708.
5. Field, J. E., discussion of "The design of rock-fill dams," by J. D. Galloway. Transactions, American Society of Civil Engineers, vol 104 (1939), pp 45-47.
6. Metcalf, J. R., "Angle of repose and internal friction." International Journal of Rock Mechanics and Mining Science, vol 3, No. 2 (May 1966), pp 155-161.
7. Department of the Army, Engineering and Design: Laboratory Soils Testing. Engineer Manual 1110-2-1906, Washington, D. C., 10 May 1965.
8. U. S. Bureau of Reclamation, Earth Manual. 1st ed., revised reprint, Denver, Colo., 1963.
9. Lane, E. W., "Design of stable channels." Transactions, American Society of Civil Engineers, vol 120 (1955), pp 1234-1260.
10. Simons, D. B., and Albertson, M. L., "Uniform water conveyance channels in alluvial material." Transactions, American Society of Civil Engineers, vol 128, Part I (1963), pp 65-107.
11. Melton, M. A., "Debris-covered hillslopes of the southern Arizona desert, consideration of their stability and sediment contribution." Journal of Geology, vol 73, No. 5 (September 1965), pp 715-729.
12. Farouki, O. T., and Winterkorn, H. F., "Mechanical properties of granular systems," in Mechanical and Physico-Chemical Properties of Soils. Highway Research Record No. 52, Highway Research Board, National Academy of Science - National Research Council, Washington, D. C., 1964, pp 10-58.
13. Vallergera, B. A., and others, "Effect of shape, size, and surface roughness of aggregate particles on the strength of granular materials." Symposium on Road and Paving Materials, STP 212, American Society for Testing Materials, Philadelphia, Pa. (1957), pp 63-74.
14. Wilson, S. D., "Application of soil mechanics to stability of open pit mines." Colorado School of Mines Quarterly, vol 54, No. 3 (July 1959), pp 93-113.

15. Lewis, J. G., "Shear strength of rockfill." Proceedings, Second Australia-New Zealand Conference on Soil Mechanics and Foundation Engineering, Christchurch, N. Z. (1956), pp 50-51.
16. Mackey, R. D., "The shearing resistance of granular soils." Civil Engineering and Public Works Review, vol 59, No. 698, London (September 1964), pp 1085, 1087, and 1089.
17. Taylor, J. N., "Selected design aspects of Burrendong Dam." Proceedings, Third Australia-New Zealand Conference on Soil Mechanics and Foundation Engineering, Sydney, Australia (1960), pp 121-129.
18. Kirkpatrick, W. M., "Effects of grain size and grading on the shearing behavior of granular materials." Proceedings, Sixth International Conference on Soil Mechanics and Foundation Engineering, Montreal, vol 1 (1965), pp 273-277.
19. Huang, E. Y., "A test for evaluating the geometric characteristics of coarse aggregate particles." American Society for Testing and Materials, Proceedings, vol 62 (1962), pp 1223-1242.
20. Krumbein, W. C., and Pettijohn, F. J., Manual of Sedimentary Petrography. D. Appleton-Century Co., Inc., New York, N. Y., 1938.
21. Krumbein, W. C., and Sloss, L. L., Stratigraphy and Sedimentation. 2d ed., W. H. Freeman and Co., Publishers, San Francisco, Calif., 1963.
22. Mackey, R. D., "The measurement of particle shape." Civil Engineering and Public Works Review, vol 60, No. 703, London (February 1965), pp 211-214.
23. Marsal, R. J., "Contact forces in soils and rockfill materials." Proceedings, Second Panamerican Conference on Soil Mechanics and Foundation Engineering, Sao Paulo, Brazil, vol II (1963), pp 67-98.
24. Pettijohn, F. F., Sedimentary Rocks. 2d ed., Harper & Brothers, New York, N. Y., 1957.
25. U. S. Army Engineer Waterways Experiment Station, CE, "CRD-C 119-53: Method of test for flat and elongated particles in coarse aggregates." Handbook for Concrete and Cement, with quarterly supplements (Vicksburg, Miss., August 1949).
26. State of California, Department of Public Works, Division of Highways, Bank and Shore Protection in California Highway Practice. Sacramento, Calif., November 1960.
27. Morris, C. H., "Effect of particle shape and texture on the strength of noncohesive aggregates." Papers on Soils, 1959 Meetings, STP 254, American Society for Testing Materials, Philadelphia, Pa. (1960), pp 350-363.
28. Simons, D. B., and Lane, E. W., Angle of Repose of Non-Cohesive Materials. Unpublished research report, Colorado State University, Fort Collins, Colo., 1956.

29. Terzaghi, Karl, and Peck, R. B., Soil Mechanics in Engineering Practice. John Wiley & Sons, Inc., New York, N. Y., 1948.
30. Nugent, R. C., and Banks, D. C., Project Danny Boy: Engineering-Geologic Investigations. PNE 5005, U. S. Army Engineer Nuclear Cratering Group, CE, Livermore, Calif., November 1966.
31. Blanc, G. J., "The Derbendi Khan project." Water Power, vol 15, Nos. 10 and 11 (October-November 1963), pp 423-431 and 447-456.
32. Frandsen, A. D., Project Pre-Schooner II: Postshot Geologic and Engineering Properties Investigations. PNE 516, U. S. Army Engineer Nuclear Cratering Group, CE, Livermore, Calif. (In preparation.)
33. Strohm, W. E., Jr., Ferguson, J. S., Jr., and Krinitzsky, E. L., Project Sedan: Stability of Crater Slopes. Miscellaneous Paper No. 3-662, U. S. Army Engineer Waterways Experiment Station, CE, Vicksburg, Miss., July 1964.
34. Benfer, R. H., and others, Project Zulu II: Phase I Summary Report. U. S. Army Engineer Nuclear Cratering Group, CE, Livermore, Calif. (In preparation.)
35. Bagnold, R. A., Physics of Blown Sand and Desert Dunes. Methuen, London, 1941.
36. Frandsen, A. D., Post-Shot Field Investigations, Buckboard Mesa, Nevada Test Site. NCG Technical Memorandum 65-4, U. S. Army Engineer Nuclear Cratering Group, CE, Livermore, Calif., 9 August 1965.
37. Whitman, R. V., Getzler, Zvi, and Hoeg, Kaare, The Response of Soils to Dynamic Loadings: Static Tests upon Thin Domes Buried in Sand. Report 12, Massachusetts Institute of Technology, Cambridge, Mass., also Contract Report 3-26, U. S. Army Engineer Waterways Experiment Station, CE, Vicksburg, Miss., December 1962.
38. Kolbuszewski, J. J., "An experimental study of the maximum and minimum porosities of sand." Proceedings, Second International Conference on Soil Mechanics and Foundation Engineering, Rotterdam, vol 1 (1948), pp 158-165.
39. U. S. Army Engineer Waterways Experiment Station, CE, Method for Predicting the Shape of Explosion-Produced Craters, by J. N. Strange, and A. J. Hendron, Jr. Miscellaneous Paper 1-677, Vicksburg, Miss., October 1964.
40. Hughes, B. C., Benfer, R. H., and Foster, F. H., Study of the Shape and Slope of Explosion-Produced Craters. NCG Technical Memorandum No. 65-8, U. S. Army Engineer Nuclear Cratering Group, CE, Livermore, Calif., November 1965.
41. Deresiewicz, H., "Mechanics of granular matter," in H. L. Dryden and Th. von Karman, ed., Advances in Applied Mechanics, vol V. Academic Press (New York, N. Y., 1958), pp 233-306.
42. Langhaar, H. L., and Boresi, A. P., Engineering Mechanics. McGraw-Hill Book Co., Inc., New York, N. Y., 1959.

43. Koons, Donaldson, "Cliff retreat in the southwestern United States." American Journal of Science, vol 253, No. 1 (January 1955), pp 44-52.
44. Ritchie, A. M., "Evaluation of rockfall and its control," in Stability of Rock Slopes. Highway Research Record No. 17, Highway Research Board, National Academy of Science - National Research Council, Washington, D. C., 1963, pp 13-28.
45. Huang, E. Y., and others, "Effect of geometric characteristics of coarse aggregates on strength of soil-aggregate mixtures." American Society for Testing and Materials, Proceedings, vol 64 (1964), pp 922-933.
46. Knappen, T. T., and Lowe, John, III, "Earth dams," in C. V. Davis, ed., Handbook of Applied Hydraulics, 2d ed., Section 5. McGraw-Hill Book Co., Inc. (New York, N. Y., 1952), pp 149-206.
47. Taylor, D. W., Fundamentals of Soil Mechanics. John Wiley & Sons, Inc., New York, N. Y., 1948.
48. Bishop, A. W., "The strength of soils as engineering materials." Geotechnique, vol 16, No. 2 (June 1966), pp 91-128.
49. Seed, H. B., and Goodman, R. E., "Earthquake stability of slopes of cohesionless soils." Proceedings, American Society of Civil Engineers, vol 90, No. SM6, Paper 4128 (November 1964), pp 43-73.
50. Tan Ek-Khoo, "Stability of soil slopes." Proceedings, American Society of Civil Engineers, vol 73, No. 1 (January 1947), pp 19-38.
51. Jones, O. T., "Design of Benmore earth dam." New Zealand Engineering, vol 20, No. 1 (January 1965), pp 13-24.
52. Rinkert, Arme, "Measurements of the pressures of filling materials against walls; earth pressure from friction soils." Proceedings, Swedish Geotechnical Institute, No. 17, Stockholm (1959), pp 3-46.
53. Twenhofel, W. H., Principles of Sedimentation. McGraw-Hill Book Co., Inc., New York, N. Y., 1939.
54. Allen, J. R. L., "Sedimentation to lee of small underwater sand waves: an experimental study." Journal of Geology, vol 73, No. 1 (January 1965), pp 95-116.
55. Davis, E. H., "An investigation for an iron ore storage area." Proceedings, Third Australia-New Zealand Conference on Soil Mechanics and Foundation Engineering, Sidney, Australia (1960), pp 155-160.
56. Behre, C. H., Jr., "Talus behavior above timber in the Rocky Mountains." Journal of Geology, vol 41, No. 6 (August-September 1933), pp 622-635.
57. Sharpe, C. F. S., Landslides and Related Phenomena. Columbia University Press, New York, N. Y., 1938.
58. Miner, N. A., "Talus slopes of the Gaspé Peninsula." Science, vol 79, No. 2045 (9 March 1934), pp 229-230.



59. Nitchiporovitch, A. A., "Deformations and stability of rockfill dams." Transactions, Eighth International Congress on Large Dams, Edinburgh, vol III (1964), pp 879-894.
60. Bening, R. G., and Larner, K. L., Phenomenology of the Formation of a Crater by Detonation of a One Pound Charge Buried at a Depth of Burst of Two Feet in the Zulu II Moist Sand. NCG Technical Memorandum 66-5, U. S. Army Engineer Nuclear Cratering Group, CE, Livermore, Calif., 26 February 1966.
61. Banks, D. C., and Saucier, R. T., Engineering Geology of Buckboard Mesa, Nevada Test Site. PNE 5001P, U. S. Army Engineer Waterways Experiment Station, CE, Vicksburg, Miss., July 1964.
62. Ash, R. L., "The mechanics of rock breakage; material properties, powder factor, blasting cost." Pit and Quarry, vol 56, No. 5 (November 1963), pp 109-111 and 114-118.
63. Bishop, R. H., and others, Project Stagecoach: 20-ton HE Cratering Experiments in Desert Alluvium, Final Report. SC-4596 (RR), Sandia Corporation, Sandia Base, Albuquerque, N. Mex., May 1962.
64. The Council for Codes of Practice, British Standards Institution, Earthworks. CP 2003, London, 1959.
65. Bogert, C. L., "Earth excavation," in Robert Peele, ed., Mining Engineers' Handbook, 3d ed., vol 1, Section 3. John Wiley & Sons, Inc. (New York, N. Y., 1948).
66. Boyle, J. C., and Barrows, W. R., "Rockfill dams: Lemolo No. 1 Dam." Transactions, American Society of Civil Engineers, vol 125, Part II (1960), pp 322-335.
67. Cates, L. S., "Factors affecting bank slopes in steam-shovel operations." Transactions, American Institute of Mining and Metallurgical Engineers, vol 74 (1925-1926), pp 818-825.
68. Carnegie-Illinois Steel Corporation, USS Steel Sheet Piling. Pittsburgh, Pa., 1931.
69. Compton, J. R., and Steinriede, W. B., Jr., Visit to Western Open-Pit Mines, 18-28 April 1966. Unnumbered memorandum, U. S. Army Engineer Waterways Experiment Station, CE, Vicksburg, Miss., 24 May 1966.
70. Davis, C. V., "Rockfill dams: The Derbendi Khan Dam." Transactions, American Society of Civil Engineers, vol 125, Part II (1960), pp 635-653.
71. Mathews, C. W., "Hints and helps." Rock Products Mining and Processing, vol 67, No. 6 (June 1964), p 56.
72. MacDonald, D. F., Some Engineering Problems of the Panama Canal in Their Relation to Geology and Topography. Bulletin 86, U. S. Bureau of Mines, Washington, D. C., 1915.
73. May, R. F., "Predicting outcrops of spoil banks." Mining Congress Journal, vol 50, No. 4 (April 1964), pp 104-105.

74. Galloway, J. D., "The design of rock-fill dams." Transactions, American Society of Civil Engineers, vol 104 (1939), pp 1-24.
75. Sherard, J. L., and others, Earth and Earth-Rock Dams. John Wiley & Sons, Inc., New York, N. Y., 1963.
76. Lowe, John, III, discussion of "Rockfill dams: dams with sloping earth cores," by J. P. Growdon. Transactions, American Society of Civil Engineers, vol 125, Part II (1960), pp 227-236.
77. Growdon, J. P., "Rockfill dams: dams with sloping earth cores." Transactions, American Society of Civil Engineers, vol 125, Part II (1960), pp 207-225.
78. Steele, I. C., and Cooke, J. B., "Rockfill dams: Salt Springs and Lower Bear River concrete face dams." Transactions, American Society of Civil Engineers, vol 125, Part II (1960), pp 74-116.
79. Lanner, Vilgot, discussion of "Rockfill dams: Brownlee sloping core dam," by Torald Mundal. Transactions, American Society of Civil Engineers, vol 125, Part II (1960), pp 564-574.
80. Lacy, W. C., "Quantitizing geological parameters for the prediction of stable slopes." Transactions, Society of Mining Engineers, vol 226, No. 3 (September 1963), pp 272-276.
81. Inman, D. L., Ewing, G. C., and Corliss, J. B., "Coastal sand dunes of Guerrero Negro, Baja California, Mexico." Geological Society of America Bulletin, vol 77, No. 8 (August 1966), pp 787-802.
82. Hollister, S. C., "Concrete," in L. C. Urquhart, ed., Civil Engineering Handbook, 2d ed., Section 7. McGraw-Hill Book Co., Inc. (New York, N. Y., 1940), pp 533-623.
83. Gillette, H. P., Earthwork and Its Cost. 3d ed., McGraw-Hill Book Co., Inc., New York, N. Y., 1920.
84. Tournier, E. J., and Judd, E. K., "Storage and mill transport." in A. F. Taggart, ed., Handbook of Mineral Dressing, Section 18, John Wiley & Sons, Inc. (New York, N. Y., 1945) pp 18-01 through 18-107.
85. Douglas, W. J., "Masonry and masonry structures," in Thaddeus Merriman and T. H. Wiggins, ed., American Civil Engineers' Handbook, 5th ed., vol 2, Section 10. John Wiley & Sons, Inc. (New York, N. Y., 1930), pp 849-1014.
86. Weigel, W. M., "Hoisting plant, shaft pockets and ore bins," in Robert Peele, ed., Mining Engineers' Handbook, 3d ed., vol 1, Section 12. John Wiley & Sons, Inc. (New York, N. Y., 1941).
87. Reynolds, C. E., "Foundations and earthwork," in C. E. Prockter, ed., Kempe's Engineers Year-Book for 1961, vol II, 66th ed. Morgan Brothers, Ltd. (London, 1961), pp 919-964.
88. Spruill, J. L., and Videon, F. F., Project Pre-Buggy II: Studies of the Pre-Buggy II Apparent Craters. PNE 315F, U. S. Army Engineer Nuclear Cratering Group, CE, Livermore, Calif., June 1965.

89. Spruill, J. L., and Paul, R. A., Project Pre-Schooner: Crater Measurements. PNE 502F, U. S. Army Engineer Nuclear Cratering Group, CE, Livermore, Calif., March 1965.
90. Vesić, A. S., and others, Engineering Properties of Nuclear Craters; Theoretical Studies of Cratering Mechanisms Affecting the Stability of Cratered Slopes, Phase II. Technical Report 3-699, Report 2, U. S. Army Engineer Waterways Experiment Station, CE, Vicksburg, Miss., October 1965.
91. Fulmer, C. V., Cratering Characteristics of Wet and Dry Sand. D2-90683, The Boeing Company, Seattle, Wash., October 1965.
92. Perret, W. R., and others, Project Scooter: Final Report. SC-4602 (RR), Sandia Corporation, Sandia Base, Albuquerque, N. Mex., October 1963.
93. U. S. Army Engineer Waterways Experiment Station, CE, Project Pre-Buggy: Emplacement and Firing of High-Explosive Charges and Crater Measurements, by A. D. Rooke, Jr., and L. K. Davis. Miscellaneous Paper No. 1-663, Vicksburg, Miss., February 1965.
94. Vortman, L. J., and others, Project Buckboard: 20-Ton and 1/2-Ton High Explosives Cratering Experiments in Basalt Rock, Final Report. SC-4675 (RR), Sandia Corporation, Sandia Base, Albuquerque, N. Mex., August 1962.
95. Nordyke, M. D., and others, Project Dugout: Technical Director's Summary Report. PNE 600F, Lawrence Radiation Laboratory, Livermore, Calif., May 1965.
96. Hughes, B. C., and others, Project Pre-Schooner II: Technical Director's Summary Report. PNE 507, Lawrence Radiation Laboratory, Livermore, Calif. (In preparation.)

APPENDIX A: EMPIRICAL DATA ON COHESIONLESS SLOPES  
(EXCLUDING CRATERING STUDIES)

1. Available empirical data on slopes in cohesionless materials are reviewed below. The data are reviewed according to the type and source of information, since the materials and methods followed are often peculiar to each source. In general, emphasis has been placed on materials produced from hard rocks by blasting. Where data are tabulated, they are usually given under the heading "Slope Angle," rather than angle of deposition or angle of repose. Although the text provides some attempt to designate which angle was measured, this is quite uncertain in some cases. Also, reference to the specific angle may be misleading; for example, if slope angles were measured before and after a failure, they are angles of repose and deposition, respectively, but they cannot be related since their order of occurrence is incorrect.

Laboratory Investigations

Van Burkalow

2. A quite comprehensive series of laboratory studies was conducted by van Burkalow,<sup>4\*</sup> who also summarized previous investigations. Great care was taken in the experimental studies to isolate each important factor (such as size, shape, and surface texture) and to evaluate its influence. However, some tests were based on unusual materials (such as wooden blocks and lead shot), and many data are incomplete. The slopes are generally formed by the undermining of piles of particles, though a few were formed from freely falling particles, and the resultant slope angles corresponded more closely to angles of deposition than to angles of repose. When the larger wooden particles were used, the slope length was equal to only 10 to 30 particle diameters, and, perhaps in consequence, many measured inclinations were very steep (up to 60 deg). Nevertheless, the test results may reflect the relative influences of various factors on the slope angle and have been cited in Part III. Selected test results are summarized below.

3. To illustrate the effect of particle size and angularity on the

---

\* Raised numbers refer to similarly numbered items in the Literature Cited at the end of the main text of this report.

slope angle, a relatively bulky and angular sand from New Jersey was compared with a bulky and well-rounded St. Peter sand from Minnesota. Samples of uniform particle size were taken from each material, piled in a loose condition, and when undermined, produced the following slope angles:

Particle Size in.	Slope Angle, deg	
	Angular Material	Rounded Material
0.002 to 0.005	35	34
0.016 to 0.02	34	33

A similar comparison for loose, uniform rhinestones gave results as follows:

Average Particle Size in.	Slope Angle deg
0.09	37
0.16	33

These tests showed an inverse relation between particle size and angle of deposition for uniformly sized material.

4. In tests conducted on well-graded samples of the angular New Jersey sand the range of particle sizes was increased by increasing the maximum particle size of each sample. The following slope angles were obtained by the undermining of piles of loose material:

Particle Size in.	Slope Angle deg
0.002 to 0.005	35
0.002 to 0.02	36
0.002 to 0.08	37
0.002 to 0.26	42

In this case, the results showed a direct relation between particle size and angle of deposition. This relation is supported by tests of a well-graded, crushed traprock, which produced the following slope angles:

Average Particle Size, in.	Slope Angle, deg
0.25	42
0.38	44
0.62	46
0.75	50

5. Tests were next performed in which the relative density of the same well-graded New Jersey sand was increased by vibration before the piles were undermined; the following slope angles were produced:

<u>Particle Size, in.</u>	<u>Slope Angle, deg</u>	
	<u>Loose Material</u>	<u>Dense Material</u>
0.002 to 0.005	35	--
0.002 to 0.02	36	37
0.002 to 0.08	37	39
0.002 to 0.26	42	--

An increase in angle of deposition with an increase in relative density was apparent in these results. This increase was also shown by the undermining of piles of the well-graded sand that had been sprinkled (allowed to fall freely) from various heights; relative density increased with the height of fall. These tests gave the following results:

<u>Particle Size in.</u>	<u>Slope Angle, deg</u>		
	<u>Loose Material</u>	<u>Material Densified by Falling</u>	
		<u>3-in. Fall</u>	<u>9-in. Fall</u>
0.002 to 0.02	36	35	36
0.002 to 0.08	37	38	39

6. Piles that formed naturally by deposition of freely falling particles had erratic slope inclinations that were approximately averaged as follows:

<u>Particle Size in.</u>	<u>Slope Angle, deg</u>		
	<u>Formed by Undermining Loose Pile</u>	<u>Formed by Fall- ing onto Pile</u>	
		<u>3-in. Fall</u>	<u>9-in. Fall</u>
0.002 to 0.02	36	32	31
0.002 to 0.08	37	36	35

Here the results illustrated the decrease in angle of deposition with increasing initial velocity of the particles.

7. Loose piles of the same well-graded New Jersey sand were undermined to form slopes curved in plan, with the following results:

Particle Size in.	Slope Angle, deg				
	Linear Slope	Concave in Plan		Convex in Plan	
		8-in. Radius	4-in. Radius	8-in. Radius	4-in. Radius
0.002 to 0.02	36	36	37	36	34
0.002 to 0.08	37	38	40	37	35

This final series of tests showed that the effect of increasing curvature is an increase in the angle of deposition of a concave slope and a decrease in the angle of deposition of a convex slope.

#### Twenhofel

8. Twenhofel<sup>53</sup> reported studies of the sedimentation of cohesionless materials underwater (presumably by means of laboratory tests); the studies showed the following angles of deposition:

Particle Size in.	Particle Angularity	Slope Angle deg
0.002 to 0.02	--	33
0.02 to 0.08	Rounded	35
0.02 to 0.08	Angular	38
0.08 to 0.16	Subangular to angular	43

#### Tan

9. In conjunction with a study of the mechanism of slope failure by means of laboratory models, Tan<sup>50</sup> performed a few tests to determine the angle of repose of a "fine to coarse" sand (possibly 0.002 to 0.1 in.) by the tilting of a model slope about 2 ft long and 1.5 ft wide. The angle of repose was 36 deg regardless of whether the material was loose or dense, and after surficial movement ceased, the material came to rest at an angle of 33 deg. Gravels were similarly tested, with the following results:

Particle Size in.	Slope Angle, deg	
	Before Movement	After Movement
0.002 to 0.1	36	33
0.38	36	31
0.75	42	27

#### Bustamante

10. Model tests conducted by Bustamante<sup>1</sup> to study the effect of earthquake motions on rock-fill embankments included several static tests

in which the models, having slopes from 2.0 to 3.3 ft high and almost 15 ft long, were tilted to induce failure. Also, a number of companion laboratory tests were performed to measure the angles of static friction and internal friction. The material was a uniform, subangular sand of volcanic origin from the Federal District in Mexico; it had the following characteristics:

- a. Maximum particle size = 0.25 in.
- b. Average particle size = 0.16 in.
- c. Coefficient of uniformity = 1.39
- d. Coefficient of curvature = 0.99
- e. Specific gravity = 2.62
- f. Water content = 0.5 percent

11. Laboratory direct shear tests under low normal stresses (less than 35 psf) gave the following values for the angle of internal friction of the material:

<u>Initial Porosity percent</u>	<u>Maximum Angle of Internal Fric- tion, deg</u>	<u>Ultimate Angle of Internal Fric- tion, deg</u>
50 (loose)	58	40
46 (dense)	62	42

These values agreed closely with values obtained by triaxial compression tests under equally low confining pressures. Static friction tests of particles on surfaces of similar material indicated an angle of static friction of about 26 deg.

12. Two other types of tests were performed by Bustamante to aid in correlating the direct shear tests with the model tests. First, thin (0.2- to 4-in.-deep) layers of the material were placed in a shallow, 5-ft-square box, which was slowly tilted until significant surface movement occurred; the surface inclination at failure averaged 42 deg for both the loose ( $n = 50$  percent) and dense ( $n = 46$  percent) materials, irrespective of layer thickness. Second, a circular pile of the material was formed by feeding material onto the apex of the pile at a low rate through a sieve maintained 0.5 ft above the apex. The slope angle was found to decrease with increasing height of the pile, varying from 37 deg when the pile was



about 1 ft high to 32 deg as the height approached 3 ft.

13. The model embankments were compacted within forms and, after removal of the forms, were tilted until significant surface movement occurred. Thus, the maximum inclination of these plane slopes corresponds to the angle of repose of the compacted material, and the inclination of the material after movement represents an angle of deposition. Further tilting of each model after the first failure permitted a measurement of the angle of repose of the material as it had been deposited by sliding. The results from eight selected models are shown in fig. A1 and the average values are summarized as follows:

Initial Porosity percent	Slope Angle, deg			
	First Failure		Second Failure	
	Before Movement	After Movement	Before Movement	After Movement
50 (loose)	45	33	36	35
46 (dense)	47	33	36	35

As shown in fig. A1, the angle of repose decreased slightly in the first

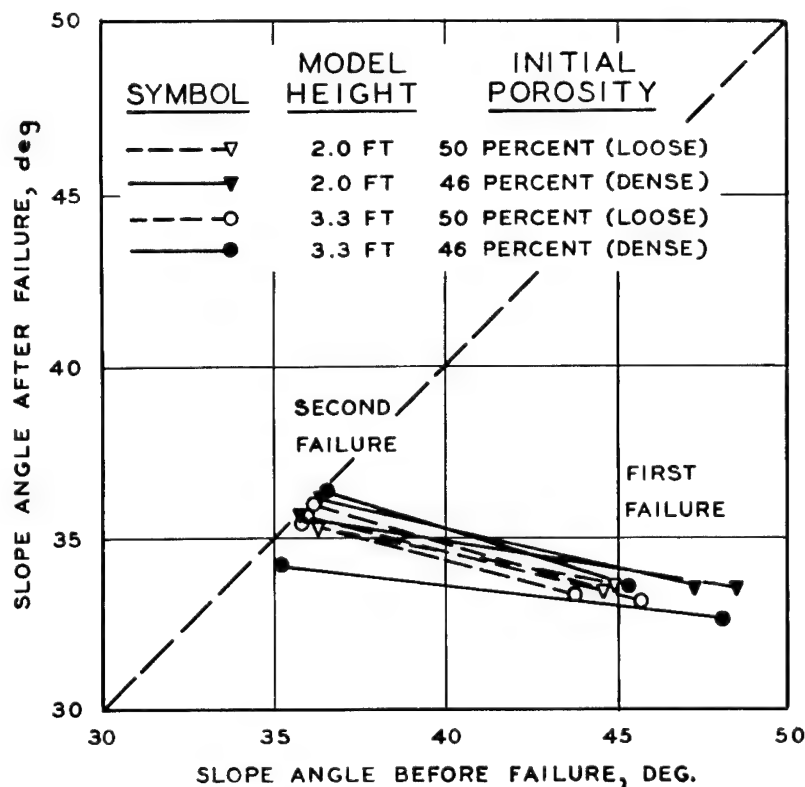


Fig. A1. Relation between angle of deposition and initial slope angle found in model tests by Bustamante<sup>1</sup>

failures with decreasing initial relative density, and then decreased markedly in the second failures with the sharp decrease in relative density; this decrease in relative density was assumed to have resulted from the disturbance of the material by the first failures. A comparison of the slope angles after the first failures with those after the second failures shows a distinct increase in angle of deposition with a decrease in kinetic energy of the moving material (the decrease in kinetic energy resulting from the failure of the flatter slopes).

#### Rinkert

14. Rinkert<sup>52</sup> performed direct shear tests of pebbles (rounded and generally oval particles, 0.6 to 1.2 in. in diameter) and macadam (believed to be angular particles of crushed rock, 1.2 to 2.4 in. in diameter), and found the angle of internal friction to be about 40 deg for each material. When the materials were shoveled into heaps (apparently circular, and at least 3 ft high), the average slope angle was 40 deg for each material when on the verge of failing.

#### Morris

15. As previously noted, Morris<sup>27</sup> tested a number of materials composed of uniformly sized particles (approximately 0.12 in.) that had been artificially roughened or smoothed. Although the shape, angularity, and surface texture of the particles are not explicitly known, they have been shown in table A1 as inferred from the treatment given to the particles. Each material was placed in a wooden box 18 in. long by 4 in. wide by 1 in. deep and the box was vibrated to densify the material. Then the box was tilted longitudinally until surficial movement indicated what Morris called the dense angle of repose, which should correspond closely to the maximum angle of repose. These angles are shown in table A1 together with results of triaxial compression tests of the same materials vibrated in a similar manner. The increase in angle of repose with increased particle angularity and surface roughness is clear.

#### Metcalfe

16. In a study specifically directed toward understanding the phenomenon of angle of repose, Metcalfe<sup>6</sup> performed laboratory tests of several materials, as shown in table A2, to determine (a) the angle of

Table A1

Results of Tests by Morris<sup>27</sup> of Uniform Materials, and  
Inferred Characteristics of Individual Particles

Material	Shape	Angularity	Surface Texture	Dense Angle of Repose,* deg	Angle of Internal Friction,** deg	Designations of Samples in Ref.
Basalt	Bulky (spherical)	Well-rounded	Deeply etched (48 hr in acid)	46	50	H, 43
			Very smooth	46	50	B, 60
			Lightly etched (12 hr in acid)	47	51	C, 34
	Nonbulky	Rounded	Moderately etched (24 hr in acid)	48	52	D, 56
			Deeply etched (48 hr in acid)	48	53	E, 61
			Rough	51	54	G, 35
River deposit containing 17 distinct types of material	Possibly nonbulky	Well-rounded	Rough	52	52	F, 62
			Very rough	54	51	A, 54, 63
	Probably nonbulky	Subrounded	Very smooth	44	44	L, 64
			Smooth	45	48	I, 31
			Predominantly smooth	48	50	J, 65
Pumice	Probably nonbulky	Subangular	Moderately rough	49	51	M, 14
			Predominantly rough	51	50	K, 66
Clay house brick	Probably nonbulky	Subrounded	Smooth	49	50	O, 67
			Rough	55	47	N, 68
			Rough	54	48	P, 69

\* Shallow box vibrated to densify material and then tilted to cause surficial movements.

\*\* Based on maximum  $\sigma_1$  from triaxial compression tests with  $\sigma_3$  of 0.97 ton/sq ft.

Table A2

Results of Tests by Metcalf<sup>6</sup> of Crushed Materials\*

Type of Material	Angle of Internal Friction		Angle of Kinetic Sliding Friction deg	Angle of Deposition deg
	Loose Material	Dense Material		
Rock salt	--	30	30	30
Shale, weathered**	30	32	33	33
Coal, hard, high volatile	28	35	36	36
Coal, coking	23	35	37	36
Coal, dry steam	18	--	38	38
Anhydrite	31	36	37	37
Sand, washed	32	36	37	37
Sandstone, crushed, hard	36	40	39	39
Coke	32	40	--	40

\* Presumably widely graded, with almost all particles finer than 0.25 in.

\*\* Presumably a cemented shale occurring in conjunction with coal deposits.

deposition, as defined in this report, (b) the angle of internal friction, for material in both loose and dense states, and (c) the angle of kinetic sliding friction. The materials were crushed until almost all particles were smaller than 0.25 in., and presumably each material was widely graded. Angles of deposition were measured after piles "a few inches high" of loose material had been undermined to cause a free flow of the material. Angles of internal friction were determined as follows. A 1-in.-thick layer of the material was placed in a 4.5-in.-wide box having glass plates for the longer sides and a wooden block, which could slide horizontally between the glass sides, for one of the shorter sides. Then, the wooden block was moved inward under a horizontal force until a sliding surface formed through the mass; the inclination of this surface with respect to the horizontal was used to compute the angle of internal friction. These shear tests (actually plane strain compression tests) were performed for each material in a loose condition (created by gently feeding material from the periphery of the box so that particles came to rest from movement on a slope rather than from falling vertically) and in a dense condition (created by repeatedly stabbing into the mass). Angles of kinetic sliding friction were determined by pushing a particle of each material across a flat surface sawed in a piece of the same material; the maximum inclination of the pushing force possible during movement was taken as the angle of kinetic friction. Interpretations by Metcalf of these tests were presented previously.

17. Metcalf also studied the angle of deposition of mixtures of materials. For example, varying the proportions of shale ( $\delta = 33$  deg) and coal ( $\delta = 36$  deg) in a mixture gave the following angles of deposition:

<u>Proportions of Mixture, %</u>		<u>Angle of Deposition, deg</u>
<u>Shale</u>	<u>Coal</u>	
>25	<75	33
10 to 20	80 to 90	34
5	95	35
<5	>95	36

#### Stockpiles and Waste Dumps

##### Simons

18. A rather extensive study of the maximum slopes of cohesionless

materials, based on measurements of stockpiles, was conducted by Simons<sup>10,28</sup> after earlier investigations initiated by Lane.<sup>9</sup> Twenty-four outdoor stockpiles of gravel and crushed rock were examined as well as several piles of sand in the laboratory. The stable slopes of the piles were undermined to induce sliding, and the inclinations of the resulting slopes were measured; thus, these were all angles of deposition. Particle size analyses were made, the angularity of particles was estimated, and the height of each pile was measured. Most of the materials were relatively uniform in size, and the effect of gradation on the slope angles for the nonuniform materials was indefinite. The piles ranged in height from 3 to 25 ft. The results are summarized as follows:

Average Particle Size in.	Slope Angle, deg	
	Angular Particles	Rounded Particles
0.01	32	29 to 30
0.1	35 to 36	30
1	40 to 41	35
10	42	39

A strong trend of increasing slope angle with increasing average particle size can be seen.

#### Compton and Steinriede

19. Compton and Steinriede<sup>69</sup> found that waste removed from the Bingham Canyon open-pit copper mine in Utah was being dumped to form slopes 700 to 800 ft high at an angle of 37 deg, though the slope angles of older deposits were 34 to 35 deg. At Ruth, Nevada, measurements of dumps formed of waste from the Liberty open-pit copper mine were as follows:

Name of Dump	Height of Slope ft	Number of Measurements	Average Slope Angle deg
Puritan	150	11	34 to 35
Sunshine	100	3	35
Keystone	200	6	36
Juniper	100	4	37

Similar waste dumps at Miami, Arizona, had a maximum height of 400 ft and a slope angle of about 37 deg.

### Metcalf

20. From a study of published photographs of waste dumps, Metcalf<sup>6</sup> reported the following slope angles:

<u>Type of Dump</u>	<u>Material</u>	<u>Slope Angle, deg</u>
Mining waste	Quartzite, predominantly	37
Ore-treatment waste	Quartzite	35 to 37
Coal-washing waste	Shale, predominantly	33
Stockpiles (20 ft high)	Anhydrite	37

### Davis

21. Davis<sup>70</sup> reported the results of laboratory direct shear tests on the -0.05-in. fraction of an iron ore having the following characteristics:

- a. Maximum particle size = 0.83 in.
- b. Average particle size = 0.06 in.
- c. Coefficient of uniformity = 12
- d. Coefficient of curvature = 0.7
- e. Specific gravity = 4.61

The angle of internal friction was found to increase from 38 to 49 deg with a decrease in porosity from 42 to 34 percent. Observations of outdoor stockpiles of this material revealed slope angles varying from 34 to 45 deg with variations in the porosity from 44 to 38 percent.

### Miscellaneous sources

22. Computations of the areas covered by conical stockpiles of ore have been based on a slope angle of 37 deg.<sup>71</sup> It has been noted<sup>72</sup> that waste dumped out of most lode mines rested at an angle of 37 deg, and many measurements of sandstone and shale spoil banks averaging 60 ft in height at coal mines in Kentucky gave an average slope angle of 37 deg.<sup>73</sup>

### Rock-Fill Dams

23. A common method for constructing a rock-fill dam is to dump the material in high lifts (say 50 to 100 ft) and permit it to seek its natural slope angle. A relatively sound, blasted rock is used, the material is often sluiced with large quantities of water from high-pressure monitors as it is being dumped from trucks, and the material may be graded to contain particles ranging from sand and gravel sizes to 10 to 20 tons apiece. Thus,

dumped rock-fill dams offer excellent sources of information on the slopes formed naturally by materials of large particle size under these specified conditions. The Corps of Engineers does not follow the practice of dumping rock-fill materials. The materials are placed in relatively thin compacted lifts so as to minimize settlement, deflection, and resultant cracking. Table A3 shows slope angles formed by dumped rock fill for dams constructed in many parts of the world. The small range of angles (36 to 40 deg) is quite clear.

24. An extremely small variation in slope angle among different materials and with varying particle size was also found by Galloway,<sup>74</sup> who noted that a loose rock fill of graduated particle sizes would generally assume a natural angle of about 37 deg if the particles were permitted to roll down the slope. Sherard and others<sup>75</sup> have observed that the stable slope angle for rock- and gravel-fill materials varies from 30 deg for rounded stream gravels to about 40 deg for angular quarried rock. However, when compacted in thin lifts, ordinary quarried rock fill can be stable with slopes as steep as 45 deg.

25. Jones<sup>51</sup> reported comparative tests of two materials used for constructing Benmore Dam in New Zealand. The first was rock fill derived from rippable graywacke and argillite, and the second was a river gravel having well-rounded particles of hard graywacke. These materials had the following characteristics:

<u>Characteristic</u>	<u>Rockfill</u>		<u>River Gravel</u>	
	<u>Coarse Grading</u>	<u>Fine Grading</u>	<u>Coarse Grading</u>	<u>Fine Grading</u>
Maximum particle size, in.	24	1.5	18	3.0
Average particle size, in.	4.5	0.13	4.0	0.39
Coefficient of uniformity	17	40	13	65
Coefficient of curvature	1.3	1.8	1.2	1.9

26. Laboratory triaxial compression tests of the fine gradings of each material showed angles of internal friction ranging from 42 to 46 deg for the rock fill with an increase in relative density from 55 to 83 percent, and about 39 deg for the river over a variation of relative density from 52 to 75 percent.



Table A3

## Slope Angles Formed by Construction of Dumped Rock-Fill Dams

Name and Location of Dam	Type and Particle Size of Rock Fill	Height of Dam ft	Height of Lift ft	Slope of Dam	Slope Angle deg	Reference
Binga, Philippines	Metamorphized rock	338	--	Downstream	36	76
Derbendi Khan, Iran	Limestone, moderately hard, fine-textured, dense to porous, usually massively bedded; 70 percent between 1 and 36 in., well-graded, some smaller particles flat or elongated	410	40 to 80	Both	37	31, 70
Nantahala, North Carolina	Arkose, very hard, massive, up to 60 in., widely graded	249	50 to 130	Downstream	37 to 38	77
Queens Creek, North Carolina	Arkose, but less massive than that at Nantahala, quarry run, largest particles placed at slope	78	--	Downstream	38	
Bear Creek, and others, North Carolina	Schist, good quality, much softer than Arkose, quarry run, largest particles placed at slope	--	--	Downstream	38	
Lemolo No. 1, Oregon	Basalt, generally 30 to 60 in., less than 5 percent finer than 4 in.	121	About 40	Downstream	38	66
Hirfanli, Turkey	Gabbro, hard and dense, specific gravity over 3.10	263	--	Downstream	38	76
Lower Bear River No. 2, California	Granodiorite, fine-textured; finer and more widely graded than upstream	125	60 to 120	Downstream	36 to 38 average 37	78
Lower Bear River No. 1, California	Granodiorite, fine-textured; 36 to 70 in. selected loads		40 to 105	Upstream	37 to 40, average 39	
	Granodiorite, fine-textured; over 50 percent between 30 and 80 in., 5 percent finer than 4 in.	233	45 to 85	Upstream	37 to 40, average 38	
Trangslæt, Sweden	Porphyry, 70 percent finer than 20 in., 10 percent finer than 2 in., not sluiced	400	to 65	Downstream	39	79

27. Measurements of slopes 20 ft high formed by dumping the rock fill from trucks gave angles of 37 deg for the fine grading and 40 deg for the coarse; excavation of the toe of these rock-fill embankments produced stable slopes as steep as 42 to 45 deg. Slopes formed by truck-dumping the river gravel into embankments up to 30 ft high averaged 35 deg in inclination. When excavated at the toe, a high stockpile of river gravel would attain slopes as steep as 45 deg, though these would flatten to 35 to 37 deg over a period of time.

28. Nitchiporovitch<sup>59</sup> stated that the angle of deposition of rock-fill slopes formed by allowing the material to roll down a slope is approximately 38 to 40 deg. If a slope is formed by undermining, however, its inclination will depend on the porosity of the material. He reported the following slope angles formed by undermining:

<u>Material</u>	<u>Porosity percent</u>	<u>Slope Angle deg</u>
Crushed rock	44	36
	37	40
Gravel	50	42
	40	47

#### Quarries and Open-Pit Mines

29. When the working face of a quarry or of a bench in an open-pit mine is blasted, the fragmented material slumps to form a slope. Relatively little momentum is imparted to the particles by the blast since the explosive energy in any efficient mining operation is spent on fragmenting the rock rather than moving it. Such slopes, which probably had bench heights of about 50 ft, were examined by Lacy<sup>80</sup> at several open-pit copper mines in Arizona. His observations are summarized as follows:

<u>Material</u>	<u>Slope Angle, deg</u>
Schist	33 to 35
Andesite	33 to 35
Altered limestone	33 to 35
Fanglomerate	34 to 36
Conglomerate	35 to 36

<u>Material</u>	<u>Slope Angle, deg</u>
Monzonite	35 to 42
Rhyolite	36
Diabase	36
Silty limestone	36
Alaskite	36 to 38
Quartz diorite	39
Intrusive breccia	40 to 42

The average of all the measurements he reported was close to 37 deg.

30. Cates<sup>67</sup> also gave slope angles for broken copper ore as measured on the benches of open-pit mines in arid regions. These angles are as follows:

<u>Material</u>	<u>Bench Height, ft</u>	<u>Slope Angle, deg</u>
Porphyry	30 to 90	32
Porphyry	70 (avg)	34
Porphyry	30 to 60	37
Monzonite porphyry	30	45

#### Natural Deposits

31. Slopes formed by natural geological processes are subject to secondary influences resulting from erosion, frost action, groundwater, and weathering. Nevertheless, the study of some natural deposits can be meaningful, especially as the size of the particles may be in the range (e.g. 10 to 100 in.) of those expected to be produced by a cratering explosion in hard rock.

32. Sand dunes are wind-formed piles of extremely uniform, relatively bulky, well-rounded and polished quartz particles. The particle sizes may be about 0.004 to 0.04 in., but in any given deposit the range of sizes is usually less than 0.02 in., according to Bagnold.<sup>35</sup> The particles are rolled by the wind up and over the windward slope of a dune where they fall gently upon the lee slope, sometimes in the presence of an upward, return current of air. Larger particles tend to gather near the bottom of

the lee slope whereas the smaller ones collect near the top with a steeper slope until a slide occurs. Inman, Ewing, and Corliss,<sup>81</sup> found on the lee slopes of coastal dunes in Baja, California, that after each slide the material came to rest at a consistent angle of 33 deg and in layers about 1 in. thick. According to Twenhofel,<sup>53</sup> one investigator (S. Passarge) observed slope angles of 30 to 33 deg, and another investigator (G. B. Cressey) observed that the inclination of dune slopes along Lake Michigan in Indiana never exceeds 32 deg. Studies of Libyan sand dunes by Bagnold<sup>35</sup> indicated the angle of repose to be 34 deg. It is to be noted that dune sands are among the most uniform and well-rounded materials that can be found, so slope angles should approach a minimum for this manner of deposition. Furthermore, since this manner of deposition is relatively gentle and the upward air-currents tend to create a loose arrangement of the particles, the slope might be considered to have an angle of repose approaching the smallest possible for any material.

33. The formation of sand waves by flowing water is similar in character to the formation of sand dunes by flowing air, and the slope angles produced tend to be the same in both cases. Allen<sup>54</sup> performed experiments in a laboratory flume using a uniform sand with well-rounded particles to study the growth of sand waves in water. At low rates of horizontal flow the material deposited near the top of the lee slope would attain a maximum angle averaging 38 deg and would then, intermittently, slide in a mass 5 to 10 average particle diameters thick to rest at a slope averaging 32 deg. When the rate of flow was increased to a certain level the material deposited on the lee slope would continuously slide in a mass with a depth of 5 to 10 average particle diameters and would come to rest at a slope averaging only 30 deg. These results illustrate the decrease in angle of deposition with an increase in horizontal component of the initial velocity.

34. Talus is a deposit of rock debris which accumulates in a pile at the foot of a cliff or lies in a sheet on an inclined surface below the cliff.<sup>57</sup> The material is produced by mechanical weathering of the parent rock mass, which causes blocks or slabs, as defined by the joint pattern, to slide or fall onto the crest of the talus slope. The particles can be

very large, are generally angular, and sometimes fall an appreciable distance before striking the talus. Therefore, the manner of deposition can be similar in character to the deposition of fallback in an explosion crater. Several geomorphologists have studied the inclination of talus slopes, though their reports frequently fail to differentiate between particles resting on a talus of similar particles and those resting on an otherwise bare rock slope. Also, observations of talus can be confused by effects of weathering and creep.

35. From numerous observations in the Rocky Mountains, Behre<sup>56</sup> concluded that the maximum angle of talus slopes, regardless of the size and angularity of the particles, is 42 deg, though the infrequency of this angle and the thinness of the talus wherever it was measured led him to reject the figure for most generalizations. By far the most common maximum angle found is 36 deg for the particles of greatest size and angularity. For other than these largest size particles, the slope angles in an area of active talus formation might be generally as follows:

<u>Average Particle Size, in.</u>	<u>Average Slope Angle, deg</u>
0.5 to 1	26 to 31
0.5 to 2	31 to 32
0.5 to 4	32 to 34
0.5 to 6	35
0.5 to 12	35

He observed that the larger particles remained near the crest of the slope, causing it to be concave in cross section, and only exceptionally large particles rolled to the bottom. Behre believed that the particles deposited on a given talus slope have about the same size initially and that as weathering reduces their size, they move downward to form a concave slope in accordance with his generalized relation, given above, between size and slope angle. The same range of slope angles given by Behre, that is, 26 to 36 deg, was considered by Sharpe<sup>57</sup> to be the usual range of the angle of repose of talus materials, but no reference was made to particle sizes.

36. Talus slopes below retreating cliffs in the southwestern United

States were observed by Koons<sup>43</sup> to have the following average angles:

<u>Material</u>	<u>Particle Size, in.</u>	<u>Slope Angle deg</u>
Basalt	2 to 90	24 to 30
Sandstone	2 to 70	30 to 34
Limestone	1 to 35	31 to 33

In the formations he investigated, the rock debris lay in sheets averaging 3 to 6 ft thick upon rock slopes inclined at angles averaging 36 deg. He advanced the notion that such taluses are formed not by a continual dribble of material from the cliffs but by periodic massive slides or falls from cliffs upon the bare rock slopes below, these lower slopes having been denuded of earlier slide debris. This would represent a severe manner of deposition.

37. A limited number of measurements of talus slopes around Buckboard Mesa at the U. S. Atomic Energy Commission Nevada Test Site by WES personnel<sup>61</sup> indicated that the lower portions of slopes usually varied in inclination between 20 and 30 deg, and the upper portions varied between 30 and 35 deg. Slope angles as large as 40 deg were found, but the average was about 32 deg. The material consisted of generally bulky and angular particles of basalt widely graded to a maximum size of 50 in., the average size being about 10 to 20 in. These slopes were 60 to 80 ft high and the talus formed a veneer only a few feet thick upon an inclined rock surface.

38. Miner<sup>58</sup> was surprised by the extreme steepness of talus slopes along the south side of the St. Lawrence River in Quebec. He believed that the angle of repose of coarse cohesionless material does not usually exceed 35 deg, but these slopes stand at angles generally between 38 and 40 deg with heights as great as 175 ft and with marked surface stability. The material consists of angular, elongated particles of calcareous shale and slate ranging in size from 0.5 to 5 in., with most particles 1 to 3 in. in size. He observed that the particles lay with their long axes essentially parallel to the slope, with each surface particle overlapped by the one upslope of it, in an echelon arrangement "so orderly that, viewed as a whole, it gave the appearance of having been laid by hand."

39. Melton<sup>11</sup> made detailed observations and measurements of numerous debris-covered slopes at least 60 ft long in southern Arizona. As a rule, these slopes had been formed by the in-place weathering and detachment of particles from the parent rock rather than by the fall of particles onto the slopes. His findings are summarized as follows:

Type of Parent Rock	Average Particle Size in.	Maximum Angle of Deposition* deg	Maximum Slope Angle deg
Granitic	3 to 13	28	38
Volcanic	5 to 11	28	34

\* Defined by whether a dropped particle (bulky and greater than average particle size) would roll to the bottom of the slope.

Although he found, at most, a very weak relation between slope angle and particle size, he suggests that particle size is a function of the slope angle. He believes that the angles of repose and deposition are, in effect, equal to the angles of static and kinetic sliding friction, respectively.

#### Handbooks and Codes

40. Handbooks of civil and mining engineering practice invariably contain tabulated values of the angle of repose of various materials. Some codes for construction or excavation practice also present such angles. The following are typical and pertinent values from these sources:

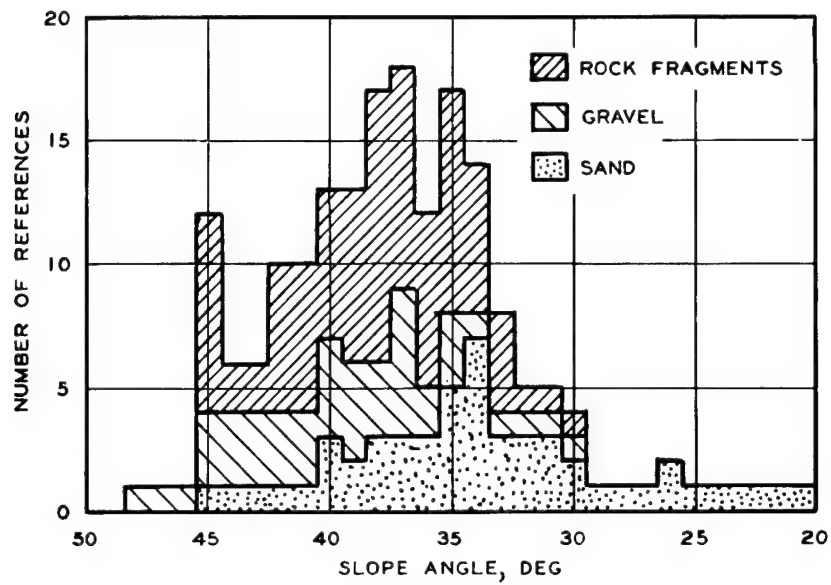
Material	Slope Angle deg	Reference
Sand, dry	20 to 35	82
Sand, dry	38	83
Sand, fine, dry	31 to 37	84
Sand, clean, loose, dry	34	65, 68, 85, 86
Sand, uniform, loose	30 to 35	87
Sand, uniform, compact	35 to 40	87
Sand, well graded, loose	35 to 40	87
Sand, well graded, compact	40 to 45	87
Sandy gravel	26	84
Gravel, round to angular	30 to 48	82

Material	Slope Angle deg	Reference
Gravel	35 to 45	87
Gravel	40	83
Gravel, clean, loose, dry	37	65, 68, 85
Gravel, dry	37 to 45	84
Shingle	39	83
Iron ore, soft, broken	35	84, 86
Ore, various	38 to 42	84
Ore, broken	45	86
Shale, broken	30 to 35	87
Shale, fragments	34 to 38	64
Shale, fragments	37	68
Shale, crushed	39	86
Marl, fragments	33 to 36	64
Chalk, fragments	33 to 36	64
Chalk, broken	35 to 45	87
Metamorphic rock, fragments	34 to 38	64
Rock, crushed	35 to 45	87
Stone, crushed	37	84
Stone, broken	38	83
Soft rotten rock	37	85
Hard rotten rock	45	85
Limestone, fragments	38 to 42	64
Limestone, fragments	45	68
Sandstone, soft	33 to 37	64
Sandstone, hard	38 to 42	64
Sandstone, fragments	45	68
Igneous rock	37 to 42	64
Rock, hard (riprap)	45	65
Rubble	45	83

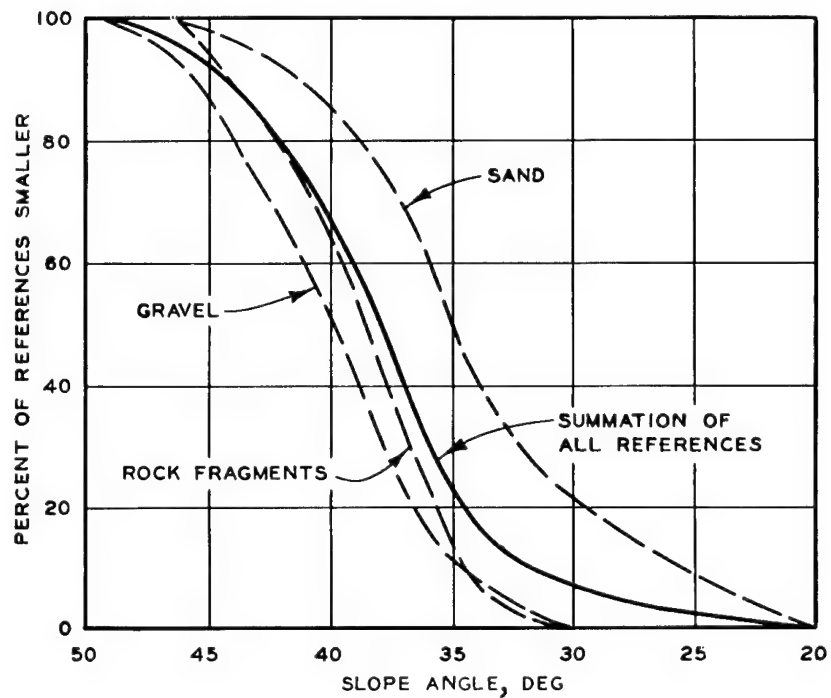
A histogram of all these values is plotted in fig. A2a, and a cumulative curve for each of the three approximate classes of material (sand, gravel, and rock fragments) is shown in fig. A2b along with a summary curve. The



average slope angle varies from 35 deg for sand to 40 deg for gravel, and the average of all the values is 38 deg.



(d) HISTOGRAM OF VALUES



(b) CUMULATIVE CURVE OF VALUES

Fig. A2. Summary of values of angle of repose given in handbooks and codes

## APPENDIX B: COHESIONLESS SLOPES IN EXPLOSION-PRODUCED CRATERS

### Explosion-Produced Craters

1. The redeposition of blasted material into craters formed by the detonation of buried explosives results in slopes of special interest in this study. Many cratering experiments using chemical explosives have been made for military purposes, but the reported data are often incomplete with regard to slope inclinations. However, some cratering experiments, using both nuclear and chemical explosives, conducted at the Nevada Test Site have been thoroughly reported and a selected number of these are described below. Only those cratering data pertaining to buried explosions at or near optimum depth of burst are considered.

2. As shown in fig. B1, the dimensions used to describe a crater for most purposes are:

<u>Symbol</u>	<u>Dimension</u>
D <sub>ob</sub>	Depth of burst
R <sub>c</sub>	Cavity radius
R <sub>a</sub>	Apparent crater radius
D <sub>a</sub>	Apparent crater depth
R <sub>al</sub>	Apparent lip crest radius
H <sub>al</sub>	Apparent lip crest height

and these are measured from the preshot ground surface vertically above the zero point or center of the explosion.<sup>88\*</sup> To compare craters formed by explosions of different energy yields  $W$ , the dimensions are usually scaled by dividing by the 3.4 root of the yield in kilotons (kt) of nuclear energy or the equivalent for a chemical explosive;<sup>89</sup> this gives units of ft per kt<sup>1/3.4</sup>. The crater dimensions vary with the depth of burst for a given yield of explosion, and the relations are expressed in scaled units. For studying the geometry and stability of crater slopes, it is preferable to establish coordinate axes with respect to the planar, upper portion of the fallback slope,<sup>89</sup> as shown in fig. B1. This introduces an additional

---

\* Raised numbers refer to similarly numbered items in the Literature Cited at the end of the main text of this report.

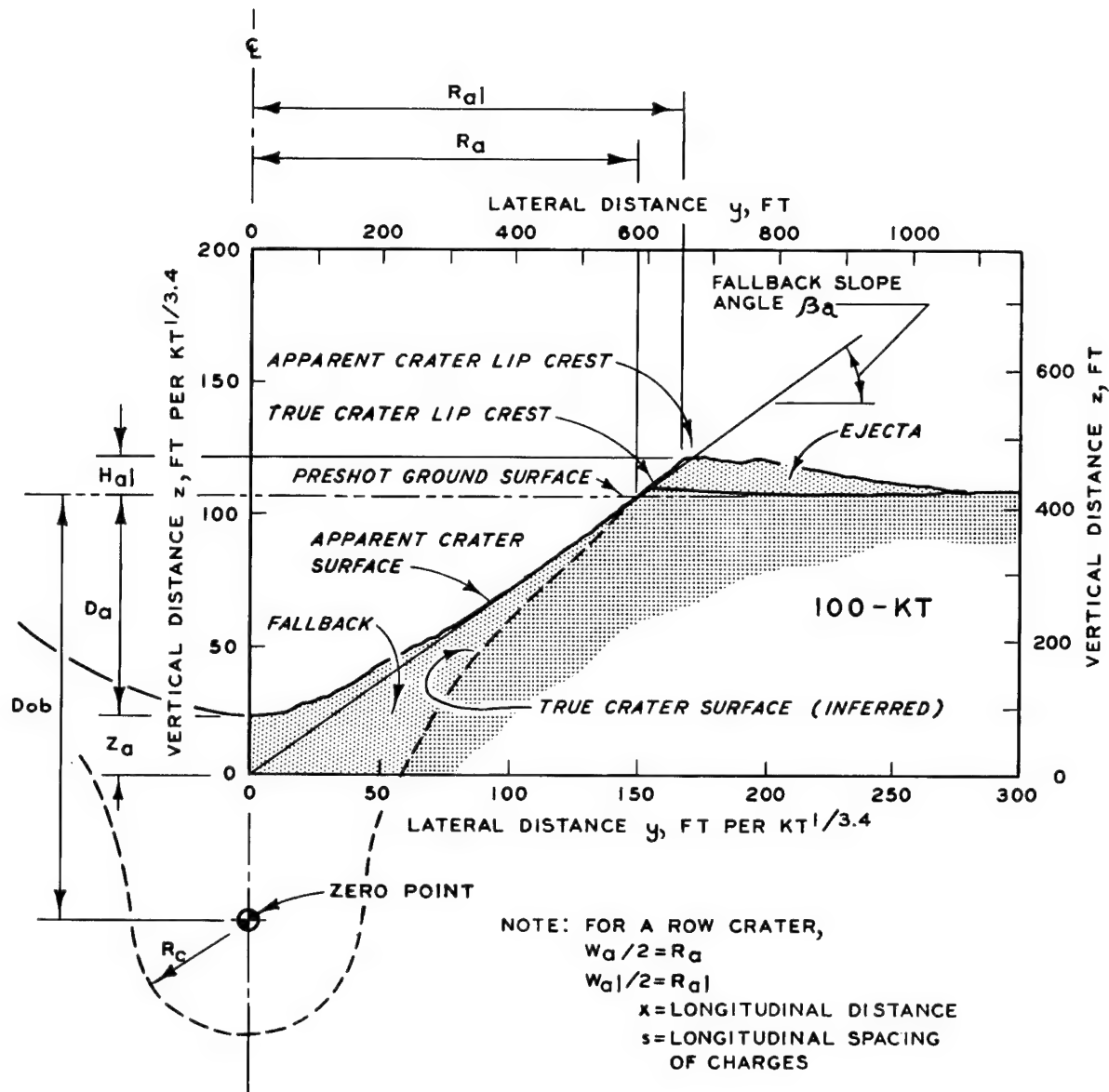


Fig. B1. Section through Sedan crater showing crater nomenclature and dimensions and coordinate axes used for slope stability studies

dimension  $Z_a$  to locate the origin of the coordinate system with respect to the apparent crater bottom. The distances on the new axes can also be scaled in terms of the yield. In this report, the fallback slope angle is always as shown in fig. B1, that is, the inclination of the line best fitting the more planar, upper portion of the fallback, disregarding both the steeper slope immediately below the crest (sometimes caused by the protrusion of the true crater lip) and the more curved lower portion of

the crater. In general, this line is tangent to the apparent crater surface at the level of the preshot ground surface. The average fallback slope angle is the line similarly fitted to the profile of an equivalent crater having, in plan, the same area at every elevation but with a regular shape (circular for a single crater and rectangular for a length of a row crater).<sup>40</sup>

### Crater Formation

3. To understand the characteristics of a slope formed by the deposition of cohesionless material, it is important to know the manner of deposition. Unfortunately, the manner in which an explosion crater is produced, particularly with regard to the deposition of fallback, is not fully known. Some insight into this phenomenon, however, can be gained from the model cratering experiments conducted by the NCG<sup>60</sup> and by Vesić, and others.<sup>90</sup> These experiments suggest that most of the fallback material slides or rolls into a final position of rest when the crater is produced by an explosion near the optimum depth of burst (at which the apparent crater radius is a maximum). A large portion of the material may not be detached and thrown upward by the explosion, but, in fact, may be the debris from failures of the instantaneously steep surface formed by the upward expansion of the cavity. Of the portion of material that is thrown into the air by the explosion, relatively little should fall directly into a position of rest within the crater, even if the areal distribution is uniform; this is due to the slope of the crater during the later stages of formation. It is certain that the uppermost layer of fallback material moves by sliding or rolling down the slope, as is shown by the segregation of particles by size along the apparent crater surface. Thus, it can be assumed that fallback slopes form by massive slumping, followed by falling and feeding at a rapidly decreasing rate.

4. Although sufficient material may be deposited near the true crater lip to develop fully the maximum angle of deposition in successful cratering experiments, this may not be true if the depth of burst is not near optimum. This is illustrated by Fulmer<sup>91</sup> in a series of cratering experiments that used single spherical 1-lb TNT charges in a compacted plaster sand having the following characteristics:

- a. Maximum particle size = 0.10 in.
- b. Average particle size = 0.018 in.
- c. Coefficient of uniformity = 1.9
- d. Coefficient of curvature = 1.2

The results of over 30 experiments, with the sand both dry (less than 0.5 percent water content) and wet (water content between 6 and 22 percent, the latter value giving complete saturation), are shown in fig. B2. These results show a distinct decrease in the average fallback slope angle with departure of the depth of burst in either direction from optimum. Information on the density of the sand is not available.

5. A somewhat similar variation in fallback slope angle with depth of burst appears in the results of Project Zulu II,<sup>34</sup> a series of cratering experiments by the NCG using single spherical 1-lb charges of compound C<sup>4</sup> in a compacted concrete sand (see fig. 10, page 15 herein) having the following characteristics:

- a. Maximum particle size = 0.19 in
- b. Average particle size = 0.028 in.
- c. Coefficient of uniformity = 5.5
- d. Coefficient of curvature = 0.70
- e. Specific gravity = 2.69

The individual particles were subrounded to subangular and about 10 to 20 percent by weight were nonbulky (either flat or elongated). The material was compacted in layers to achieve a porosity of about 33 percent (relative density about 65 percent) with a water content between 6 and 7 percent. Laboratory triaxial compression tests suggest that the angle of internal friction is about 43 deg with a cohesion intercept of about 0.2 ton per sq ft for the material as compacted. Postshot porosity of the fallback material averaged about 42 percent (relative density about zero). Fig. B3 shows the results of 15 experiments that display the decrease in fallback slope angle with departure from optimum depth (primarily as the depth of burst increases) of the depth of burst. It is important to note the variation of crater dimensions and slope angle with the depth of burst; at a scaled depth of burst greater than about 150 ft/kt<sup>1/3.4</sup> (where the slope angle decreases sharply) no crater is formed by the explosion.

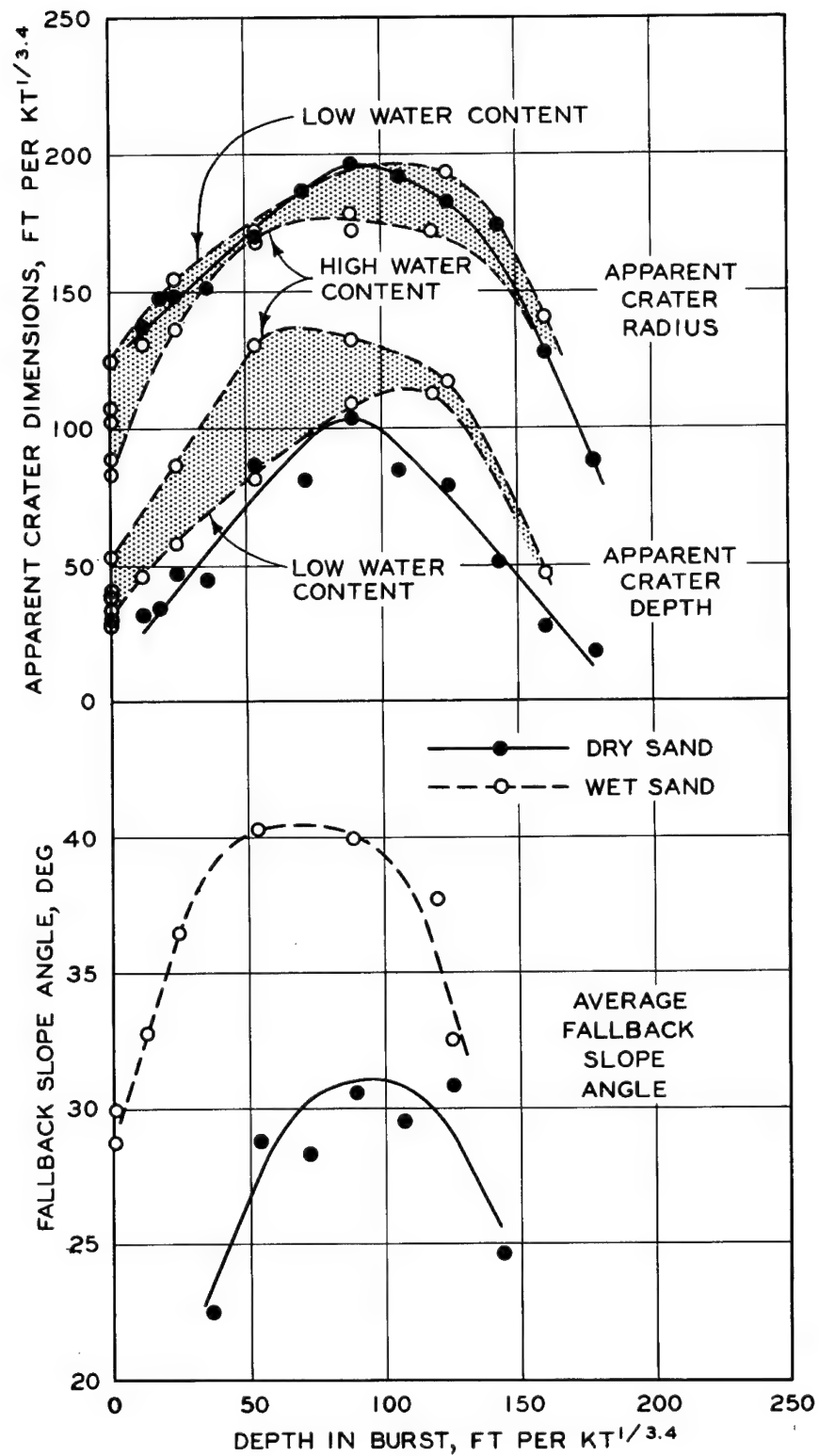


Fig. B2. Variation in average fallback slope angle with depth of burst of single 1-lb TNT charges in sand found in experiments by Fulmer

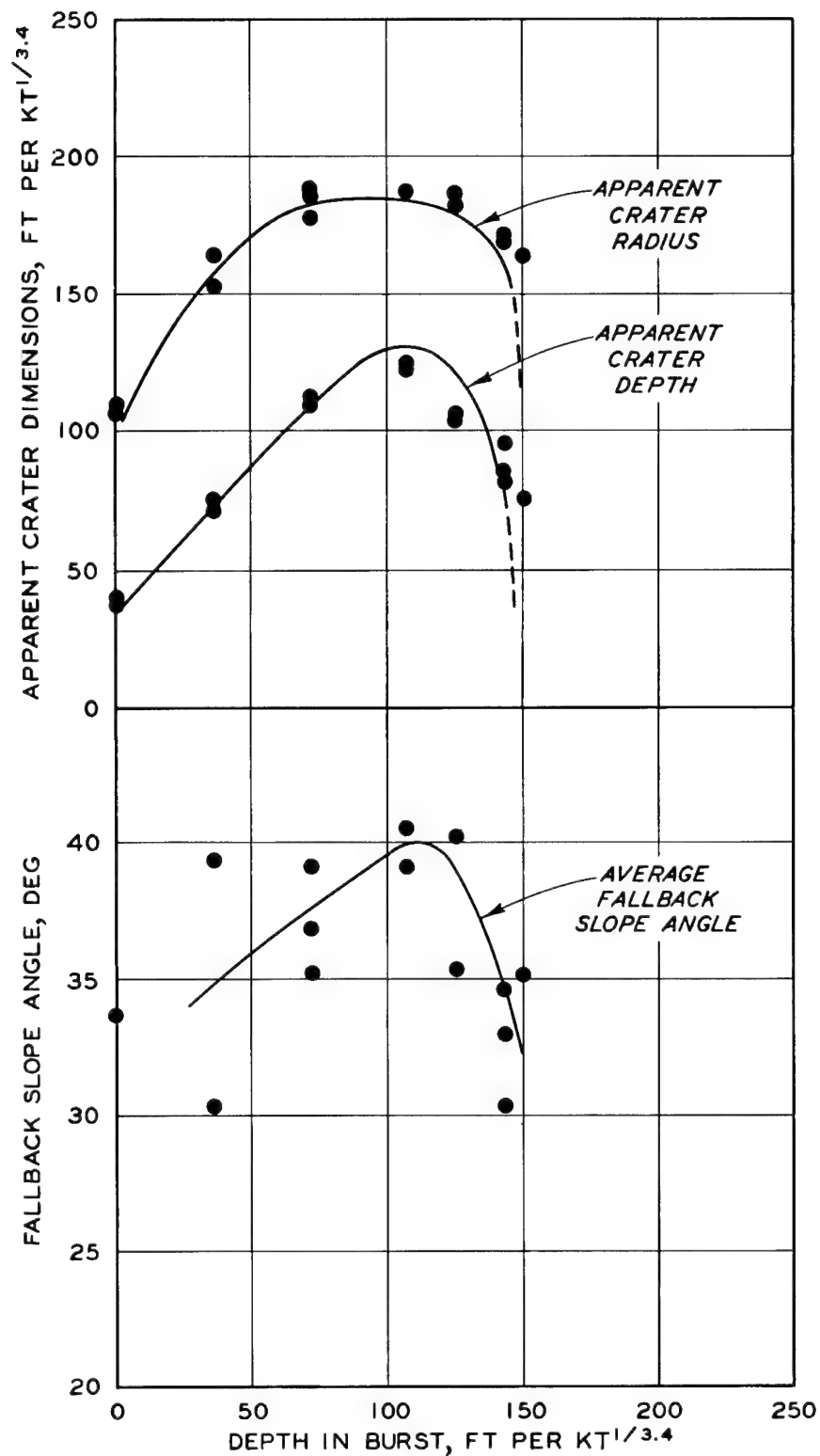


Fig. B3. Variation in average fallback slope angle with depth of burst of single 1-lb C<sup>4</sup> charges in sand found in results of Project Zulu II

## Craters in desert alluvium

6. The largest crater produced in the desert alluvium of the Nevada Test Site was that of Project Sedan,<sup>33</sup> in which a single 100-kt nuclear explosion produced an apparent crater with the dimensions given in table B1. Profiles of the apparent crater are shown in fig. B4. The average

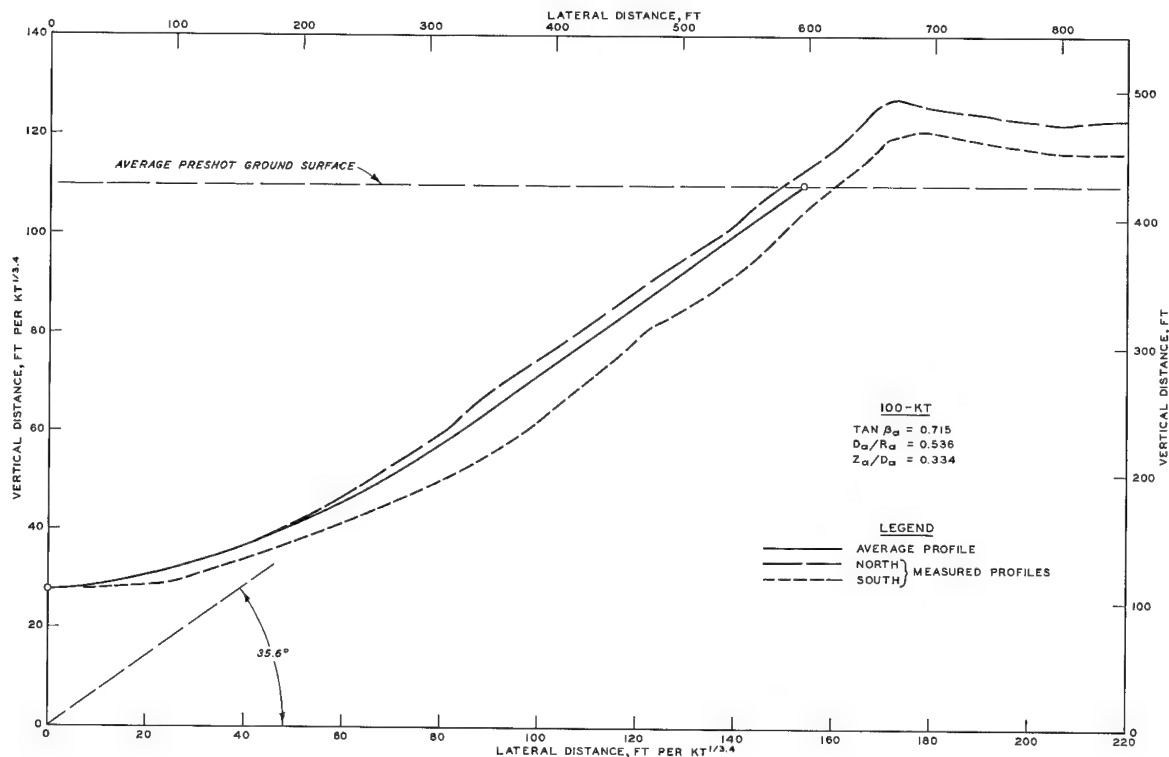


Fig. B4. Typical and average profiles of apparent crater of Project Sedan produced by single 100-kt nuclear explosion in desert alluvium

fallback slope angle was about 36 deg and was a fully developed angle of deposition as evidenced by the appearance of the slope and by the fact that an average-size particle dropped onto the slope from a low height would invariably roll all the way to the bottom. The material at the Sedan crater is a widely graded desert alluvium (see fig. 10) having relatively bulky, subrounded to subangular particles and the following typical characteristics:

- a. Maximum particle size = 3.0 in.
- b. Average particle size = 0.025 in.
- c. Coefficient of uniformity = 35



Table B1

Dimensions of Selected Explosion-Produced Craters

Material Cratered	Name of Crater Project	Event	Dimensions of Explosion					Dimensions of Average Apparent Crater										References							
			Yield or Weight of Each Charge	Type of Explosive	Energy Equivalent of Yield, Wt	Spacing of Charges, s	Depth of Burst, Dob	Apparent Crater R <sub>a</sub> or W <sub>a</sub> /2	Apparent Crater Depth, D <sub>a</sub>	Fallback Slope Angle, θ <sub>a</sub>	Fallback Slope Ratio, tan θ <sub>a</sub>	Profile Shape Ratio, D <sub>a</sub> <sup>3/2</sup> /s <sub>a</sub>	Profile Roundness Ratio, Z <sub>a</sub> <sup>3/2</sup> /s <sub>a</sub>												
														Number of Charges	ft	ft	ft		ft	ft	ft	ft	ft	ft	ft
Desert Alluvium	Sedan	-	1	100 kt	Nuclear	100.0	-	635	164	597.0	154	320.0	83	33	35.6	0.715	0.536	0.334	40,33						
	Teapot	ESS	1	1.2 kt	Nuclear	1.2	-	67.0	63	146.0	139	90.0	85	13	42.6	0.92	0.616	0.494	15						
	Johnnie Boy	-	1	0.5 kt	Nuclear	0.5	-	1.9	2	60.3	74	30.7	38	10	36.4	0.736	0.509	0.446	40						
	Scooter	-	1	1,000,000 lb	TNT	0.5	-	125.0	153	154.4	189	74.5	91	12	36.3	0.735	0.483	0.523	40,92						
	Stagecoach	2	1	40,000 lb	TNT	0.0197	-	17.0	54	50.4	160	23.6	75	5	35.1	0.702	0.468	0.500	63,40						
		3	1	40,000 lb	TNT	0.0197	-	34.2	108	58.2	194	23.9	91	6	35.5	0.715	0.497	0.439	63,40						
		1	1	40,000 lb	TNT	0.0197	-	50.0	252	57.0	180	7.0	23	6	22.0	0.40	0.12	2.3	63						
		1	1	1,000 lb	NM	0.000556	-	15.0	137	21.3	194	9.9	90	3	38.8	0.805	0.465	0.731	40,93						
		2	1	1,000 lb	NM	0.000556	-	16.6	150	22.2	200	9.5	86	3	32.0	0.526	0.428	0.463	40,93						
		3	1	1,000 lb	NM	0.000558	-	13.2	164	20.1	181	8.1	73	2	31.0	0.60	0.403	0.483	40,93						
Desert Alluvium	Pre-Bugy	6	1	1,000 lb	NM	0.000552	-	19.6	178	20.0	181	8.1	73	2	33.4	0.659	0.410	0.507	40,93						
		4	1	1,000 lb	NM	0.000553	-	19.8	180	20.1	182	9.1	83	2	33.7	0.667	0.453	0.472	40,93						
	Row A	5	1	1,000 lb	NM	0.000553	20.6	1.00	19.8	22.2	202	12.1	113	6	33.4	0.66	0.545	0.211	93						
	Row D	5	1	1,000 lb	NM	0.000557	23.2	1.12	19.3	21.4	194	5.4	158	7	29.4	0.56	0.299	0.383	93						
	Row C	5	1	1,000 lb	NM	0.000553	25.3	1.25	19.8	19.3	175	4.4	140	5	28.4	0.54	0.288	1.37	93						
	Row B	5	1	1,000 lb	NM	0.000562	30.9	1.50	19.8	16.5	151	4.9	145	5	32.1	0.63	0.295	1.13	93						
	F-3	1	1	950 lb	TNT	0.000468	-	18.3	174	21.2	202	11.1	105	3	36.1	0.729	0.524	0.391	40,88						
	F-4	1	1	950 lb	TNT	0.000468	-	15.3	175	21.9	203	10.8	102	3	35.3	0.721	0.493	0.482	40,88						
	F-1	1	1	1,000 lb	NM	0.000553	-	19.8	180	22.2	202	11.4	104	3	37.5	0.77	0.513	0.395	88						
	Row C	5	1	1,000 lb	NM	0.000553	20.6	0.94	19.8	24.3	225	15.4	140	40.7	0.60	0.521	0.395	88							
Basalt	Pre-Bugy II	5	1	1,000 lb	NM	0.000556	23.2	1.06	19.8	23.6	213	13.7	125	7	35.4	0.712	0.531	0.225	88						
	Row D	5	1	1,000 lb	NM	0.000556	25.8	1.17	19.8	23.4	213	11.7	105	7	35.0	0.700	0.500	0.329	88						
	Row B	5	1	1,000 lb	NM	0.000555	20.6	0.94	23.0	209	23.1	7.5	69	7	31.1	0.602	0.329	0.390	88						
	Row C**	5	1	1,000 lb	NM	0.000557	20.6	0.94	23.0	209	190	9.3	95	7	34.3	0.652	0.445	0.533	88						
	Row H	13**	1	1,000 lb	NM	0.000553	20.6, 0.94 25.8, 1.17 30.9, 1.40	19.8, 19.8, 19.8	24.8, 23.4, 20.1	225, 213, 153	14.7, 13.0, 10.5	134, 119, 95	34.7, 34.3, 34.3	0.693, 0.682, 0.682	0.593, 0.555, 0.522	0.169, 0.227, 0.307	88, 88, 88								
	Danny Boy	-	1	0.42 kt	Nuclear	0.42	-	110.0	142	109.0	141	62.0	80	20	35.6	0.718	0.569	0.262	40,30						
	Buckboard	11	1	40,000 lb	TNT	0.0197	-	25.5	80	44.4	140	24.7	78	5	32.6	0.641	0.555	0.153	40,94						
		12	1	40,000 lb	TNT	0.0197	-	42.7	135	56.5	179	34.9	11.0	3	37.1	0.757	0.617	0.227	40,94						
		13	1	40,000 lb	TNT	0.0197	-	53.8	195	36.8	116	16.0	50	12	25.5	0.50	0.435	0.149	40,94						
	Pre-Schooner	Delta	1	40,000 lb	NM	0.0219	-	41.9	128	46.2	141	25.5	78	9	32.2	0.689	0.552	0.139	40,89						
Chert		1	40,000 lb	NM	0.0213	-	50.2	155	49.5	153	23.7	79	10	31.0	0.600	0.519	0.155	40,89							
		1	40,000 lb	NM	0.0217	-	53.0	179	51.2	153	23.2	72	12	31.4	0.61	0.453	0.347	40,89							
	Dugout	5	1	40,000 lb	NM	0.0224	45.0, 0.90	58.7	180	68.0	210	35.2	108	24	34.8	0.595	0.513	0.342	95						
Chert	Pre-Schooner II	-	1	171,000 lb	NM	0.0946	-	71.1	142	95.2	190	50.7	121	17	38.0	0.782	0.638	0.286	96						

\* Row C\* was an extension of Row C crater and vented into the existing crater before venting upward.

\*\* Four spaces of 20.6 ft, four of 25.5 ft, and four of 30.9 ft.

d. Coefficient of curvature = 0.71

e. Specific gravity = 2.59

The gradation varied extremely; some 10- to 20-in. boulders were present, and the average particle size of various samples ranged from less than 0.02 to more than 0.2 in. Segregation was apparent among the larger-sized particles, with the larger ones resting at the crater bottom and the size of the particles decreasing with distance up the concave slope. However, the material at the bottom contained a greater percentage of the finer (e.g. less than 0.02 in.) sizes than did the material up the slope. An increase in porosity and a decrease in water content with height above the crater bottom were also observed. Measurements made about 18 in.

beneath the surface showed porosities ranging from about 41 percent (with 4 to 7 percent water content) at the bottom to 49 percent about one-fourth the way up, and 57 percent (with 1 percent water content) about halfway up the slope. The average of all porosity measurements was about 44 percent. Laboratory triaxial compression tests of the material compacted to various porosities (with about 15 percent water content) suggested the angle of internal friction to be 35 deg at a porosity of about 44 percent.

7. Numerous other single craters have been produced in the desert alluvium; the dimensions of the larger ones, ranging in equivalent energy yield from 0.00055 to 1.2 kt, are given in table B1. Figure B5 shows the crater-scaling relations developed from these and other single craters in the desert alluvium together with the average fallback slope angle for each crater. It should be

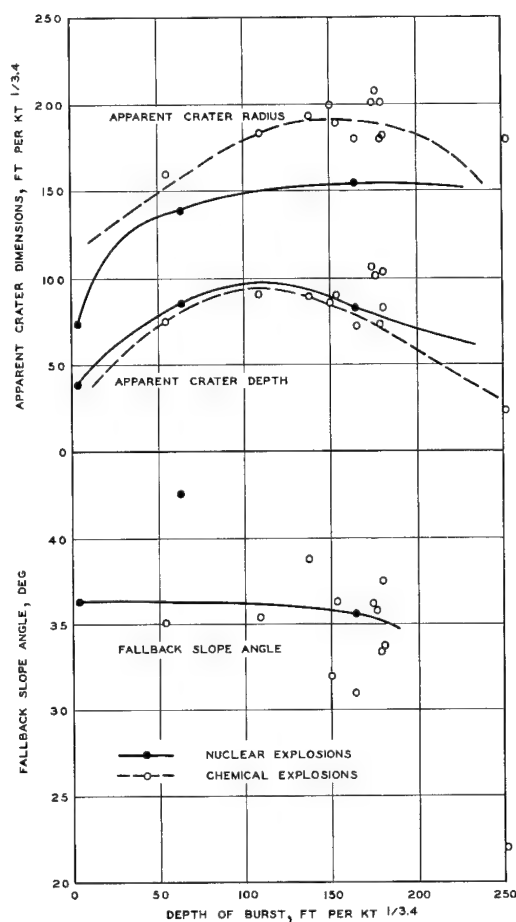


Fig. B5. Variation in average fallback slope angle with depth of burst of single explosions in desert alluvium

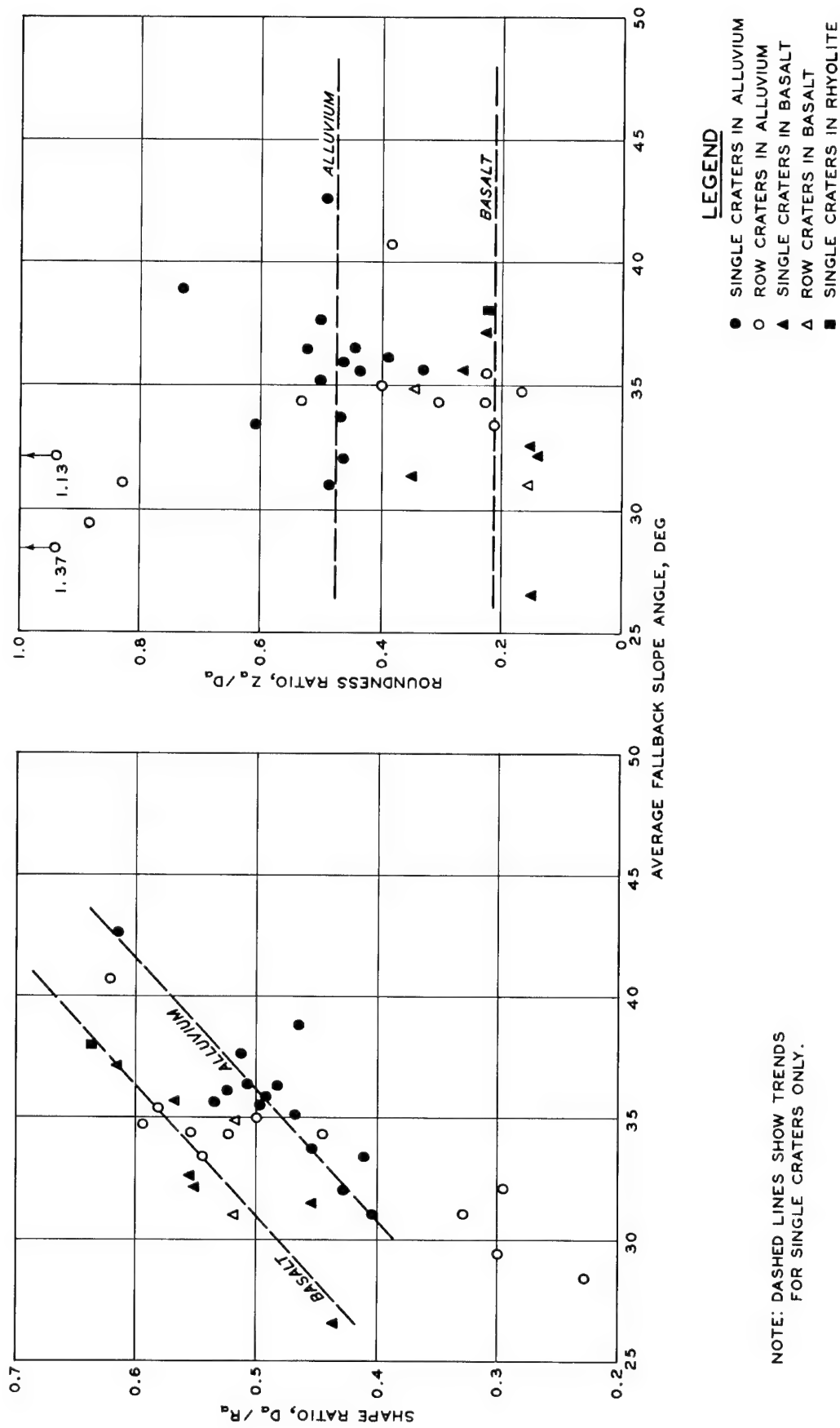


Fig. B6. Profile shape and roundness ratios for explosion-produced craters

noted that there appears to be no relation between the average fallback slope angle and the depth of burst such as that found in the model cratering experiments described earlier. The two profile ratios,  $D_a/R_a$  and  $Z_a/D_a$ , are plotted in fig. B6 for all the explosion craters described in this report. For the single craters in alluvium, there is a discernible tendency for the shape ratio to vary directly with the average fallback slope angles; the shape ratio ranges between 0.40 and 0.55 for slope angles ranging between 31 and 39 degrees. Over this range of slope angles, the roundness ratio varies erratically between 0.30 and 0.75, though most of the values are between 0.40 and 0.55.

8. The apparent crater formed by a linear row of several closely spaced, simultaneous explosions (with the spacing  $s$  equal to or slightly greater than the apparent crater radius of a single crater) tends to have a smaller profile roundness ratio than a single crater. In other words, the upper portions of the fallback slopes are quite planar in section and there is relatively little rounding at the bottom. This difference may result from several factors. First, and probably most influential, is the different areal distribution of falling material thrown into the air by the explosion. Since the ratio of true crater volume to perimeter is greater for a row crater, a relatively larger volume of material falls on the lip of a row crater than on the lip of a single crater. Because of this increased volume of material (as well as the interaction of the explosions), row craters are wider, deeper, and have higher side lips than equivalent single craters,<sup>88</sup> and the fallback slopes can fully develop planar angles of deposition. Second, since the fallback slopes of a row crater are linear in plan, there would not be present the converging flow of material as in the case of a single crater, the slope of which has concave curvature.

9. The difference in apparent crater shapes is clearly shown by the results of Project Pre-Buggy II<sup>88</sup> in which rows of spherical 1000-lb nitromethane (NM) charges were exploded at several spacings and depths of burst in the desert alluvium of the Nevada Test Site. These results are also presented in table B1. The average slope angle was about 34 deg. From the typical section through one crater (Row H), shown in fig. B7, it

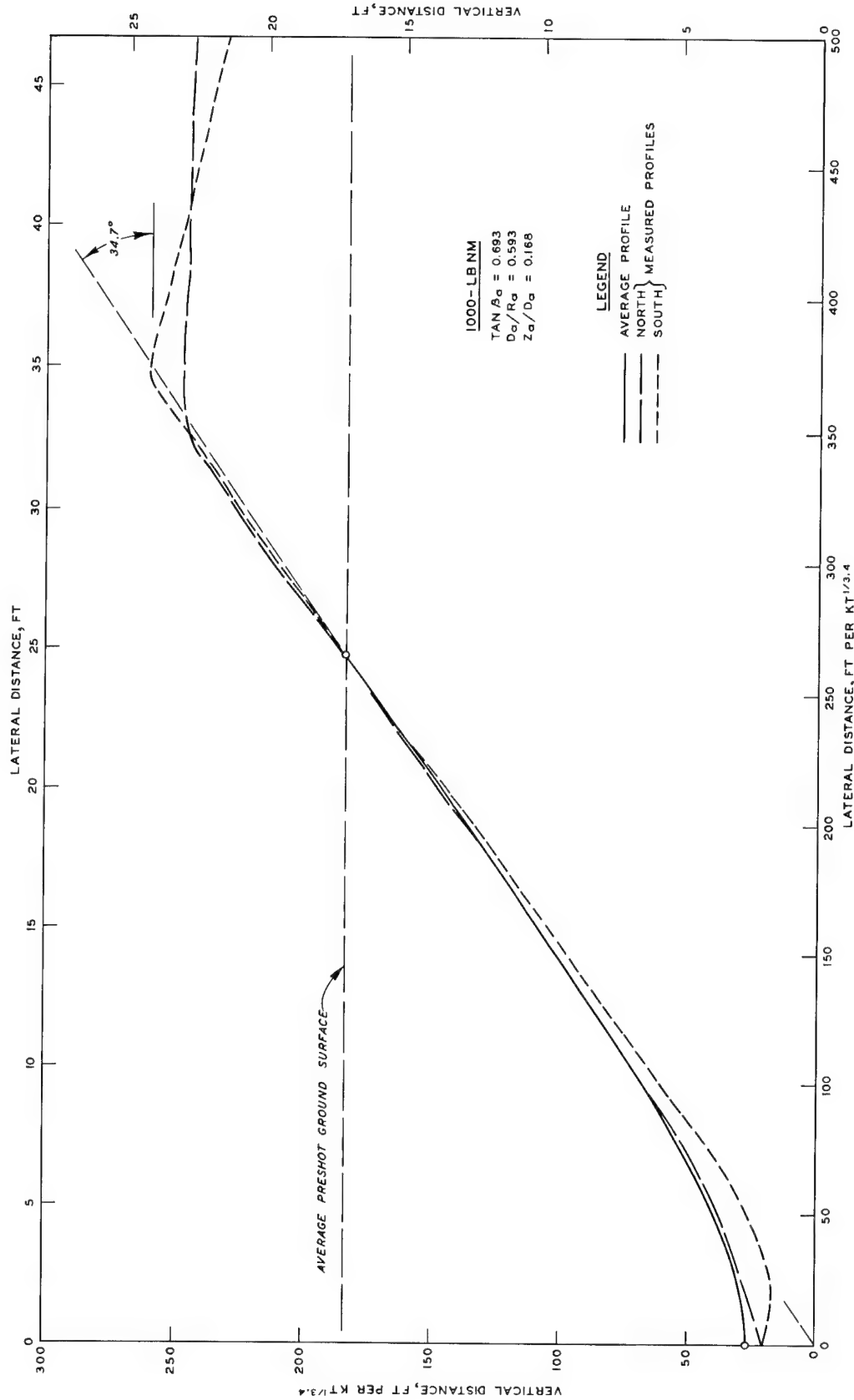


Fig. B7. Typical and average profiles of apparent crater of Row H (at charge No. 5) of Project Pre-Buggy II produced by row of 1000-lb nitromethane explosions in desert alluvium

can be seen that the slope is plane over a substantial height. Photographs of these craters show segregation of particles by size on the slopes, indicating that the last particles deposited could move freely. The profile roundness ratios for these craters, as shown in fig. B6, tend to be smaller than those for the single craters, though the data are erratic; the roundness ratio for the well-developed crater of Row H is definitely smaller.

#### Craters in basalt

10. Several craters have been produced in the basalt cap of Buckboard Mesa at the Nevada Test Site. The largest of these was that of Project Danny Boy,<sup>30</sup> produced by a single 0.42-kt nuclear explosion. Profiles of the apparent crater are shown in fig. B8 and the dimensions are

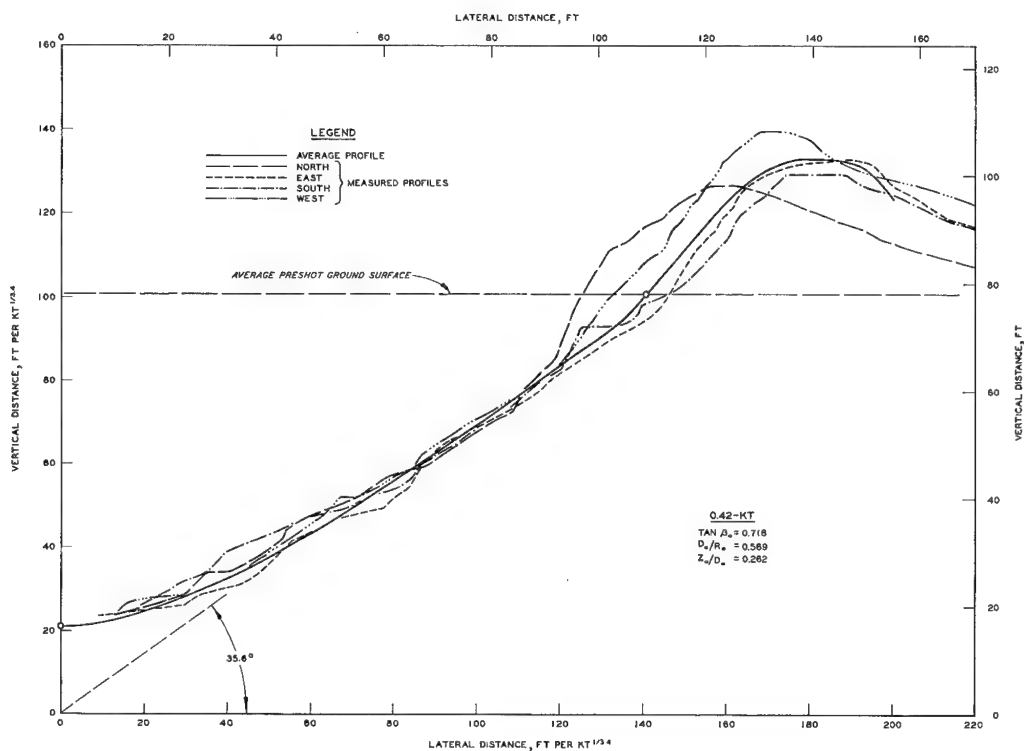


Fig. B8. Typical and average profiles of apparent crater of Project Danny Boy produced by single 0.42-kt nuclear explosion in basalt

given in table B1. The average fallback slope angle was about 36 deg. The fallback and ejecta material consisted of vesicular and dense basalts that had been shattered by the explosion into generally bulky, angular particles with the following typical characteristics:

- a. Maximum particle size = 72 in.\*
- b. Average particle size = 15 in.
- c. Coefficient of uniformity = 35
- d. Coefficient of curvature = 2.6
- e. Bulk specific gravity = 2.76\*\*

There appears to be a correspondence of ejecta particle sizes with spacings of natural joints in the parent material, as shown in fig. B9; this suggests

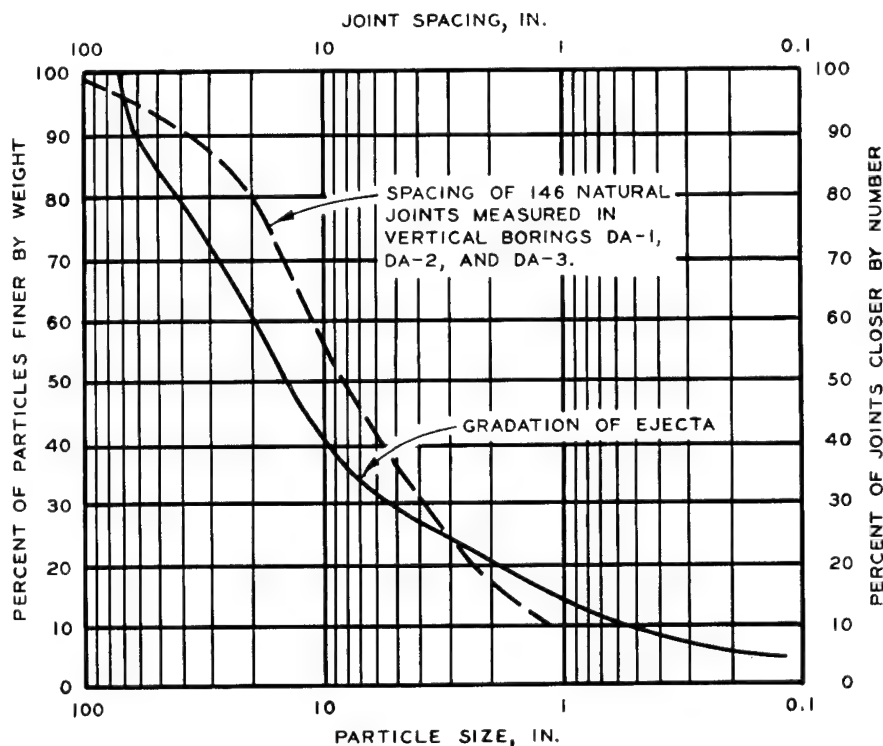


Fig. B9. Comparison of particle size distribution of ejecta with natural joint spacing distribution at Danny Boy crater

the possibility of predicting the gradation of fallback and ejecta material on the basis of preshot subsurface explorations. The slant height of the fallback slope was equal to only 50 to 100 average particle diameters, and the radius of areal curvature was relatively small compared to the average particle size.

\* These characteristics are based on the particle-size analysis of the ejecta, as shown in fig. 10. Actually, the largest particles (up to 100 in.) were concentrated near the bottom of the crater.

\*\* This bulk specific gravity is for the densest basalt; with increased vesicularity this value became as low as 2.16.

11. Dimensions of the other single craters in basalt are given in table B1 and are plotted in fig. B10 along with the crater-scaling relations based on all the single explosions in the basalt of Buckboard Mesa. Three differences can be noted between single craters formed in basalt and those formed in alluvium. First, the average fallback slope angles are slightly smaller in basalt, varying from 27 to 37 deg. Second, the average fallback slope angles in basalt tend to decrease slightly with an increase in the depth of burst beyond optimum, as was the case in Project Zulu II (again, the sharp decrease in apparent crater dimensions beyond this point must be kept in mind). Finally, the upper portions of the fallback slopes in basalt are more planar in section and, as shown in fig. B6, the profile roundness ratios are distinctly smaller; excluding one value of 0.35, the ratios range from 0.15 to 0.25. These differences may be due to the relatively large ratio of volume of fallback material to volume of true crater; the bulking factor for the material at the Delta crater of Project Pre-Schooner averaged 1.67,<sup>36</sup> and that at the Sedan crater was essentially 1.00.<sup>33</sup> Also, much more of the explosion energy in basalt is consumed in forming and extending the cavity, and less horizontal acceleration is imparted to the detached material than in alluvium, so more of the fallback may be redeposited vertically into the center of the crater rather than initially falling near the periphery.

12. The only row crater on Buckboard Mesa is that of Project Dugout,<sup>95</sup> which involved the simultaneous explosion of five spherical 40,000-lb NM charges to produce an apparent crater with the dimensions given in table B1. The dimensions of this crater were appreciably greater than those of the craters of Project Pre-Schooner. However, the charges were spaced too closely ( $s = 0.9 R_g$ ) to produce a linear crater, and the result was a crater elliptical in plan. The fallback slopes were particularly smooth and planar in section, as shown in fig. B11, and averaged about 36 deg in inclination. It should be noted that the profile roundness ratio is about the same for this row crater as for the single craters, which is in contrast to the difference noted between the row and single craters in alluvium.



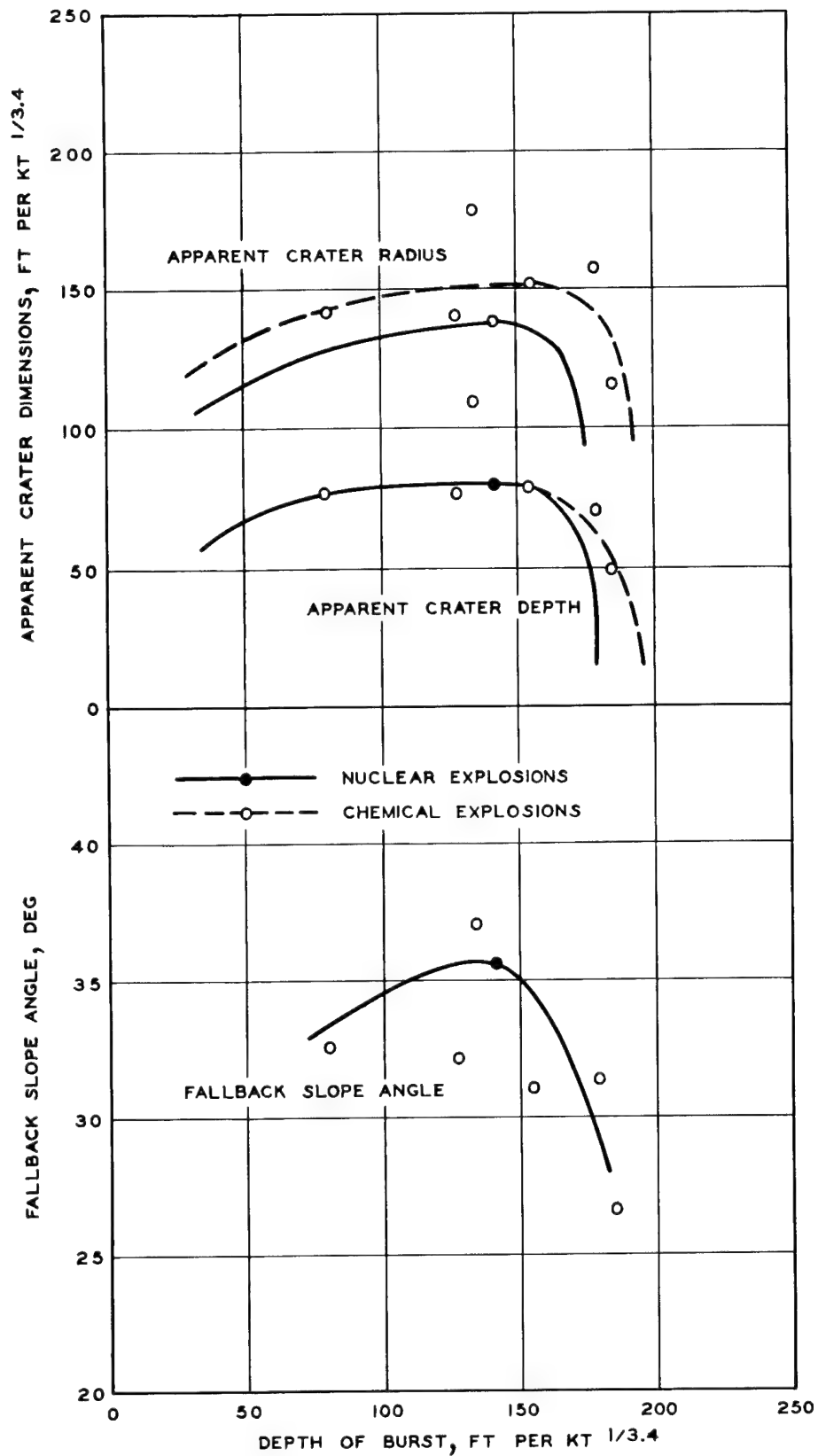


Fig. B10. Variation in average fallback slope angle with depth of burst of single explosions in basalt of Buckboard Mesa

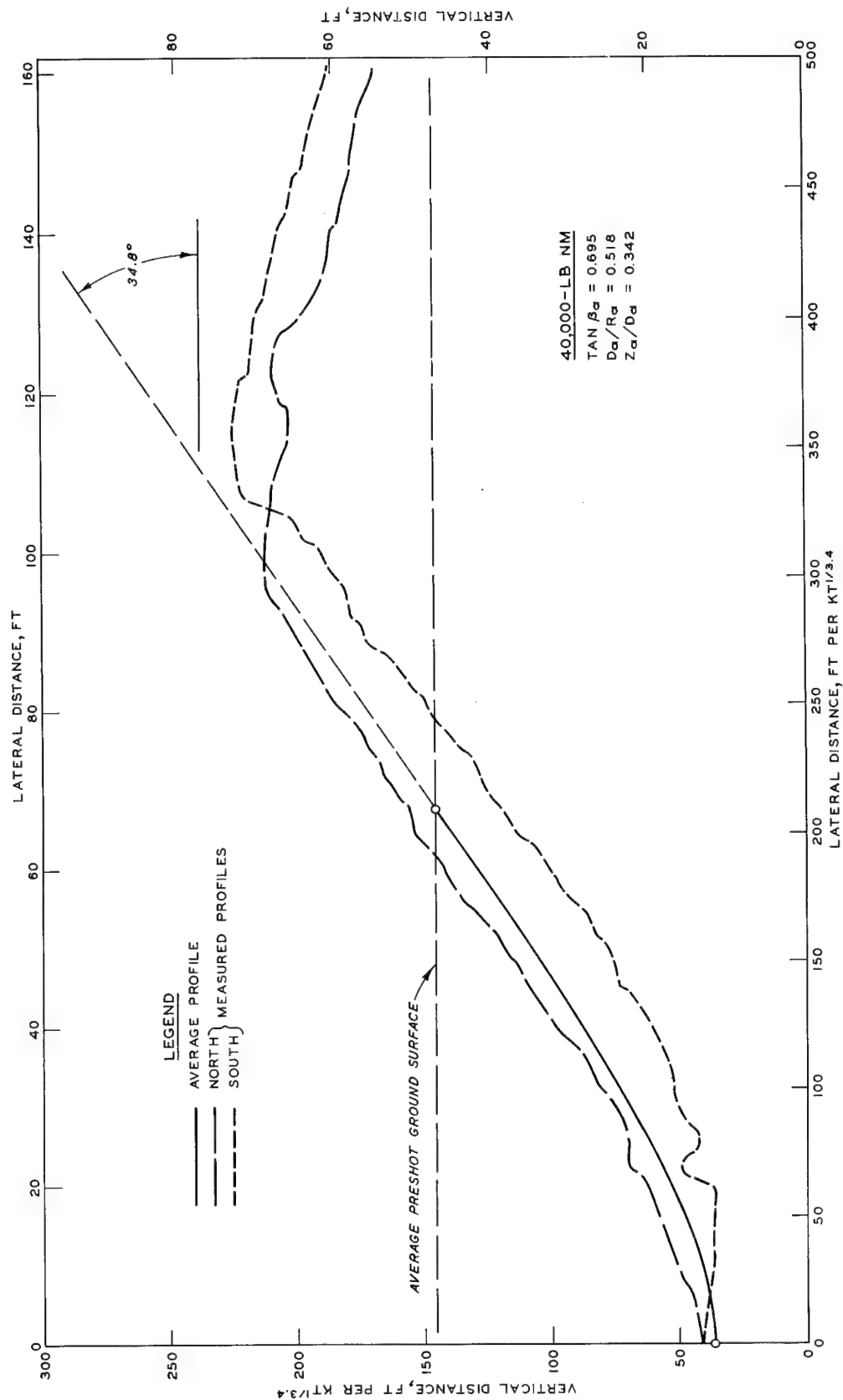


Fig. B11. Typical and average profiles of apparent crater of Project Dugout produced by row of 40,000-lb nitromethane explosions in basalt

### Crater in rhyolite

13. The only large cratering experiment described in this report that was not conducted at the Nevada Test Site is Project Pre-Schooner II.<sup>32,96</sup> This crater was produced by a single 171,000-lb NM explosion in the extensively fractured vitrophyre (including a thick layer of breccia) and felsite comprising the top of Bruneau Plateau in southwestern Idaho. The fallback material consisted of generally bulky and angular, though sometimes subrounded, particles of vitrophyre and felsite having the following characteristics (see fig. 10):

- a. Maximum particle size = 75 in.
- b. Average particle size = 0.63 in.
- c. Coefficient of uniformity = 60
- d. Coefficient of curvature = 0.90
- e. Bulk specific gravity = 2.37

The porosity of the fallback material averaged 29 percent, indicating a bulking factor of only 1.40, which is significantly less than that for the basalt of Buckboard Mesa. The fallback slopes were relatively planar in section and quite steep; the average fallback slope angle was 38 deg.

14. Removal of the fallback material for density and particle-size determinations provided an opportunity to steepen the slope on this material to a condition of imminent surficial failure, that is, to the angle of repose. Trenches were excavated by a dragline on roughly diametrically opposite radials from the center of the crater; over 200,000 cu ft of fallback material were so removed. The trenches undermined the remaining portions of the slope, especially in the southwestern quadrant of the crater where the steepened slope became both planar in section and somewhat linear in plan. Fig. B12 shows in four profiles the steepening of the slope along bearing S40°W from 37 to 42 deg, and the subsequent surficial readjustment of the steepened slope to form a final slope inclined at an angle of 38 deg. The slope along bearing S15°W was similarly steepened from 38 to 43 deg. Thus, it can be concluded that the slope on the Pre-Schooner II crater was formed having an initial factor of safety against surficial failure (i.e. against readjustment) of about 1.2.

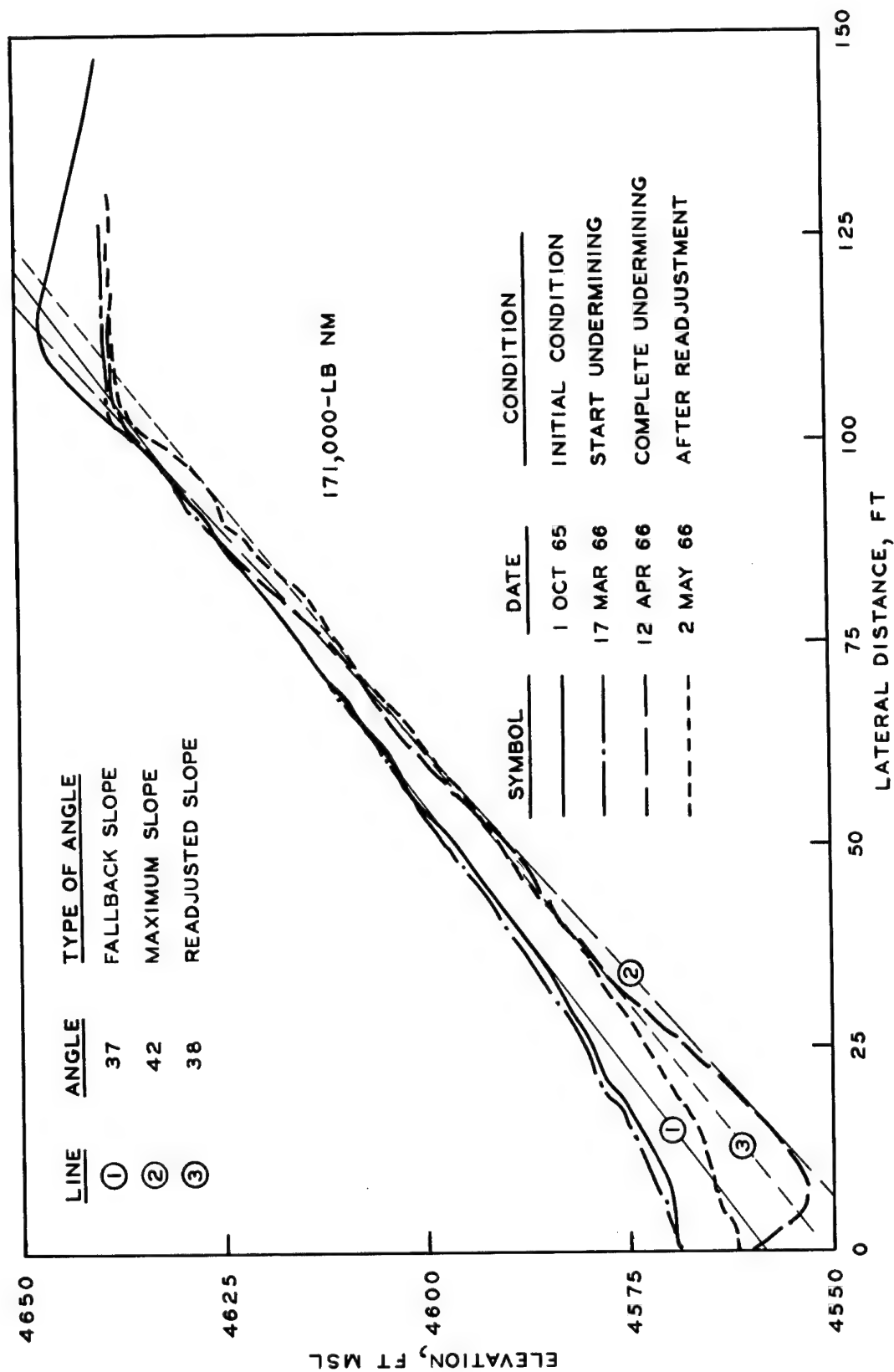


Fig. B12. Profiles along bearing S40°W of apparent crater of Project Pre-Schooner II showing steepening of slope by undermining

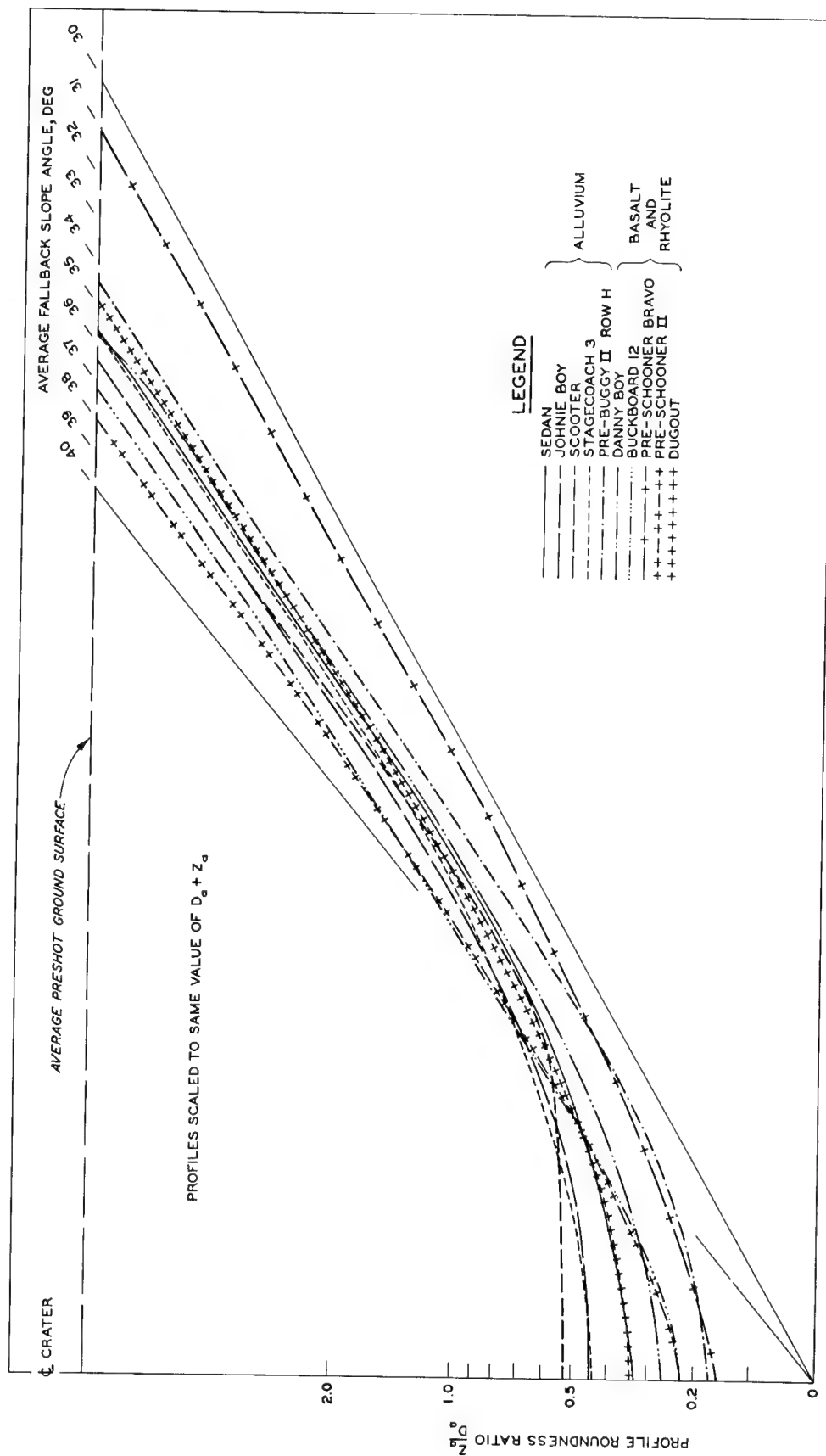


Fig. B13. Comparison of selected average apparent crater profiles

### Comparison of crater profiles

15. The dimensions of several craters considered in this report are given in table B1, plotted in scaled units in figs. B5 and B10, and shown as profile shape and roundness ratios in fig. B6. Nevertheless, it is revealing to compare directly the profiles of these craters when scaled to the same size. Figure B13 shows the average apparent crater of ten of the larger craters scaled to the same value of  $R_a \tan \beta_a$ , that is to the same sum of  $D_a$  and  $Z_a$ . The average fallback slope angles can be seen lying within a rather narrow range despite the differences in material cratered and in the geometry of the explosion.

# DISTRIBUTION LIST

	<u>No. of Copies</u>
LRL Internal Distribution	
Director's Office	
Information Department	30
R. Batzel	
J. Bell	
J. Carothers	
W. Decker	
S. Fernbach	
R. Goeckermann	
J. Gofman	
E. Goldberg	
J. Hadley	
W. Harford	
C. Haussmann	
R. Herbst	
G. Higgins	
A. Holzer	2
E. Hulse	
J. Kane	
J. Knox	2
J. Kury	
C. McDonald	
M. Nordyke	2
J. Rosengren	

Distribution List (continued)

	<u>No. of Copies</u>
B. Rubin	
D. Sewell	
P. Stevenson	2
H. Tewes	2
C. Van Atta	
G. Werth	
LRL Berkeley	
R. K. Wakerling	
D. M. Wilkes	
E. Teller	
LRL Mercury	
L. Crooks	
External Distribution	
TID-4500, UC-35, Nuclear Explosions - Peaceful Applications	277
Department of Mines and Technical Surveys Canada	
D. J. Convey	2
Oil and Gas Conservation Board Canada	
G. W. Govier	2
U. S. Army Engineer Division, Lower Mississippi Valley Vicksburg, Mississippi	
U. S. Army Engineer District, Memphis Memphis, Tennessee	
U. S. Army Engineer District, New Orleans New Orleans, Louisiana	



Distribution List (continued)

No. of Copies

U. S. Army Engineer Waterways Experiment Station  
Vicksburg, Mississippi

75

U. S. Army Engineer District, St. Louis  
St. Louis, Missouri

U. S. Army Engineer District, Vicksburg  
Vicksburg, Mississippi

U. S. Army Engineer Division, Mediterranean  
APO, New York

U. S. Army Liaison Detachment  
New York, New York

U. S. Army Engineer District, GULF  
APO, New York

U. S. Army Engineer Division, Missouri River  
Omaha, Nebraska

U. S. Army Engineer District, Kansas City  
Kansas City, Missouri

U. S. Army Engineer District, Omaha  
Omaha, Nebraska

U. S. Army Engineer Division, New England  
Waltham, Massachusetts

U. S. Army Engineer Division, North Atlantic  
New York, New York

U. S. Army Engineer District, Baltimore  
Baltimore, Maryland

U. S. Army Engineer District, New York  
New York, New York

U. S. Army Engineer District, Norfolk  
Norfolk, Virginia

U. S. Army Engineer District, Philadelphia  
Philadelphia, Pennsylvania

U. S. Army Engineer Division, North Central  
Chicago, Illinois

U. S. Army Engineer District, Buffalo  
Buffalo, New York

Distribution List (continued)

No. of Copies

U. S. Army Engineer District, Chicago  
Chicago, Illinois

U. S. Army Engineer District, Detroit  
Detroit, Michigan

U. S. Army Engineer District, Rock Island  
Rock Island, Illinois

U. S. Army Engineer District, St. Paul  
St. Paul, Minnesota

U. S. Army Engineer District, Lake Survey  
Detroit, Michigan

U. S. Army Engineer Division, North Pacific  
Portland, Oregon

U. S. Army Engineer District, Portland  
Portland, Oregon

U. S. Army Engineer District, Alaska  
Anchorage, Alaska

U. S. Army Engineer District, Seattle  
Seattle, Washington

U. S. Army Engineer District, Walla Walla  
Walla Walla, Washington

U. S. Army Engineer Division, Ohio River  
Cincinnati, Ohio

U. S. Army Engineer District, Huntington  
Huntington, West Virginia

U. S. Army Engineer District, Louisville  
Louisville, Kentucky

U. S. Army Engineer District, Nashville  
Nashville, Tennessee

U. S. Army Engineer District, Pittsburgh  
Pittsburgh, Pennsylvania

U. S. Army Engineer Division, Pacific Ocean  
Honolulu, Hawaii

U. S. Army Engineer District, Far East  
APO, San Francisco, California

Distribution List (continued)

No. of Copies

U. S. Army Engineer District, Honolulu  
Honolulu, Hawaii

U. S. Army Engineer District, Okinawa  
APO, San Francisco, California

U. S. Army Engineer Division, South Atlantic  
Atlanta, Georgia

U. S. Army Engineer District, Canaveral  
Merritt Island, Florida

U. S. Army Engineer District, Charleston  
Charleston, South Carolina

U. S. Army Engineer District, Jacksonville  
Jacksonville, Florida

U. S. Army Engineer District, Mobile  
Mobile, Alabama

U. S. Army Engineer District, Savannah  
Savannah, Georgia

U. S. Army Engineer District, Wilmington  
Wilmington, North Carolina

U. S. Army Engineer Division, South Pacific  
San Francisco, California

U. S. Army Engineer District, Los Angeles  
Los Angeles, California

U. S. Army Engineer District, Sacramento  
Sacramento, California

U. S. Army Engineer District, San Francisco  
San Francisco, California

U. S. Army Engineer Division, Southwestern  
Dallas, Texas

U. S. Army Engineer District, Albuquerque  
Albuquerque, New Mexico

U. S. Army Engineer District, Fort Worth  
Fort Worth, Texas

U. S. Army Engineer District, Galveston  
Galveston, Texas

Distribution List (continued)

No. of Copies

U. S. Army Engineer District, Little Rock Little Rock, Arkansas	
U. S. Army Engineer District, Tulsa Tulsa, Oklahoma	
U. S. Army Coastal Engineering Research Board Washington, D. C.	
Mississippi River Commission Vicksburg, Mississippi	
Rivers and Harbors, Boards of Engineers Washington, D. C.	
Corps of Engineers Ballistic Missile Construction Office Norton Air Force Base, California	
U. S. Army Engineer Center Ft. Belvoir, Virginia	
U. S. Army Engineer Reactors Group Ft. Belvoir, Virginia	
U. S. Army Engineer Training Center Ft. Leonard Wood, Missouri	
U. S. Army Engineer School Ft. Belvoir, Virginia	
U. S. Army Engineer Nuclear Cratering Group Livermore, California	74

Unclassified

Security Classification

DOCUMENT CONTROL DATA - R & D		
(Security classification of title, body of abstract and indexing annotation must be entered when the overall report is classified)		
1. ORIGINATING ACTIVITY (Corporate author)		2a. REPORT SECURITY CLASSIFICATION
U. S. Army Engineer Waterways Experiment Station Vicksburg, Mississippi		Unclassified
		2b. GROUP
3. REPORT TITLE		
ENGINEERING PROPERTIES OF NUCLEAR CRATERS; THE FORMATION AND INITIAL STABILITY OF SLOPES ON COHESIONLESS MATERIALS		
4. DESCRIPTIVE NOTES (Type of report and inclusive dates)		
Report 4 of a series		
5. AUTHOR(S) (First name, middle initial, last name)		
Bruce N. MacIver		
6. REPORT DATE	7a. TOTAL NO. OF PAGES	7b. NO. OF REFS
August 1967	113	96
8a. CONTRACT OR GRANT NO.	9a. ORIGINATOR'S REPORT NUMBER(S)	
b. PROJECT NO.	Technical Report No. 3-699	
c.	9b. OTHER REPORT NO(S) (Any other numbers that may be assigned this report)	
d.	PNE-5009	
10. DISTRIBUTION STATEMENT		
Distribution of this document is unlimited.		
11. SUPPLEMENTARY NOTES		12. SPONSORING MILITARY ACTIVITY
		U. S. Army Nuclear Cratering Group Livermore, California
13. ABSTRACT		
<p>The purpose of the study of engineering properties of nuclear craters is to identify and describe the physical properties that will control the use of a nuclear crater for engineering purposes. One of the prime considerations in the engineering use of a nuclear crater is the stability of the crater slopes. The late time mechanism of explosion crater formation is a deposition phenomenon. The inclination of a slope formed by deposition of cohesionless material is termed the angle of deposition, and the maximum possible inclination of the slope is termed the angle of repose. This definition differs from some common definitions of angle of repose. The factor of safety of a slope formed by deposition is defined as the ratio of the tangent of the angle of repose to the tangent of the angle of deposition. Variations are recognized in the angle of deposition with the manner of deposition, and in the angle of repose with varying relative density and particle orientation. Such factors as particle size, shape, and angularity, structure of particle aggregations, manner of deposition, and geometry of slopes are discussed with regard to their relative influence on each of the aforementioned angles. A few simple analytical relations are given to aid in understanding the behavior of particles during deposition and their stability on an inclined surface. Empirical data from laboratory tests, stockpiles, rock-fill dams, natural slopes, explosion-produced craters, etc., are presented and compared. It is concluded that angles of deposition for cohesionless rock and soil materials vary between 22 and 42 deg, and generally lie between 34 and 37 deg for angular particles, whereas angles of repose range between 27 and 47 deg, and generally lie between 37 and 47 deg for angular particles. The initial factor of safety of a slope formed by deposition will probably exceed 1.1 but will be no more than 1.5 in most cases.</p>		

DD FORM 1473 REPLACES DD FORM 1473, 1 JAN 64, WHICH IS OBSOLETE FOR ARMY USE.

Unclassified

Security Classification

Unclassified

Security Classification

14.	KEY WORDS	LINK A		LINK B		LINK C	
		ROLE	WT	ROLE	WT	ROLE	WT
	Angle of repose Cohesionless soils Craters and cratering Nuclear craters Slope stability						

Unclassified

Security Classification